FILMWISE CONDENSATION OVER A TIER OF SPHERE

A THESIS SUBMITTED TO
THE GRADUATE SCHOOL OF NATURAL AND APPLIED SCIENCES
OF
MIDDLE EAST TECHNICAL UNIVERSITY

BY

TAMER ÇOBANOĞLU

IN PARTIAL FULFILLMENT OF THE REQUIREMENTS
FOR
THE DEGREE OF MASTER OF SCIENCE
IN
MECHANICAL ENGINEERING

DECEMBER 2006

Approval of the Graduate School of Natural and Applied Sciences

_____
Prof. Dr. Canan ÖZGEN
Director

I certify that this thesis satisfies all the requirements as a thesis for the degree of Master of Science.

_____
Prof. Dr. S. Kemal İDER
Head of Department

This is to certify that we have read this thesis and that in our opinion it is fully adequate, in scope and quality, as a thesis for the degree of Master of Science.

_____
Assoc. Prof. Dr. Cemil YAMALI
Supervisor

Examining Committee Members

Prof. Dr. Faruk ARINÇ (METU,ME) _____

Assoc. Prof. Dr. Cemil YAMALI (Affiliation) _____

Prof. Dr. Kahraman ALBAYRAK (Affiliation) _____

Asst. Prof. Dr. Tahsin ÇETİNKAYA (Affiliation) _____

Asst. Prof. Dr. İbrahim ATILGAN (GAZI UNIV.) _____

I hereby declare that all information in this document has been obtained and presented in accordance with academic rules and ethical conduct. I also declare that, as required by these rules and conduct, I have fully cited and referenced all material and results that are not original to this work.

Name, Last name :

Signature :

ABSTRACT

FILMWISE CONDENSATION OVER A TIER OF SPHERE

ÇOBANOĞLU, Tamer
M.S., Department of Mechanical Engineering
Supervisor:Assoc. Prof. Dr.Cemil YAMALI

December 2006 , 131 pages

The objective of this study is to determine the mean heat transfer coefficient and heat transfer rate and to analyse the effect of inclination angles,the effect of subcooling temperatures and the effect of vapour velocity for laminar filmwise condensation of water vapour on a vertical tier of spheres experimentaly and analyticaly. For this purpose, the experimental aparatus were designed and manufactured. In the free condensation experimental study Ø50mm and Ø60 mm O.D. spheres were used to analyse the diameter effect . In the experimental studies of free and forced condensation Ø60mm O.D. spheres on which vapour flows at 2,75 bars were used to analyse the effect of vapour velocity. For the experimental study of the annular condensation in the concentric spheres the effect of vapour velocity

was studied by forcing the vapour to flow in the area between two concentric spheres.

In the free condensation experiments it is observed that at smaller diameters the heat flux and mean heat transfer coefficients for sphere is higher. In the free and forced condensation experiments increasing the velocity of vapour increases the mean heat transfer coefficient. At the experiments with annular condensation between the concentric spheres high mean heat transfer coefficient values have been obtained compared to the free and forced condansation over the surface of spheres experimental studies.

Keywords: Laminar, film condensation, sphere, inclination angle, forced condensation.

ÖZ

DİKEY SIRALANMIŞ KÜRELER ÜZERİNDEN
FİLM YOĞUŞMASININ İNCELENMESİ

ÇOBANOĞLU , Tamer
Y.Lisans, Makine Mühendisliği Bölümü
Tez Yöneticisi: Doç. Dr.Cemil YAMALI

Aralık 2006 , 131 sayfa

Bu çalışmanın amacı, deneysel ve analitik yöntemler kullanılarak, dikey sıralanmış küreler üzerinden akan su buharının laminar yoğuşması esnasında gerçekleşen ortalama ısı transfer katsayılarının hesaplanması ve buhar hızı, eğim açısı ile buhar ve yüzey sıcaklık farkı etkisinin analiz edilmesidir. Bu amaç için, bir deney seti tasarlanarak imal edilmiştir. Deneyler 3 aşamalı olarak gerçekleştirilmiştir. Serbest yoğuşma deneyinde, Ø50mm ve Ø60mm çaplarında küreler kullanılarak çap etkisi incelenmiştir. Serbest ve zorlanmış yoğuşma deneyinde üzerinden 2,75 bar buhar akan Ø60mm küreler kullanılarak, durağan ve hızlı akan buhar etkisi incelenmiştir. İç içe geçirilmiş eş merkezli iki küre deneyinde serbest ve zorlanmış yoğuşma etkisi incelenmiştir.

Serbest yoğuşma deneyi sonucunda küçük çaplı kürede ortalama ısı transferi katsayısının daha yüksek çıktığı görülmektedir. Serbest ve zorlamalı yoğuşma deneyi sonucunda yüksek buhar hızlarında film kalınlığının düştüğü ve ortalama ısı transferi katsayısının yükseldiği görülmektedir. İç içe geçirilmiş eşmerkezli küreler deneyinde elde edilen ortalama ısı transferi katsayılarının diğer deneylerde elde edilen değerlerden daha yüksek çıktığı görülmektedir.

Anahtar kelimeler: Laminar, film yoğuşması,küre, tırmanma açısı, hızlı buhar.

ACKNOWLEGEMENTS

I would like to thank my supervisor, Assoc. Prof. Dr. Cemil YAMALI for his continuous guidance, support and valuable contribution throughout this study. I gratefully acknowledge Cengiz Akkor, Hükümdar Ertan and Hamdi Genç for their technical assistance in manufacturing and operating the setup. I am grateful to the jury members for their valuable contributions.

I express my deepest gratitude to my mother Gülsüm Çobanoğlu, my father Fuat Çobanoğlu and my wife Ahsen Çobanoğlu for their encouragements throughout my education life.

.

TABLE OF CONTENTS

LIST OF TABLES

TABLES

LIST OF FIGURES

FIGURES

LIST OF SYMBOLS

C_p	Specific heat at constant pressure, J/(kg.K)
g	Gravitational acceleration, m/s^2
h	Convective heat transfer coefficient, W/(m^2.K)
h_{fg}	Latent heat of condensation, J/kg
k	Thermal conductivity, W/m.K
$\dot{m}$	Mass Flow Rate, kg/s
Pr	Prandtl Number, $\frac{\mu C_p}{k}$
q	Heat flux, W/m^2
Q	Heat transfer rate, W
T	Temperature, K or ^{O}C
T1,…,T20	Thermocouples
t	Time, s
A	Area, m^2
ΔT	Temperature difference, K
r	Radius of the sphere, m
u	x component of velocity, m/s
x	Coordinate parallel to surface
y	Coordinate normal to surface

Subscripts

cond	Condensation
in	Inlet
out	Outlet
sat	Saturation
w	Wall

Greek Letters

δ	Film thickness of the condensate layer, m
θ	Angular position measured from the top of the sphere, rad.
μ	Dynamic viscosity, kg/(m.s)
ρ	Density, kg/m^3
τ	Shear stress, N/m^2

CHAPTER 1

1 INTRODUCTION

1.1 Condensation

Condensation phenomena occur in many industrial applications.Condensation is defined as the phase change from the vapor state to the liquid or solid state. Condensation can occur on a solid surface or in a bulk vapor. If the temperature of vapor is below its saturation temperature according to its pressure it can take place in a bulk vapor. If the temperature of the solid surface is below the saturation temperature of the vapor condensation can occur on the solid surface. The subcooling condition must be obtained for any type of condensation.

There are two idealized models of condensation, filmwise condensation and dropwise condensation.

1.1.1 Filmwise Condensation

Filmwise condensation is the former and it occurs on a cooled surface which is easily wetted. The vapor condenses in drops which grow by further condensation and coalesce to form a film over the surface, if the surface-fluid combination is wettable. Filmwise condensation is the most observed type of cendensation. The removal of the film is the result of the gravity, acceleration or other body forces.

Rates of heat transfer for film condensation can be predicted as a function of bulk and surface temperatures, total bulk pressure, surface and liquid film characteristics, bulk velocity and the presence of noncondensible gases. Even though film condensation has been investigated extensively, the majority of these studies were devoted to laminar film condensation (laminar bulk flow and laminar film). Since the vapor flow in heat exchange equipment may be turbulent, models and recent data are also reviewed for the condensation flux with a turbulent mixture flow. A simple engineering correlation or model is preferred many times for use in engineering design studies and with existing computer system analyses.

1.1.2 Dropwise Condensation

Dropwise condensation occurs if the surface is non-wetting rivulets of liquid flow away and new drops then begin to form. The phenomena of dropwise condensation results in local heat transfer coefficients which are often an order of magnitude greater than those for filmwise condensation. Even though condensation phenomena can be classified into these categories of dropwise and film condensation the initial period of condensation would evolve into a film and probably would not affect the overall pressure-temperature response unless drop condensation is promoted.

1.2 Condensate Film Structure

The condensate film characteristics depend on its flow field and the nature of the condensing surface, e.g. roughness, wetting and orientation. Forced flow induces interfacial instabilities that increase the heat transfer rates by reducing the thickness of gas phase laminar sublayer and enhancing the mixing of both the liquid (condensate film) and gas phase.

The surface finish has a major effect on the mode of condensation for a downward facing surface and it is the wetting characteristics of the surface

that ultimately determine this. Dropwise condensation is likely to exist on non-wetting surfaces and filmwise condensation is likely on wetting surfaces. In dropwise condensation mode with polished metal surfaces, the heat transfer characteristics are likely to change due to oxidation of the surface or tarnishing. Thus, one cannot precisely know the wetting characteristics as surface aging occurs.

1.3 Effects of Non-Condensable Gases

It can be observed that in actual cases some amount of non-condensable gases occurs in the condensation system. In some systems such as steam power plants because of the pressure less than atmospheric pressure air leaking occurs in the convective flow. Also in some systems the dissolved gases cause to occuring of non-condensable gases in the condensation such as water and alcohol. When the condensing vapor carries non condensable gases to the condenser surface, it acts as an empty area between the condenser surface and the condensation of vapor. Therefore the heat transfer comes to be difficult. So non-condensable gases reduce the heat transfer rate both in filmwise and dropwise condensation.

1.3.1 Stationary Vapor with a Noncondensable Gas

A noncondensable gas can exist in a condensing environment and leads to a significant reduction in heat transfer during condensation. A gas-vapor boundary layer (e.g., air-steam) forms next to the condensate layer and the partial pressures of gas and vapor vary through the boundary layer. The buildup of noncondensable gas near the condensate film inhibits the diffusion of the vapor from the bulk mixture to the liquid film and reduces the rate of mass and energy transfer. Therefore, it is necessary to solve simultaneously the conservation equations of mass, momentum and energy for both the condensate film and the vapor-gas boundary layer together with the

conservation of specied for the vapor-gas layer. At the interface, a continuity condition of mass, momentum and energy has to be satisfied.

1.3.2 Moving Vapor with a Noncondensable Gas

For a laminar vapor-gas mixture case, Sparrow, et al. (1967) solved the conservation equations for the liquid film and the vapor-gas boundary layer neglecting inertia and convection in the liquid layer and assuming the stream-wise velocity component at the interface to be zero in the computation of the velocity field in the vapor-gas boundary layer. Also a reference temperature was used for the evaluation of properties. The results showed that the effect of noncondensable gas for the moving vapor-gas mixture case is much less than for the corresponding stationary vapor-gas mixture. A moving vapor-gas mixture is considered to have a "sweeping" effect, thereby resulting in a lower gas concentration at the interface (compared to the corresponding stationary vapor-gas mixture case). Also, the ratio of the heat flux with a noncondensable gas to that without a noncondensable gas was calculated to be independent on the bulk velocity. The computed results reveal that interfacial resistance has a negligible effect on the heat transfer and that superheating has much less of an effect than in the corresponding free condensation case.

1.4 Laminar and Turbulent Flow

Boundary layer is defined as the very thin layer in the intermediate neighborhood of the body, in which the velocity gradient normal to the wall is very large. In this region, the very small viscosity of the fluid exerts an essential influence as the shearing stress may assume large values. At the wall surface, the fluid particles adhere to it and the frictional forces between the fluid layers retard the motion of the fluid within the boundary layer. In this thin layer, the velocity of the fluid decreases from its free-stream value to zero with no slip condition.

According to Prandtl, who intrctduced the boundary layer concept for the first time, under certain conditions viscous forces are of importance only in the immediate vicinity of a solid surface where velocity gradients are large. In regions removed from the solid surface where there exists no large gradients in fluid velocity, the fluid motion may be considered as frictionless, which is called potential flow. In fact, there is no precise separating line between the potential flow and boundary layer regions. However, boundary layer can be defined as the region where the velocity component parallel to the surface is less than 99% of the free-stream velocity.

An essential first step in the treatment of any flow problem is to determine whether the flow is *laminar* or *turbulent.* Surface friction and the convection transfer rates depend strongly on which of these conditions exists. There are sharp differences between laminar and turbulent flow conditions. In the laminar flow, fluid motion is highly ordered and it is possible to identify streamlines along which particles move. Fluid motion along a streamline is characterized by velocity components in both the x and y directions. Since the velocity component *v* is in the direction normal to the surface, it can contribute significantly to the transfer of momentum, energy or species through the flow layers.

In contrast, fluid motion in the turbulent flow is highly irregular and is characterized by velocity fluctuations. These fluctuations enhance the transfer of momentum, energy and species, and hence increase surface friction as well as convection transfer rates. Fluid mixing resulting from the fluctuations makes turbulent flow layer thicknesses larger and flow layer prdfiles (velocity, temperature and concentration) flatter than in laminar flow.

When the foregoing conditions for velocity distribution on a flat plate are analyzed, it is seen that the flow is initially laminar, but at some distance from the leading edge, small disturbances are amplified and transition to turbulent flow begins to occur. Fluid fluctuations begin to develop in the *transition*

region, and the boundary layer eventually becomes completely turbulent. In the fully turbulent region, conditions are characterized by a highly random, three-dimensional motion of relatively large parcels of fluid, and it is not surprising that the transition to turbulence is accompanied by significant increases in the boundary layer thicknesses, the wall shear stress and the convection coefficients.

In the turbulent flow, three different regions may be delineated. There is a *laminar sublayer* in which transport is dominated by diffusion and the velocity profile is nearly linear; there is an adjoining *buffer layer* in which diffusion and turbulent mixing are comparable; and there is a *turbulent zone* in which transport is dominated by turbulent mixing.

CHAPTER 2

2 REVIEW OF PREVIOUS STUDIES

In this section, the review of the literature with the theory background and research findings will be presented. The review is mainly based on three subjects: inclination angle, heat transfer, subcooling, film condensation, laminar boundary layer and condensation on sphere & cylinder.

Michael Ming Chen [1] studied the cases of laminar film condensation over a single and multiple horizontal tubes. In this analytical study neglecting the x-component of vapor velocity outside the boundary layer and $\mu_v\rho_v<<\mu\rho$ were assumed. Both the vapor boundary layer and the liquid film were considered to be thin compared to the radius of the tube. All properties were taken constant. Results: For single tube the temperature profiles are essentially the same as the flat-plate case. The inertia forces have a larger effect on the heat transfer of round tubes than flat plates. For vertical tubes the heat transfer results for lower tubes were found to be consistently higher than Nusselt's theory. As a result of condensation between tubes a higher heat transfer rate was predicted.

E.M.Sparrow and J.L.Gregg [2] studied the problem of laminar film condensation on a vertical plate. In this analytical study energy-convection and fluid-acceleration terms are fully considered. Solutions are obtained for $c_p\Delta T / h_{fg}$ between 0 and 2 for Prandtl numbers between 1 and 100. Solutions are obtained both with and without acceleration terms. The addition

of acceleration terms introduces the Prandtl number as an additional parameter. Negligible heat conduction across the liquid-vapor interface was assumed. As a result it is found that the Prandtl number effect on the heat transfer results is very small for high Prandtl numbers (Pr >1). So the effect of Prandtl number on the heat transfer appears negligible for the range Pr >1. The Pr=100 results are seen to coincide with those for no acceleration term. But for lower Prandtl numbers, the acceleration terms should play a more important role (Pr<1). As $c_p\Delta T / h_{fg}$ increases, the inertia effects lead to a dropping off of the Nusselt number.

Cz.O.Popiel and L.Boguslawski [3] studied the problem of heat transfer by laminar film condensation on sphere surfaces taking into account liquid wetting. Despite of horizontal tubes over sphere there was an influx of additional condensate according to the change of the section area. The neglecting of surface tensions was assumed. As a result of this study it was seen that the average heat transfer coefficients on the upper and bottom hemisphere surfaces are very close. The heat transfer coefficient decreases slowly and then over the bottom hemisphere it decreases faster and faster as it approaches the bottom stagnation point, in which it reaches zero. It is the result of faster increase of the condensate thickness, caused by vapor condensation, the decrease of the circumference, the condense flow down and the tangential component of the gravity force.

V.H.Adams and P.J.Marto [4] analyzed the problem of laminar film condensation on a horizontal elliptical tube in a pure saturated vapor for conditions of free and forced condensation. They assumed the effects of surface tension and pressure gradient in the condensate film. For free condensation an elliptical tube with the major axis vertical showed an improvement of nearly 11% in the mean heat-transfer coefficient when compared to a circular tube of equivalent surface area. For forced condensation with the same approach velocity as for a circular tube, a small decrease (≈2%) in the mean heat-transfer coefficient resulted. However, for

the same pressure drop, heat transfer performance for an elliptical tube increased by up to 16%. It can be seen that the effect of placing more of the elliptical tube surface in the direction of gravity is to increase the mean heat-transfer coefficient by 7%. The condensation rate and the condensate film velocity determine the thikness of the film. For free condensation, at the top of the elliptical tube, the increased effect of gravity (compared with the circular tube) increases the condensate velocity, resulting in a thinner film. The thinner film, however, results in a higher condensation rate, which tends to thicken the film further downstream. With vapor shear, the streamlined shape of an elliptical tube causes higher vapor velocities over the front and rear portions, but a lower vapor velocity over the middle region. For the elliptical tube, the larger shear stress at the top of the tube due to the higher vapor velocity (when compared to a circular tube) results in a thinner condensate film. This causes a higher condensation rate which leads to a thicker condensate film in this region. Over the rear portion of the elliptical tube, the now lower condensation rate combined with the higher vapor shear once again results in a thinner film than with a circular tube.

Ravi Kumar, H.K.Varma, Bikash Mohanty and K.N.Agrawal [5] studied an experimental investigation for the condensation of steam over a plain tube, CIFT (circular integral-fin tube) and a SIFT (spine integral-fin tube). The steam temperature was measured at two points, one above the test-section and the other below it. The maximum uncertanity in the determination of heat transfer coefficient was found to be 2.0 percent. The experimental values of heat transfer coefficients are higher than those predicted by the Nusselt's model in a range of 5 to 15 percent. In fact, as the coolant velocity increases, the inside tube heat transfer coefficient also increases resulting in a higher rate of condensation and thus, the thickness of condensate film over the tube surface increases. The increased thickness of condensate film offers greater thermal resistance to heat flow resulting in reduction of condensing side heat transfer coefficient. Thus, for CIFT, the condensing heat transfer coefficient is 2.21 times than that for the plain tube. The SIFT further increases the value

of h_0 by 1.29 times in comparison to CIFT and prove itself to be the best performing tube. For a given pressure (T_s=constant) the value of (T_s - T_{wo}) increases with the rise in cooling water velocity. For a given pressure the best fit line for SIFT falls below that of CIFT indicating that the performance of SIFT is better for all the pressures and coolant flow rates investigated, the value of (T_s - T_{wo}) for the plain tube is approximately 45 to 55 percent higher than that for CIFT and 60 to 80 percent higher than that for SIFT. In other words, the (T_s - T_{wo}) values for SIFT are approximately 15 to 25 percent less than CIFT. An increase in heat flux reduces the value of h_0. At higher heat flux, the rate of condensation is higher and thus the condensate layer becomes thicker, which in turn reduced the value of h_0. The SIFT and CIFT enhance the heat transfer coefficient approximately by factors of 3.2 and 2.5 respectively as compared to plain tube of diameter equal to the root diameter of finned tubes.

M.Mosaad [6] analyzed the laminar film condensation on an inclined circular tube, under the condition of combined free and forced condensation. He assumed that condensate film thickness is much smaller than the tube diameter, the inertia and pressure terms and the convection terms for the condensate film can be neglected, surface tension effect is insignificant, the condensae film flow is laminar, steady and with negligible vicous dissipation, all physical properties of the condensate film are constant. He considered the combined influence of vapour shear and gravity forces. The result for the case of the finite-length tube is that at fixed Z^- , $Nu_d(z)$ increases with increasing Fd. But for constant Fd, $Nu_d(z)$ decreases from an infinite value at the start point (Z^-=0) with increasing Z^- .

C.H.Hsu and S.A.Yang [7] studied the problem of pressure gradient and variable wall temperature effects during filmwise condensation from downward flowing vapors onto a horizontal tube. The extended model will be applicable to filmwise condensation from flowing pure vapors onto horizontal tubes, including taking account of the pressure gradient and vapor shear

effects in a general fashion, and being amendable to any physically relevant initial condition. As for the forced-convection film condensation, ingnoring the pressure gradient case investigated by Memory et all. [14], the mean condensation heat transfer increases as the wall temperature variation amplitude goes up. As a result for pure forced- convection film condensation and for isothermal tube wall , the film thickness increases continuously with ϕ. For natural convection dominated film condensation the dimensionless condensate film thickness increases directly with ϕ. For the isothermal wall, the local heat flux decreases continuously around the tube. The higher *F* or lower vapor velocity is, the higher the local heat flux is. When *P*=0, the mean heat transfer coefficient is increasing insignificantly with *A*, whereas as *P* is included and increases., the mean heat transfer coefficent decreases appreciably with *A*. The mean heat transfer coefficient is also nearly unaffected by the pressure gradient for the lower vapor velocity once its corresponding $\phi c=\pi$. As for the higher vapor velocity (or higher *F*), the mean heat transfer coefficient decreases significantly with increasing the pressure gradient effect.

S.S.Kutateladze and I.I.Gogonin [8] made an experimental study on heat transfer in film condensation of flowing vapour on horizontal tube banks. This study describes experimental results for the case of the joint influence of vapour velocity and condensate flow rate on heat transfer intensity in condensation of a practically pure vapour. The experiments were run on 10-row tube banks in a cross flow of a coolant (R21 and R12) vapour. In the experiments, the dependence of the heat flux on the vapour-wall temperature difference, vapour velocity, physical properties of the cooling agents, location of a tube in a bank and the geometry of the bank was determined. As a result at a constant heat flux the vapour- wall temperature difference increases with the number of a tube in a bank and the slope of the curves changes. Also the effect of vapour velocity is practically lacking at *Re*> 70 and the heat transfer in this case is governed by the condensate flow rate alone.

Georg Peter Fieg and Wilfried Roetzel [9] studied on calculation of laminar film condensation in/on inclined elliptical tubes. The Nusselt type laminar film condensation in or on inclined elliptical tubes was investigated analytically in this study. In this study the additional minor effect of surface tension on film flow, which occurs mainly in non-circular tubes, was neglected. For $a/b < 1$ (a=horizontal radius, b=vertical radius) the total heat transfer ratio becomes > 1 and vice versa. An elliptical deformation of a circular tube improves heat transfer only if $a/b < 1$. In the limiting case $a/b \rightarrow 0$ the ellipse turns to a vertical plate with maximum total heat transfer ratio 1.157. A more significant increase of heat transfer is obtained with inclined elliptical tubes of finite length.

Stuart W.Churchill [10] studied laminar film condensation of a saturated vapor on a vertical and isotermal surface. He studied the effect of the heat capacity of the condensate, the inertia of the condensate, the drag of the vapor and the curvature of the surface on the rate of laminar condensation . The solutions are very accurate for large Pr, but for small Pr are restricted to small values of $Cp\Delta T/\lambda$. Solutions in closed form are presented for. For $Pr < 5$ both the inertia and the drag of the vapor are found to be effective and negligible for $Pr \geq 5$. The heat capacity of the liquid increases the rate of heat transfer for $Pr > 1$ but has the opposite effect for $Pr < 1$. When a vapor condenses on the outside of a round vertical tube the effect of curvature is to provide a greater area for flow and a greater area for heat transfer for the same film thickness, thereby resulting in a greater rate of condensation.

T.Fujii, H.Uehara, K.Hırata and K.Oda [11] made an experimental study on heat transfer and condensation of saturated steam flowing through tube banks. The tests were performed in the ranges of steam pressure 0.01-0.07 bar, oncoming velocities of steam 10-40 m/s and temperatures of cooling water 5 - 20 ^{0}C. Due to the change of microscopic state of the tube surface, filmwise condensation became dominant on all tube surfaces after some experiments. Steam temperature falls more rapidly over the lower rows,

where leaked air was accumulated. That tendency was usual in the cases where mass flow rate of steam was relatively small. The overall accuracy of these experiments may be estimated to be about ten per cent. While the pressure in non-condensing cases varies almost linearly, that in condensing cases varies non- linearly owing to the variation of mass velocity. As a result the resistance coefficient of flow through tube banks c_D depends on the relation between the diameter and the spacings of tubes.

E.S.Gaddis [12] presented a method for solving the two phase boundary layer equations for the condensation of a flowing vapour on a horizontal cylinder. The ideal flow outside the vapour layer, constant physical properties, surface tension forces, achiving to steady state, ignored viscous dissipation and uniform wall surface temperature were assumed. After calculations the following numerical results were obtained. For quiescent vapour (Re=0), ignoring inertial forces in the condensate layer leads to an increase in the local Nusselt number Nu_0 and the mean Nusselt number Nu_m by 30% and 23% respectively. Ignoring the shear forces at the liquid-vapour interface increases Nu_0 and Nu_m by 19% and 24% respectively. Ignoring the inertial forces in the condensate layer and the shear forces at the interface have insignificant effect on the value of the Nusselt number for Pr=100. However, eliminating convection in the energy equation or ignoring liquid subcooling leads to a reduction of 5% in Nu_0 and Nu_m.

Tetsu Fujıı, Haruo Uehara and Chikatoshi Kurata [13] stuided the effect of vapour velocity on condensation with a single horizontal tube. Outside the boundary layer vapour flow was assumed to be potential. Numerical results; when the vapour velocity is smaller, the temperature difference is larger, and the vapour pressure is lower.when the vapour velocity is high, about 78 or 98 % of total condensate takes place where angle ø are less than 90 and 140 degrees respectively. For relatively small oncoming vapour velocity, pressure term is negligibly small , and for large one, on the other hand, the magnitudes of both terms are comparable. Experimental results; experiments were

performed with a horizontal brass tube of 0.014m o.d. and 0.0104m i.d. which intersected through a circular duct of 0.092m i.d. Eight thermocouples of 0.023m effective length were inserted in the wall of the brass tube. The temperature of tube wall is not uniform but the peripheral distribution of wall temperature is affected by both oncoming velocity U and heat flux q. The direction of steam flow is different from the situation of theoretical calculation and the experiments are not so accurate owing to small temperature rise in cooling water.

J.W.Rose [14] studied the effect of pressure gradient in film condensation on a horizontal tube. The shear stress at the condensate surface and the circumferential variation of pressure in the condensate film were included. Owing to the higher vapour density, pressure gradient effects should become important at lower velocities for the refrigerants than for steam at comparable pressures and temperatures. For steam, pressure gradient effects should be more important at relatively high pressures. Including of the pressure gradient term has two effects; it gives rise to an increase in the heat transfer coefficient over the forward part of the tube. The instability of laminar condensate film caused by an infinite rate of increase of film thickness could give rise to an appreciable increase in the heat transfer coefficient over the value calculated for laminar flow when the pressure gradient term is neglected. When $\rho_g U_\infty^2/\rho gd < 1/8$ it is found that the increase in heat tansfer for the forward half of the tube is almost balanced by a decrease for the rear half, so that the mean Nusselt number for the tube is very close to that found when the pressure gradient is neglected

The classical analysis of laminar film condensation was carried out by Nusselt [15] in 1916. He successively analyzed the condensation problem for a variety of geometrical configurations. In his analysis, an equation was obtained for condensate thickness by considering gravity and viscous forces. The heat transfer coefficient was calculated by assuming a linear temperature profile within the condensate layer. Only assuming heat conduction to take place, he neglected the effects of both energy convection

and fluid accelerations within the condensate layer. The actual heat transfer coefficients are found to be higher for fluids with moderate and high Prandtl numbers although Nusselt's theory was simple and capable of predicting the heat transfer coefficient in many cases, while the heat transfer coefficients observed for the liquid metals with small Prandtl number are considerably lower than Nusselt's theory.

H.Karabulut and E.Ataer [16] presented a numerical method for the analysis of laminar filmwise condensation of vapor flowing downwards on a horizontal tube, including the pressure gradient, inertia and convective terms to the governing equations of condensate flow. Errors due to omission of inertia and convective ternis were examined for steam and found to be insignificant except at high oncoming velocity and ΔT. The pressure drop term was also found to be insignificant upstream of the tube, but to be important in determining the location of the flow separation. The results indicated that, before the vapor boundary layer, the condensate flow becomes unstable and affects the location of the separation point, and beyond the separation point, the condensate thickness displays some instabilities due to the pressure variation, which becomes zero after the separation point.

CHAPTER 3

3 ANALYTICAL MODEL

The condensation of steam over a vertical tier of spheres is studied by both analytical and experimental methods. In analytical study firstly the principles of conservation of mass and conservation of momentum on the condensate layer were used and two equations were obtained from them. Then they are transformed into the finite difference forms. The Newton-Raphson method was used to calculate this problem on the computer. The film thickness and the velocity distribution of the condensate for each spheres were calculated by this program.

3.1 Assumptions

Only the condensate layer is to be taken into account. So the vapour boundary layer analysis is not involved in this study. To model this problem some assumptions were made to simplify the solution:

- Laminar flow and constant properties are valid for condensate film.
- The vapor is pure and at saturation temperature, T_{sat} .
- Inertia forces are insignificant, thus velocity parallel to the surface depends on only y direction, i.e., $u = u(y)$.
- The condensation taking place between the spheres is neglected.

- The shear stress at the liquid vapor interface is neglected.
- Spheres are isothermal
- Only gravity forces are acting on the condensate.
- Temperature dependence of the properties is neglected.
- Heat convection is ignored; therefore, heat is transferred across the condensate only by conduction resulting in a linear temperature profile.
- Steady-state condition is available. Therefore, heat transferred from vapor to the condensate by condensation is equal to heat transferred across the condensate by conduction.
- Geometrical dimensions of all spheres are identical and are made from the same material.

3.2 Physical Model

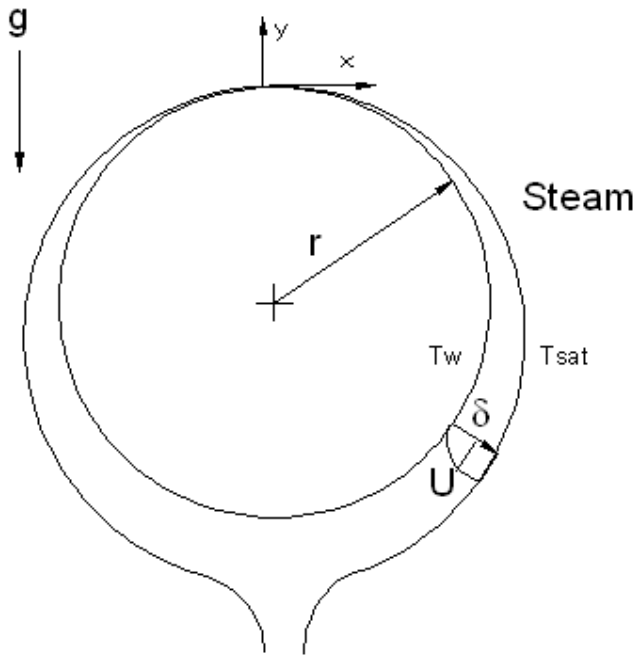

Figure 3.1 Physical Model and Coordinate System

3.3 Formulation of the Problem

The analytical problem was formulated by using the above assumptions. First a third order polynomial was assumed and derived according to the boundary conditions. Then conservation of mass and conservation of momentum equations were derived.

3.3.1 Velocity Profile

By using the following boundary conditions and third order polynomial equation 3.1 can be obtained to define the velocity profile in the condensate layer. It is expressed in terms of free stream velocity, condensate film thickness and the distance from the wall [17]:

$$At \quad y = 0, \quad x \geq 0: \qquad u = 0, \qquad \frac{\partial^2 u}{\partial y^2} = 0$$

$$At \quad y = \delta, \quad x \geq 0: \qquad u = U_\infty, \qquad \frac{\partial u}{\partial y} = 0$$

$$u = U_\infty \left[\frac{3}{2}\left(\frac{y}{\delta}\right) - \frac{1}{2}\left(\frac{y}{\delta}\right)^3 \right] \tag{3.1}$$

Two equations are needed to solve this problem. First can be obtained from conservation of mass and second from conservation of momentum principles.

3.3.2 Conservation of Mass

The conservation of mass principle is applied on the control volume shown in the following figure.

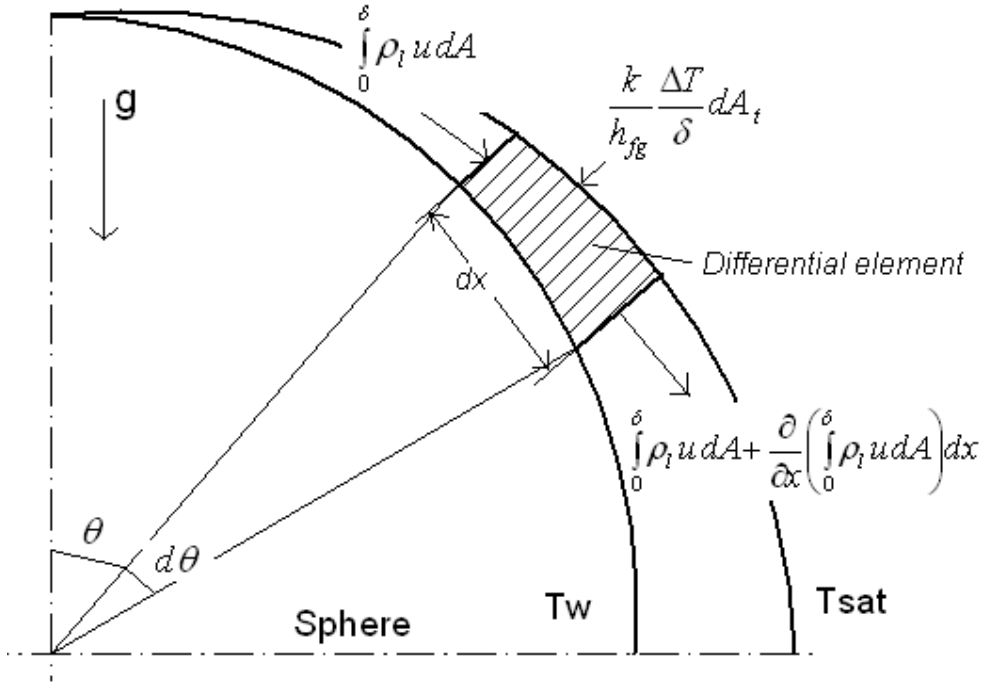

Figure 3.2 Differential Element and Energy Balance on the Liquid Film

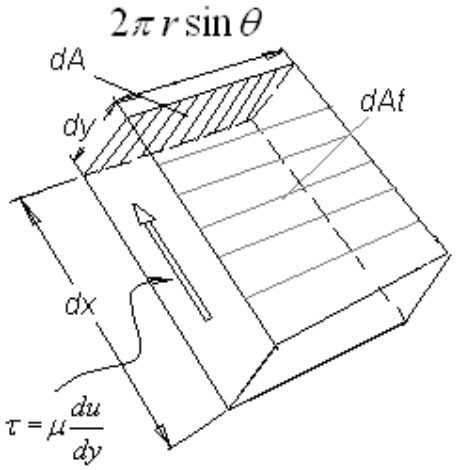

Figure 3.3 Flow Area and Heat Transfer Area on Differential Element.

$$\int_0^{\delta} \rho_l \, u \, dA + \frac{k}{h_{fg}} \frac{\Delta T}{\delta} dA_t = \int_0^{\delta} \rho_l \, u \, dA + \frac{\partial}{\partial x}\left(\int_0^{\delta} \rho_l \, u \, dA \right) dx \tag{3.2}$$

$$\frac{d}{dx}\left(\int_0^{\delta} \rho_l u \, 2\pi r \sin\theta \, dy \right) = \frac{k}{h_{fg}} \frac{\Delta T}{\delta} 2\pi r \sin\theta \tag{3.3}$$

Where;

$dA = 2\pi r \sin\theta \, dy$

$dA_t = 2\pi r \sin\theta \, dx$

Substituting Equation 3.1 into Equation 3.3:

$$\frac{d}{dx}\left(\int_0^{\delta} U_{\infty} \left[\frac{3}{2}\left(\frac{y}{\delta}\right) - \frac{1}{2}\left(\frac{y}{\delta}\right)^3 \right] \sin\theta \, dy \right) = \frac{k}{\rho_f h_{fg}} \frac{\Delta T}{\delta} \sin\theta \tag{3.4}$$

Put

$$\theta = \frac{x}{r}$$

$$\frac{d}{dx}\left(\int_0^{\delta} U_{\infty} \left[\frac{3}{2}\left(\frac{y}{\delta}\right) - \frac{1}{2}\left(\frac{y}{\delta}\right)^3 \right] \sin\left(\frac{x}{r}\right) dy \right) = \frac{k}{\rho_f h_{fg}} \frac{\Delta T}{\delta} \sin\frac{x}{r} \tag{3.5}$$

Solving the integral for y;

$$\frac{5}{4} \frac{d}{dx}\left(\sin\frac{x}{r} \delta U_{\infty} \right) - \frac{k}{\rho_f \, h_{fg}} \frac{\Delta T}{\delta} \sin\frac{x}{r} = 0 \tag{3.6}$$

$$\frac{5}{4} \frac{1}{r} \cos\frac{x}{r} \delta U_{\infty} + \frac{5}{4} \frac{d}{dx}(\delta U_{\infty}) - \frac{k}{\rho_f h_{fg}} \frac{\Delta T}{\delta} \sin\frac{x}{r} = 0 \tag{3.7}$$

3.3.3 Conservation of Momentum

The second equation can be obtained from the conservation of momentum principle. After applying this principle;

$$\frac{d}{dx}\left(\int_0^{\delta} \rho_f u^2 2\pi r \sin\frac{x}{r} dy\right) - \rho_f \delta f_x + \tau_s\big|_{y=0} = 0 \tag{3.8}$$

f_x is body force related with gravity. For the condensate around a sphere;

$$f_x = 2\pi r^2 \sin^2\theta\, g \tag{3.9}$$

The shear stress in Equation 3.8 can be expressed with Newton's law of viscosity:

$$\tau_s = \mu \left.\frac{du}{dy}\right|_{y=0} \tag{3.10}$$

Substituting u from Equation 3.1 and taking the derivative, one can obtain:

$$\tau_s = \frac{3}{2}\mu\frac{U_\infty}{\delta} \tag{3.11}$$

Recalling Equation 3.1 and integrating Equation 3.8 for y;

$$\frac{34}{35}\pi r\rho_f \frac{d}{dx}\left(\sin\frac{x}{r}\delta U_\infty{}^2\right) - \rho_f 2\pi r^2 (\sin\frac{x}{r})^2\, \delta\, g + \frac{3}{2}\mu\frac{U_\infty}{\delta} = 0 \tag{3.12}$$

$$\frac{34}{35}\pi\rho_f \cos\frac{x}{r} + \frac{34}{35}\pi r\rho_f \frac{d}{dx}\left(\delta U_\infty{}^2\right) - \rho_f 2\pi r^2 (\sin\frac{x}{r})^2\, \delta\, g + \\ + \frac{3}{2}\mu\frac{U_\infty}{\delta} = 0 \tag{3.13}$$

3.3.4 Heat Transfer Equation

Since only conduction type heat transfer mechanism is assumed at the beginning of the analysis, heat transfer at the wall in the area dA is;

$$q = k\frac{(T_{sat} - T_w)}{\delta} \tag{3.14}$$

3.4 Calculation of the Initial Values

We should make some assumptions to begin the calculation from the upper stagnation point. At the stagnation point the flow velocity is small, so we can assume that the inertia terms and the pressure gradient in the momentum equation can be neglected. The momentum equation in the condensate layer is that:

$$\frac{\partial(\rho_f uu)}{\partial x} + \frac{\partial(\rho_f vu)}{\partial \mathrm{y}} = -\frac{\partial \mathrm{P}}{\partial \mathrm{x}} + \frac{\partial}{\partial \mathrm{y}}\left[\mu_{\mathrm{f}}(\frac{\partial u}{\partial y})\right] + \rho_f g\sin\theta \tag{3.15}$$

After eliminating the inertia terms and pressure gradient the momentum equation comes this form:

$$\mu_f \frac{\partial^2 u}{\partial y^2} = -g\rho_f \sin\theta \tag{3.16}$$

After taking the derivative of u twice we can obtain the following equation;

$$u = -\frac{\mathrm{g}\rho_{\mathrm{f}}\sin\theta}{2\mu_f}\mathrm{y}^2 + \mathrm{c}_1\mathrm{y} + \mathrm{c}_2 \tag{3.17}$$

The boundary conditions are like that:

$$y = 0 \rightarrow u = 0$$
$$y = \delta \rightarrow \frac{du}{dy} = 0$$

After applying the boundary conditions Equation 3.17 can be written as :

$$u = \frac{g\rho_f \delta^2 \sin\theta}{\mu_f}\left[\frac{y}{\delta} - \frac{1}{2}\left(\frac{y}{\delta}\right)^2\right] \tag{3.18}$$

Initial velocity distribution along the liquid-vapor interface can be obtained substituting δ into Equation 3.18.

$$u = \frac{g\rho_f \delta^2 \sin\theta}{2\mu_f} \tag{3.19}$$

From an energy balance in the condensate layer [16];

$$\int_0^{\delta} h_{fg}\rho_f u 2\pi r\, dy = \int_0^{x} k_f \left(\frac{\partial T}{\partial y}\right)_{y=0} 2\pi r\, dx \tag{3.20}$$

The left hand side of this equation is the latent heat of condensation. The right hand side is the heat transferred from the condensate to the wall over a length from x=0 to x=x. Equation 3.20 can be rewritten as;

$$\int_0^{\delta} \frac{\partial}{\partial \mathrm{x}}(ru)dy = \frac{k_f}{h_{fg}\rho_f} r\left(\frac{\partial T}{\partial y}\right)_{y=0} \tag{3.21}$$

After substituting the velocity equation in the energy balance, one can obtain the following equation which gives the condensate layer thickness.

$$\delta = \left[\frac{3\upsilon_f r k_f (T_{sat} - T_w)}{h_{fg} \rho_f g} \right]^{1/4} \tag{3.22}$$

3.5 Finite Difference Equations

Equation 3.7 and Equation 3.13 must be transformed into the finite differences to solve them numerically. After transforming Equation 3.7 yields;

$$\frac{5}{4r}\cos\frac{x}{r}\delta_i U_{\infty i} + \frac{5}{4}\frac{(\delta_i U_{\infty i} - \delta_{i-1} U_{\infty i-1})}{\Delta x} - \frac{k}{\rho_f h_{fg}}\frac{\Delta T}{\delta_i}\sin\frac{x}{r} = 0 \tag{3.23}$$

and Equation 3.13 yields:

$$\frac{34}{35}\pi\rho_f \cos\frac{x}{r}\delta_i U_{\infty i}{}^2 + \frac{34}{35}\pi r\rho_f \left(\frac{\delta_i (U_{\infty i})^2 - \delta_{i-1}(U_{\infty i-1})^2}{\Delta x} \right) -$$
$$-2\pi r^2 (\sin\frac{x}{r})^2 \delta_i \rho_f g + \frac{3}{2}\mu\frac{U_{\infty i}}{\delta_i} = 0 \tag{3.24}$$

Taylor Series expension method can be used to solve these equations.

$$f(x_{i+1}) = f(x_i) + (x_{i+1} - x_i) f'(x_i) + \ldots \tag{3.25}$$

As matrix C corresponds to $f(x_i)$, matrix Ψ corresponds to derivative of the function at x_i. x_i represents δ_i and $U_{\infty i}$ variables. These are increased with δ_{inc} and U_{inc} increments, subtracted from their original states and divided by

corresponding increment. Ψ matrix is two by two square matrix and it is constituted as:

$$\psi_{(0,0)} = \frac{\left[\begin{array}{l}\frac{5}{4r}\cos\frac{x}{r}(\delta_i+\delta_{inc})U_{\infty i}+\frac{5}{4}\frac{(\delta_i+\delta_{inc})U_{\infty i}-\delta_{i-1}U_{\infty i-1}}{\Delta x}- \\ \frac{k_f\Delta T}{\rho_f h_{fg}(\delta_i+\delta_{inc})}\sin\frac{x}{r}\end{array}\right]\cdots - \left[\frac{5}{4r}\cos\frac{x}{r}\delta_i U_{\infty i}+\frac{5}{4}\frac{\delta_i U_{\infty i}-\delta_{i-1}U_{\infty i-1}}{\Delta x}-\frac{k_f\Delta T}{\rho_f h_{fg}\delta_i}\sin\frac{x}{r}\right]}{\delta_{inc}} \tag{3.26}$$

$$\psi_{(0,1)} = \frac{\left[\frac{5}{4r}\cos\frac{x}{r}\delta_i(U_{\infty i}+U_{inc})+\frac{5}{4}\frac{\delta_i(U_{\infty i}+U_{inc})-\delta_{i-1}U_{\infty i-1}}{\Delta x}\right] - \left[\frac{5}{4r}\cos\frac{x}{r}\delta_i U_{\infty i}+\frac{5}{4}\frac{\delta_i U_{\infty i}-\delta_{i-1}U_{\infty i-1}}{\Delta x}\right]}{U_{inc}} \tag{3.27}$$

$$\psi_{(1,0)} = \frac{\left[\begin{array}{l}\frac{34}{35}\pi\rho_f\cos\frac{x}{r}(\delta_i+\delta_{inc})(U_{\infty i})^2+ \\ \frac{34}{35}\pi r\rho_f\frac{(\delta_i+\delta_{inc})(U_{\infty i})^2-\delta_{i-1}(U_{\infty i-1})^2}{\Delta x}- \\ -2\pi r^2(\delta_i+\delta_{inc})\rho_f g(\sin\frac{x}{r})^2+\frac{3}{2}\mu\frac{U_{\infty i}}{(\delta_i+\delta_{inc})}\end{array}\right]\cdots - \left[\begin{array}{l}\frac{34}{35}\pi\rho_f\cos\frac{x}{r}\delta_i(U_{\infty i})^2+\frac{34}{35}\pi r\rho_f\frac{\delta_i(U_{\infty i})^2-\delta_{i-1}(U_{\infty i-1})^2}{\Delta x} \\ -2\pi r^2\delta_i\rho_f g(\sin\frac{x}{r})^2+\frac{3}{2}\mu\frac{U_{\infty i}}{\delta_i}\end{array}\right]}{\delta_{inc}} \tag{3.28}$$

$$\psi_{(1,1)} = \begin{bmatrix} \frac{34}{35}\pi\rho_f \cos\frac{x}{r}\delta_i (U_{\infty i} + U_{inc})^2 + \\ \frac{34}{35}\pi r\rho_f \frac{\delta_i (U_{\infty i} + U_{inc})^2 - \delta_{i-1}(U_{\infty i-1})^2}{\Delta x} \\ -2\pi r^2 \delta_i \rho_f g(\sin\frac{x}{r})^2 + \frac{3}{2}\mu\frac{U_{\infty i} + U_{inc}}{\delta_i} \end{bmatrix} \cdots$$

$$- \frac{\begin{bmatrix} \frac{34}{35}\pi\rho_f \cos\frac{x}{r}\delta_i (U_{\infty i})^2 + \frac{34}{35}\pi r\rho_f \frac{\delta_i (U_{\infty i})^2 - \delta_{i-1}(U_{\infty i-1})^2}{\Delta x} \\ -2\pi r^2 \delta_i \rho_f g(\sin\frac{x}{r})^2 + \frac{3}{2}\mu\frac{U_{\infty i}}{\delta_i} \end{bmatrix}}{U_{inc}} \qquad (3.29)$$

To approach to the exact values of velocity and film thickness variables C_0, C_1, $\psi_{(0,0)}$, $\psi_{(0,1)}$, $\psi_{(1,0)}$, $\psi_{(1,1)}$ equations have been iterated 20 times. After finishing the first iteration, by multiplying the inverse of matrix ψ with matrix C, a vector called as *del* is found. The velocity and film thickness variables are updated by adding this vector to the previous iteration. After 20 iterations the first exact values of velocity (U_1) and film thickness (δ_1) variables are found. This cycle is applied to calculate the 18 values of velocity and film thickness variables.

$$del = \begin{bmatrix} \psi_{0,0} & \psi_{0,1} \\ \psi_{1,0} & \psi_{1,1} \end{bmatrix}^{-1} \begin{bmatrix} C_0 \\ C_1 \end{bmatrix} = \begin{bmatrix} \delta \\ U \end{bmatrix} \qquad (3.30)$$

3.6 Calculation for the Lower Spheres

The condensing falling from the upper sphere creates a film thickness at the upper stagnation point of the lower sphere. So this film thickness is called as Δ and it goes to zero as seen in Figure 3.2. The velocity profile is uniform in

this layer. Also as a result of this falling condensing a velocity value occurs at the upper stagnation point. After completing the iterations for the first sphere, the effect of film thickness and velocity values falling from the upper sphere are taken and updated for the lower sphere by using Bernoulli equation.

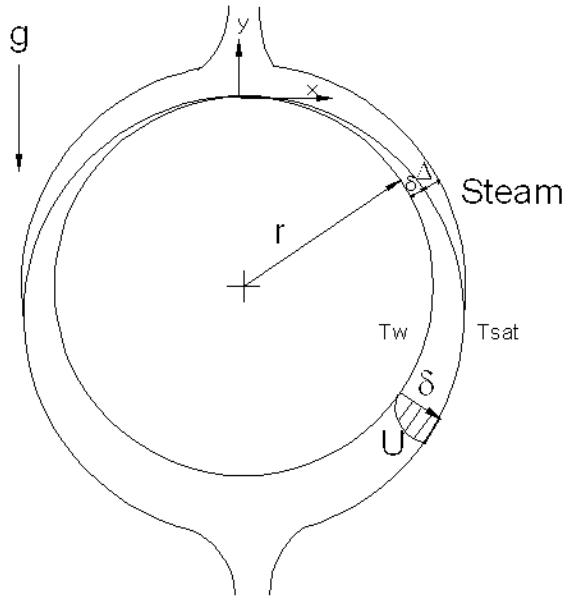

Figure 3.4 Physical Model for the Lower Spheres

The initial velocity and condensate thickness are calculated from Equations 3.16 and 3.22. After this calculation Equations 3.23, 3.24, 3.25 are used to calculate velocity and condensate thickness for upper sphere as said above.

After finishing the calculations of upper sphere , δ_{inc} and U_{inc} values are calculated from Equations 3.16 and 3.22. Then the last values of δ and U which are δ_{18} and U_{18} for upper sphere are taken. The condensate thickness and velocity values are calculated from the following equations for middle sphere.

$$U_{\infty 0} = \sqrt{(U_{\infty 18})^2 + 2\,g\,h} \tag{3.31}$$

$$\Delta_0 = \frac{U_{\infty 18}\,\delta_{18}}{U_{\infty 0}} \tag{3.32}$$

After calculating the initial values for middle sphere, the Δ thickness is calculated from the following equation;

$$\Delta_i = \frac{U_{\infty i-1}\,\delta_{i-1}}{U_{\infty i}} \tag{3.33}$$

Then the Δ thickness is added to the conservation of mass and momentum equations. After arranging Equation 3.23 the following equation is obtained;

$$\frac{5}{8r}\cos\frac{x}{r}\delta_i U_{\infty i} + \frac{5}{8}\frac{\left(\delta_i U_{\infty i} - \delta_{i-1}U_{\infty i-1}\right)}{\Delta x} - \frac{k}{\rho_f h_{fg}}\frac{\Delta T}{\delta_i}\sin\frac{x}{r} + \frac{\Delta_i U_i - \Delta_{i-1}U_{i-1}}{\Delta x} = 0 \tag{3.34}$$

And after arranging Equation 3.24 the following equation is obtained;

$$\frac{34}{35}\pi\rho_f\cos\frac{x}{r}\delta_i U_{\infty i}^{\,2} + \frac{34}{35}\pi r\rho_f\left(\frac{\delta_i\left(U_{\infty i}\right)^2 - \delta_{i-1}\left(U_{\infty i-1}\right)^2}{\Delta x}\right) - 2\pi r^2(\sin\frac{x}{r})^2\delta_i\rho_f g + \frac{3}{2}\mu\frac{U_{\infty i}}{\delta_i} + \rho_f\frac{\Delta_i(U_i)^2 - \Delta_{i-1}(U_{i-1})^2}{\Delta x} = 0 \tag{3.35}$$

After Δ goes to zero, Equation 3.23 and Equation 3.24 are used to calculate velocity and condensate film thickness for the remaining portion of the x axis.

Calculations for the bottom sphere are the same as the middle sphere calculations.

CHAPTER 4

4 EXPERIMENTAL STUDIES

The experimental studies were completly made in ERDEMİR in Machine Workshop. To do this firstly all parts from screw to the main frame were designed as 3-D model and then technical drawings were formed. These drawings were manufactured and assembled in Machine Workshop.

Here three experiments were done. The aim of the first is to measure the heat transfer rates and heat transfer coefficients for Ø50mm and Ø60mm o.d. spheres. The aim of the second is to compare the free and forced condensation results for Ø60mm o.d. sphere and to calculate the local heat transfer coefficient additionally. The aim of the third study is to obtain datas for annular condensation in concentric spheres for free and forced condensations. There are some differences between free condensation experimental setup and free&forced condensation experimental setup. The reason behind the differences between the free and free&forced condensation experimental setups is the experience gained in the free condensation experiments. After gaining some experience in the free condensation experiments, improvements were made in the free&forced condensation experimental setup.

The difference between free and free&forced condensation experimental setups are the elevation of the cooling water tank, the location of valves, the source of the water vapour, the location and the numbers of thermocouples.

4.1 Case-1 Free Condensation Experimental Study

- The tests were conducted at 0^o,12^o,20^o,30^o inclination angles and at 20^oC-30^oC-40^oC-50^oC-60^oC cooling water inlet temperatures.
- The tests were conducted at Ø50 and Ø60mm o.d.spheres.
- The spheres employed had Ø50mm o.d. Ø44mm i.d.and Ø60mm o.d. Ø54mm i.d. Inner spheres which had 30mm o.d. were placed in Ø60mm o.d. spheres and Ø24mm o.d. were placed in Ø50mm o.d. spheres. The connection of steel water pipe and sphere was achieved by tight fit.
- The elevation of the cooling water tank from test section was 2 meters.
- Valves were used to prevent the flow of the cooling water so that the cooling water tank can be filled at the exit of the cooling water distributing apparatus and three adjustment pieces which were equipped with adjustment screws were used at the end of the cooling water exit pipes to adjust the coolant mass flow rate.
- The water vapour was supplied from the steam line of the workshop.
- 11 thermocouples were used. Each sphere was equipped with 2 thermocouples.

4.2 Case-2 Free and Forced Condensation Experimental Study

- The tests were conducted at 0^o,5^o,10^o,15^o,20^o inclination angles and at 20^oC-30^oC-40^oC-50^oC-60^oC cooling water inlet temperatures.
- The tests were conducted for free and forced (only 0^o inclination angle) condensations.
- The spheres employed had 60mm o.d. and 40mm i.d. No internal spheres were used. The connection between steel water pipe and sphere was achieved by threads.
- The elevation of the cooling water tank from test section was taken as 3m.

- Six valves were used. Three of them were placed at the exit of cooling water distributing apparatus and the other three were placed at the end of the cooling water exit pipes.
- A boiler tank was used to supply water vapour to the test section for free condensation. The steamline of workshop was used for forced condensation.
- 20 thermocouples were used for free condensation. On each sphere surface 3 thermocouple and inside of each sphere 2 thermocouples were placed. 13 thermocouples were used for forced condensation.

4.3 Case-3 Annular Condensation in Concentric Spheres

- The tests were conducted at 0^o inclination angle and at 20^oC-30^oC-40^oC-50^oC cooling water inlet temperatures.
- The tests were conducted for free and forced condensations.
- A cylindrical shaped polyamid piece whose inner surface is sphere was used to make the vapour flow area smaller so that the vapour flows faster.
- The free and forced condensation experimental setup was used.
- The streamline of workshop was used for forced condensation.

4.4 Experimental Setup

The main parts of the experimental setup are the following :

- Test section
- Cooling Water Tank
- Boiler Tank
- Temperature Reading System
- Main Frame

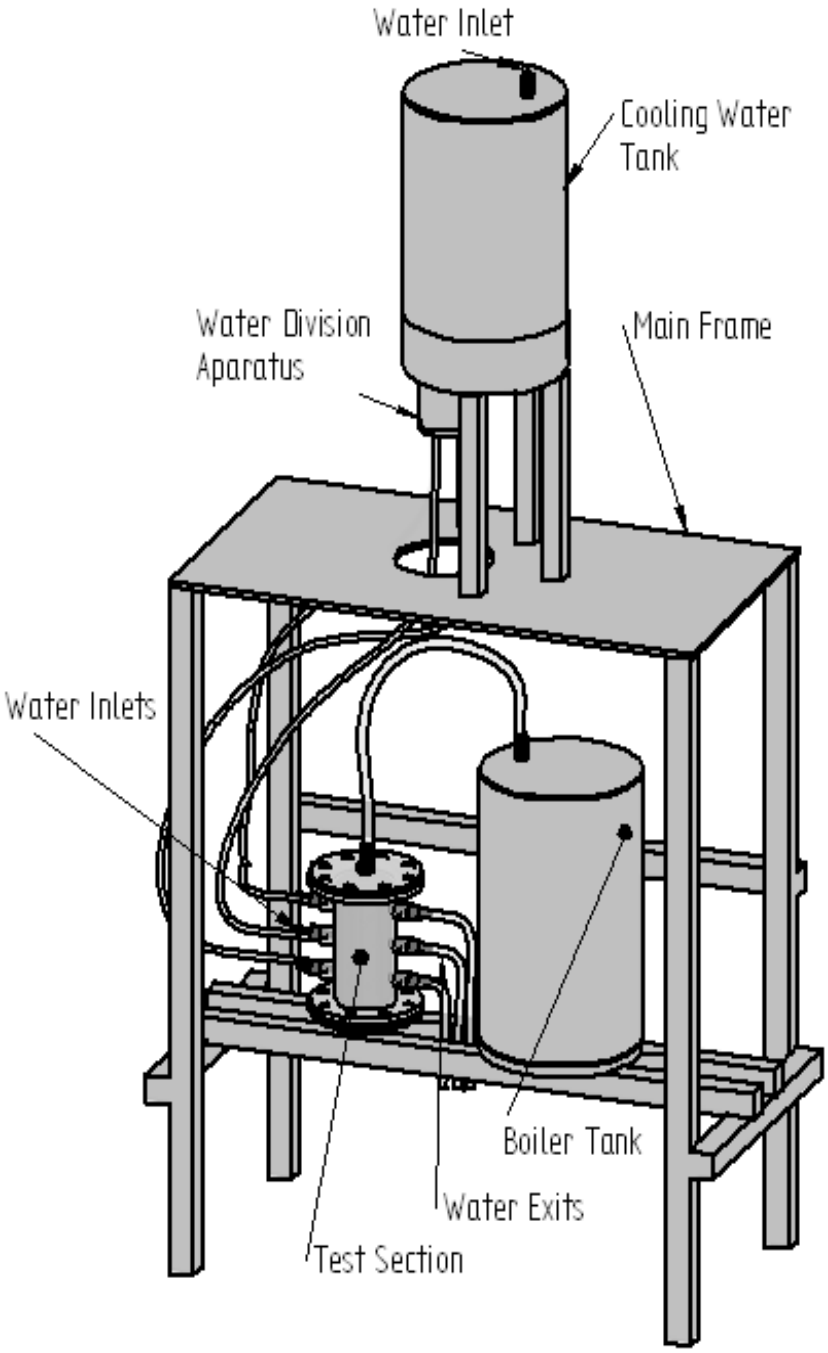

Figure 4.1 General View of the Experimental Setup

Figure 4.2 General View of the Free Condensation Experimental Setup

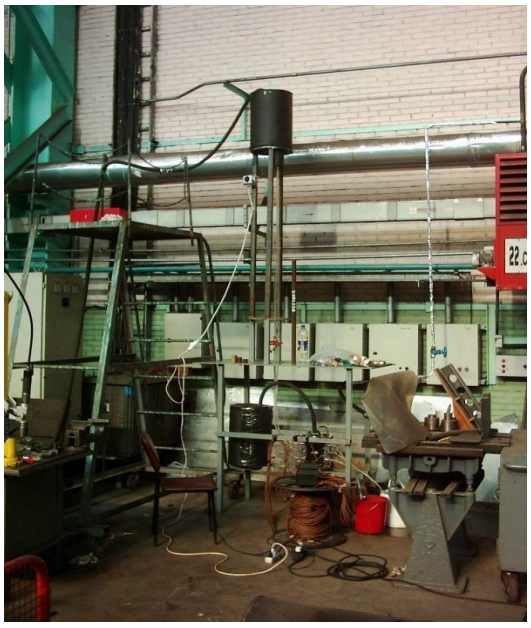

Figure 4.3 General View of the Free and Forced Condensation Experimental Setup

4.5 Cooling Water Tank

The cooling water tank was designed and manufactured in Machine Workshop in Erdemir. The aim of the cooling water tank is to supply cooling water at the desired temperature to the test section. The material from which the cooling water tank is produced is 316 stainless steel cold extruded pipe. The grade standard of the pipe material is ASTM A 312 Gr.TP 316 and the manufacturing standard of this pipe is ASTM A530.The outer diameter is Ø323.8mm and the inner diameter is Ø303.2mm. The volume of this tank is 36.1 dm^3 and the weight is 39.8 kg. The outer surface of this tank was covered by isolation material which is called as K-Flex isolation material.

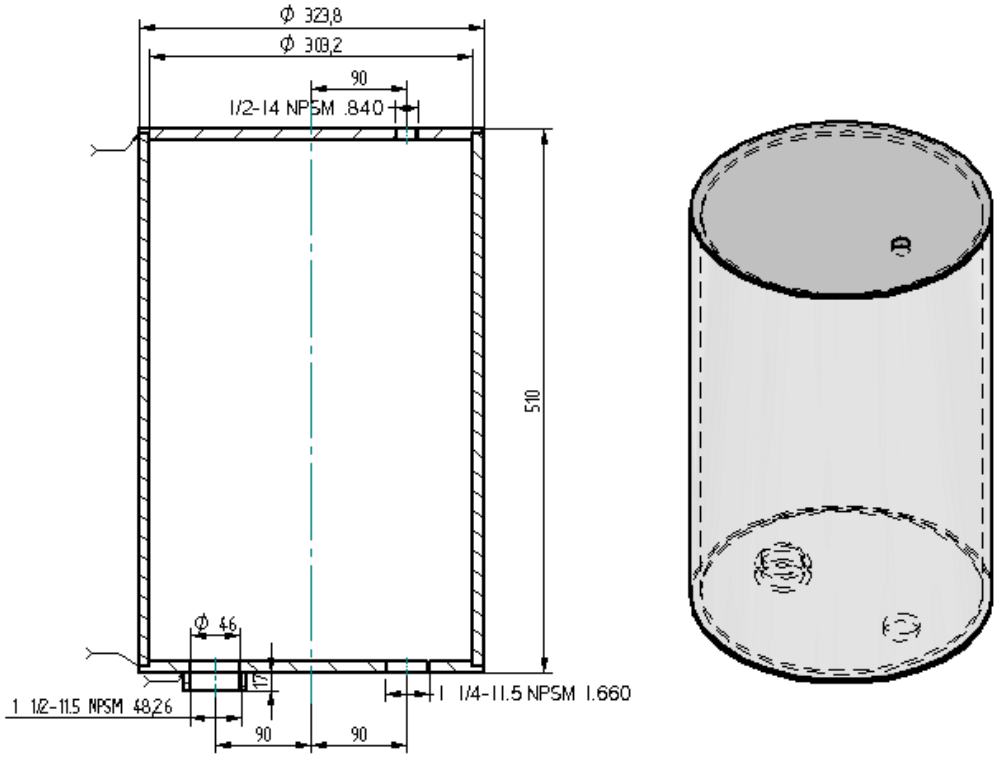

Figure 4.4 Technical Drawing of the Cooling Water Tank

First the pipe material was cut to 500 mm length at the sawing machine. Then the upper and bottom flanges of the tank were cut by plasma machine.

After flanges were welded to the top and bottom of the tank the holes were drilled at the radial drilling machine. The holes are used for assembling of cooling water distributing apparatus at the bottom .

At the free condensation experimental setup the water tank was placed 2m high from the test section. The aim here is to obtain water pressure fixed by gravity so that the mass flow rate to be the same during the experiments. The cooling water tank was used only to store water inside it. And no heater was placed inside it. Water at the desired temperature was obtained from another tank with a heater on it, which was placed above the cooling water tank. The cooling water which was caped in 20 dm^3 barrels was charged to the heater tank. The temperature of the cooling water was adjusted by means of the adjustment button of thermostat. When the temperature of cooling water reached to the desired value the valve at the exit of the cooling water heating tank was opened to allow water flow to the cooling water tank. After cooling water tank was full valves at the exit of the water distributing apparatus were opened to flow water to the test section.

At the second experimental setup the heigth of the cooling water tank was increased to 350cm from test section. Here a heater was placed inside the water tank and a thermometer was placed on the tank. Cooling water was heated up to desired value inside this tank and supplied to the test section.

4.6 Boiler Tank

Boiler Tank was manufactured from the same pipe used for cooling water tank. So the dimensions are all same as in the cooling water tank. Boiler tank has 36.1 dm^3 volume and 39.8 kg weight. The manufacturing sequence are same as the cooling water tank. All drilling operations was made by radial drilling machine.

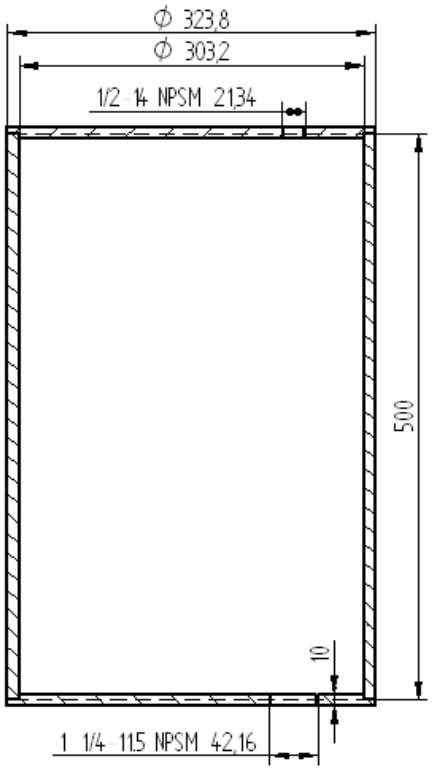

Figure 4.5 Technical Drawing of the Boiler Tank

At the free condensation experimental study the boiler tank was not used. Instead of that the vapour was obtained from the machine shop. At the free and forced condensation experimental study an electric heater was assembled at the bottom of the boiler tank with a heating capacity of 2000W.

4.7 Test Section

The test section was manufactured in Erdemir at machine shop. The material used is ASTM 316 stainless steel. The test section has three parts.

- Test section body
- Upper cap
- Lower cap

4.7.1 Test Section Body

Manufacturing of the apparatus was started with the manufacturing of the test section which has three parts. These are test tube, upper flange and lower flange. Test tube was made from 316 stainless steel material. This material was cut by sawing machine first. Then inside diameter was machined at the lathe by leaving 2mm allowance to machine after welding operation because after flanges are welded to the test tube thermal distorsions which affects the dimensions occur. This method is used to obtain desired geometrical tolerances between flanges and test tube, i.e. perpendicularity, parallelism, concentricity. The upper and lower flanges were manufactured from 316 stainless steel. At the lathe machine circular faces of flanges were machined and 8 holes were left to be drilled after welding process. After welding operation of the upper and lower flanges with test tube, the diameter of test tube and faces of flanges were finished by lathe machine to obtain desired dimensional and geometrical tolerances. Then the assemble holes over the flanges were drilled at the coordinate milling machine, which has a digital coordinate screen. After that the side holes over the test tube were drilled at the same machine by leaving some allowance to machine after welding operation of outer rings in which the stainless steel pipe of cooling water is placed. These outer rings were machined by a lathe machine by leaving some allowance in their inside diameters. After finishing of them they were welded on the side holes over the test tube. Then again the test section body was settled on the coordinate milling machine and the coarse holes of outer rings and of test tube were drilled together mutually to obtain perfect eccentricity between the opposite holes and parallelism between the upper and lower holes. After this operations the dimensional checks were made and it was seen that the eccentricity and parallelism tolerances were in the range of 0.01mm to 0.03mm. This eliminates the alignment problem of spheres.

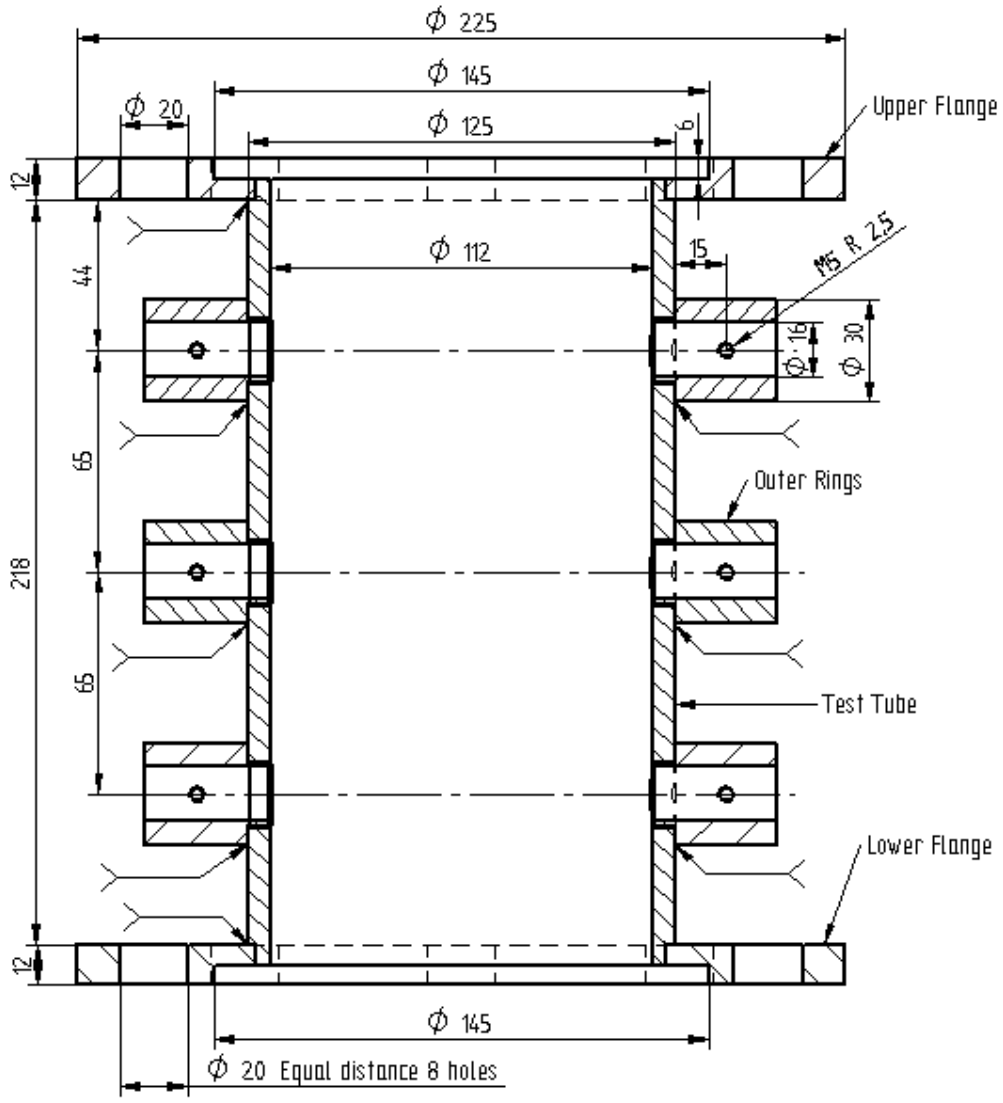

Figure 4.6 Technical Drawing of the Test Section

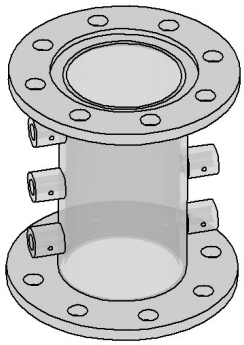

Figure 4.7 Technical Drawing of the Test Section as Isometric View

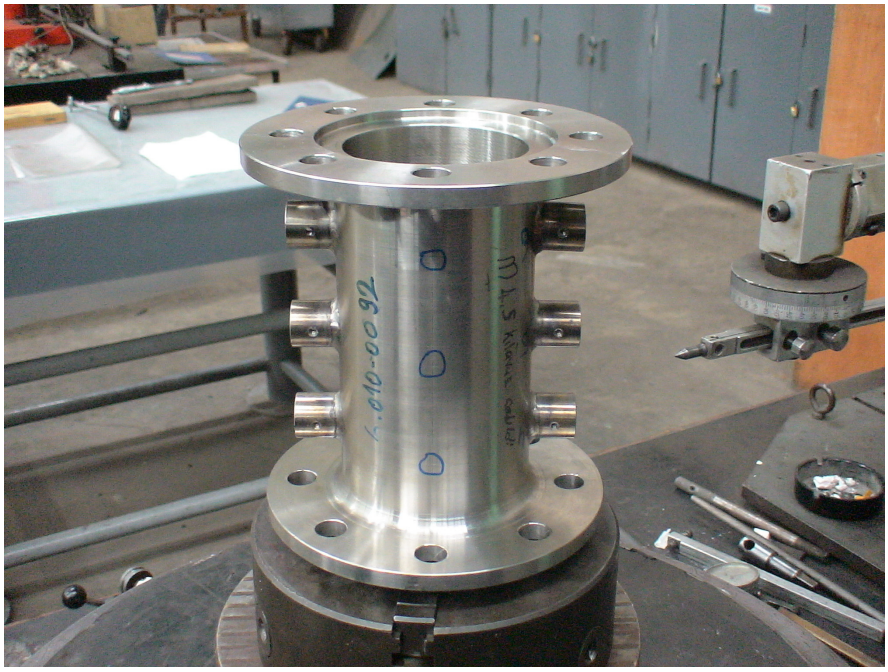

Figure 4.8 View of the Test Section After Manufacturing Processes

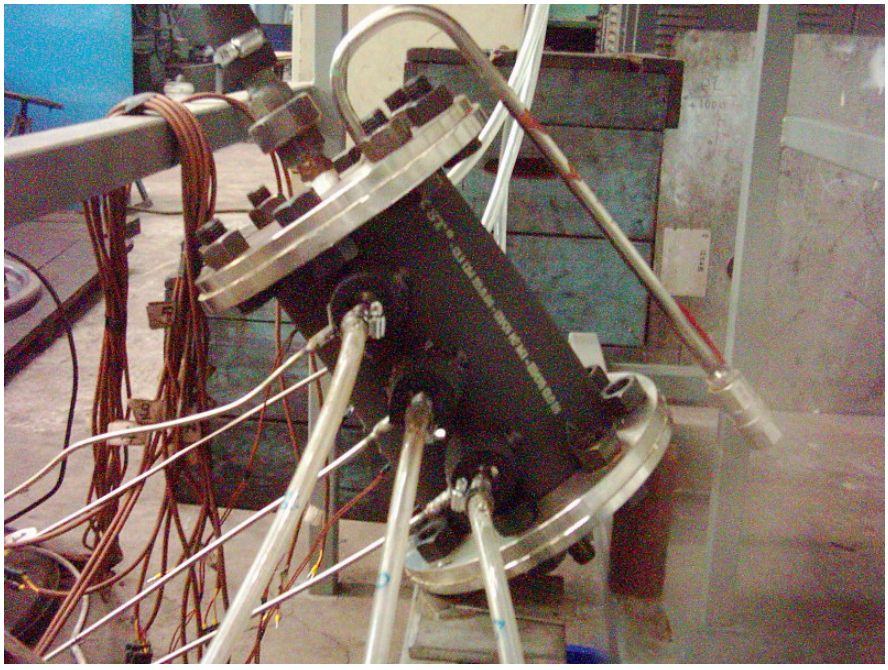

Figure 4.9 View of the Test Section During the Test.

4.7.2 Upper And Lower Caps

Finishing the test section body the upper and lower flanges were made. They also made from 316 stainless steel material. After machining them on the CNC lathe machine the mounting holes were drilled again on the coordinate milling machine. For collecting the condensates a hole drilled at the center of the lower flange. Also the inside surface of the lower flange was machined as a concave geometry of radius R900mm. A hole was drilled at the center of the upper flange in order to flow the water vapor to the test section.

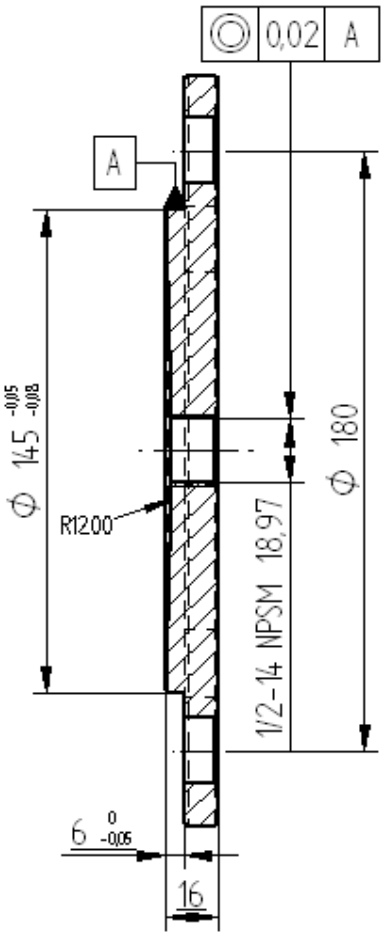

Figure 4.10 Technical Drawing of the Lower Cap

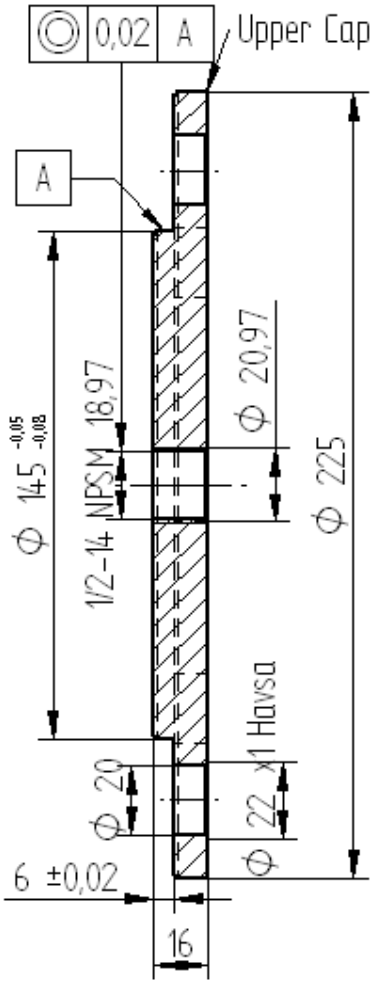

Figure 4.11 Technical Drawing of the Upper Cap

Figure 4.12 View of the Upper (left) and Lower (rigth) Caps.

4.8 Spheres

Spheres were also made in Machine Workshop in Erdemir. The material used is 316 Stainless Steel. Two different kind of spheres were used in experiments.

4.8.1 First type of sphere:

Spheres on which condensation is taking place used in the first experiment had Ø60mm and Ø50mm outer diameter. Because of the spherical shape and small wall thickness the machining of these spheres are quite difficult. These spheres were manufactured by machining two hemispheres and bonding them to each other. The bond material was Loctite Fixmaster Superior Material. Also Ø34mm diameter spheres made of teflon material the purpose of which is to accelerate and force the coolant to flow parallel to the inner surface of the spheres on which condensation is taking place were

used. Three stainless steel pins were machined to pass from the hole at the center of the Teflon spheres. Before bonding the hemispheres the Ø34mm diameter spheres were fixed at the center of the steel spheres by welding the pin to the inner surface of the sphere. Then the bonding material was applied to the contact surface of the spheres.

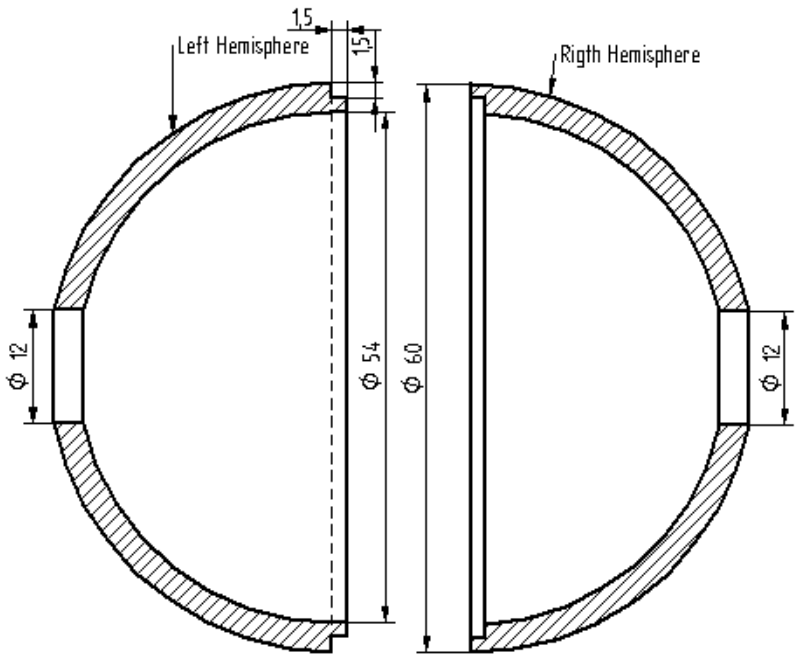

Figure 4.13 Technical Drawing of the Shpere used in the Free Condensation Experiments.

After that these hemispheres were connected and after 12 hours the bonding operation was completely finished. Then the surfaces of the spheres were polished by polishing machine about 4 hours per sphere.

Figure 4.14 First Type of Spheres After Bonding and Polishing

Figure 4.15 First Type of Hemispheres and Inner Sphere

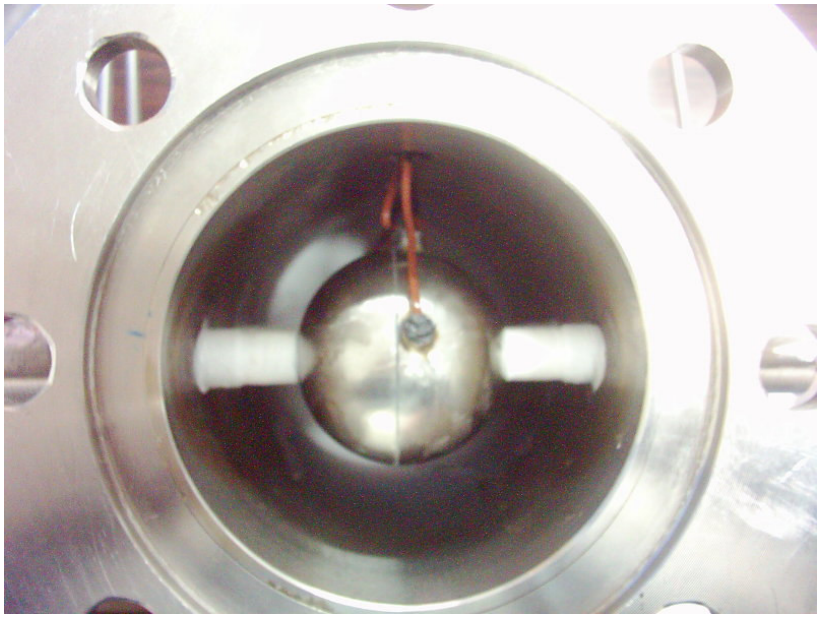

Figure 4.16 The Placements of the First Type of Spheres in the Test Section.

4.8.2 Sphere used in the Free&Forced Condensation Experiments

These spheres were used in the free and forced condensation and annular condensation in the concentric spheres experiments. These spheres also were made from 316 stainless steel material and had 60mm o.d. and 40mm i.d.So the thickness of these spheres is 10mm. There were no internal spheres on them. Similarly two hemispheres were machined to obtain one sphere. These hemispheres were joint by silver welding after placing the inner and outer thermocouples which were fastened on the outer and inner surface on which condensation is taking place by silver welding. On the contrary of the first type of sphere, instead of 10mm diameter hole a 3/8”-NPT screw was made. After silver welding process, the sphere surfaces were polished by polishing machine about 4 hours per sphere.

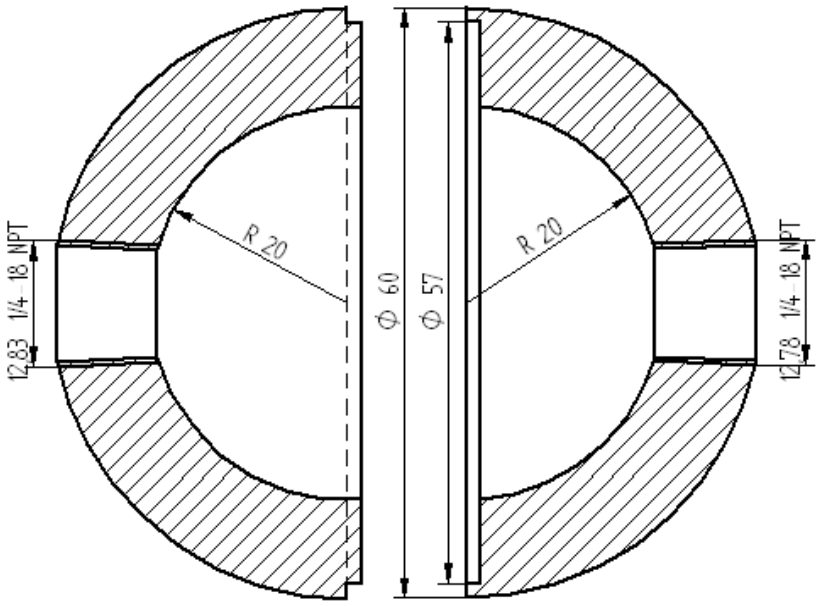

Figure 4.17 Technical Drawing of the Shpere used in the Free&Forced Condensation Experiments.

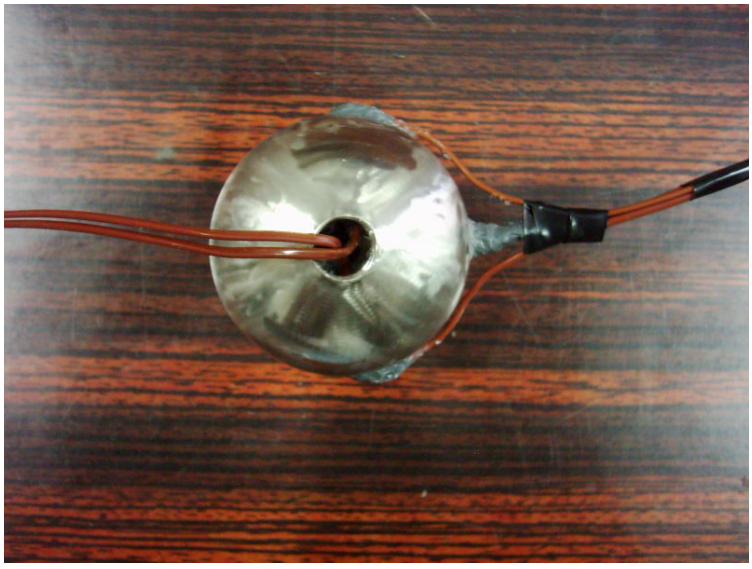

Figure 4.18 Shpere used in the Free&Forced Condensation Experiments After Silver Welding and Polishing

Figure 4.19 Second Type of Spheres with Thermocouples

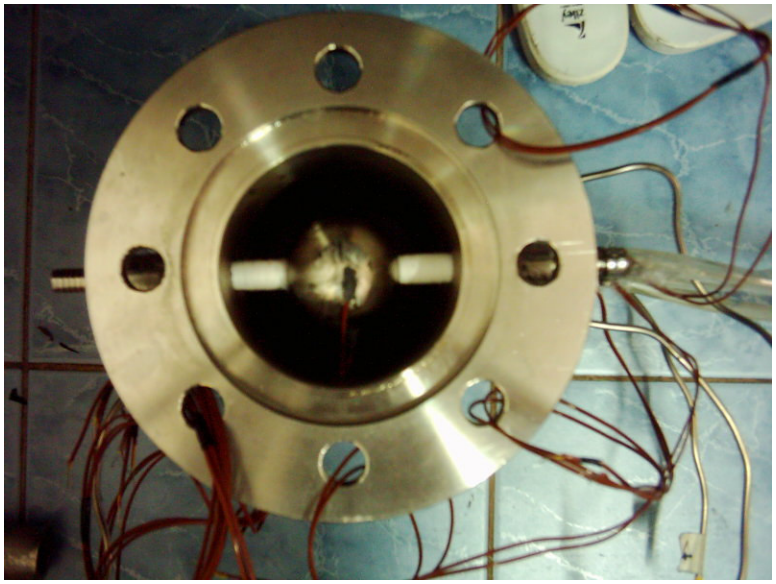

Figure 4.20 The Placement of Second Type of Spheres in the Test Section.

4.9 Vapour Accelerater for Free&Forced Condensation Experiments

In second experimental study to accelerate the vapour a cylinder was used to make the flow area, through which vapour flows, smaller. To achieve this the cylinder was placed between the spheres and the test section.

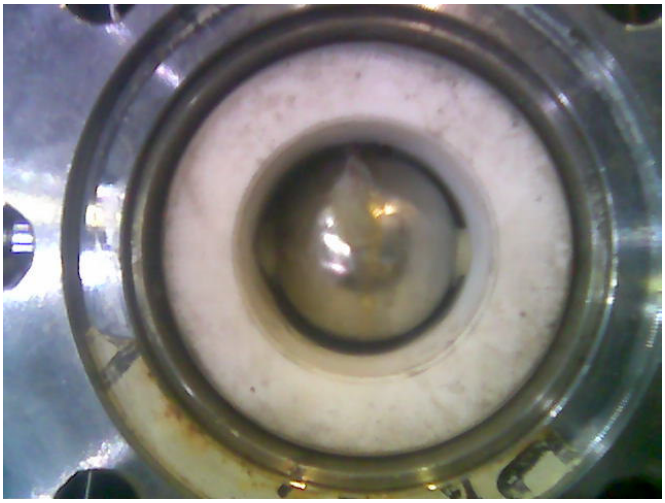

Figure 4.21 The Placement of Vapour Accelerater for Free&Forced Condensation Experiments.

4.10 Vapour Accelerater for Annular Condensation in Concentric Spheres

At the third experimental study a polyamid cylinder was used to accelerate the water vapour flowing around the sphere. The inside of this cylinder is sphere and its diameter is Ø85mm. Polyamid was choosen because being a plastic material it is easier to machine and since it has a low thermal conductivity not much condensation occurs on it.

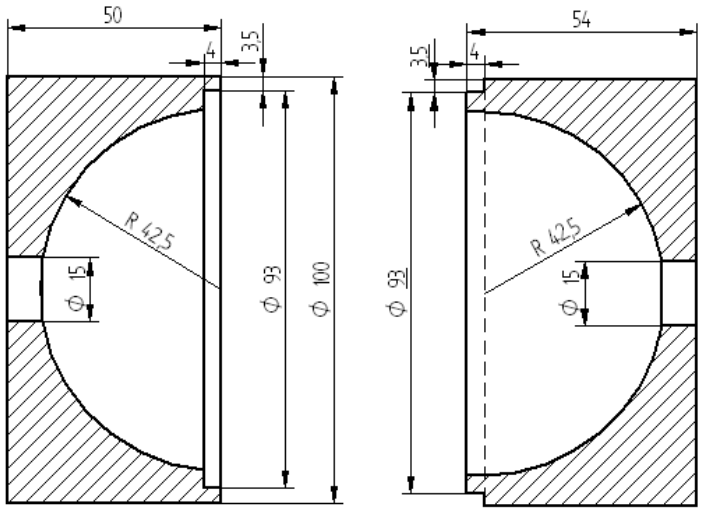

Figure 4.22 Drawing of the Vapour Accelerater for Case-3.

4.11 Stainless Steel Pipe Connectors for thr Spheres

These pipes were made from 316 stainless steel material to eliminate corrosion. They were machined at the lathe. The center was drilled from one end to other with 10mm drill. Thight fit and threaded types of pipes were manufactured.

4.11.1 Tight Fit Type of Pipe

It was used at the free condensation experiment. It has 8mm i.d. and 12mm o.d. at the tips so that it attaches to the sphere with a tight fit. There was no external screw on this pipe. The hole diameter of the test section was machined in 0.10mm tolerance to enter this pipe to the test section tigthly and centered the sphere perfectly. The connection area of sphere and pipe was insulated with Loctite silicon material to prevent water leakage from inside of sphere to the outer surface. Also the surface which was left in the test section was insulated by teflon material to eliminate the condensation on this surface.

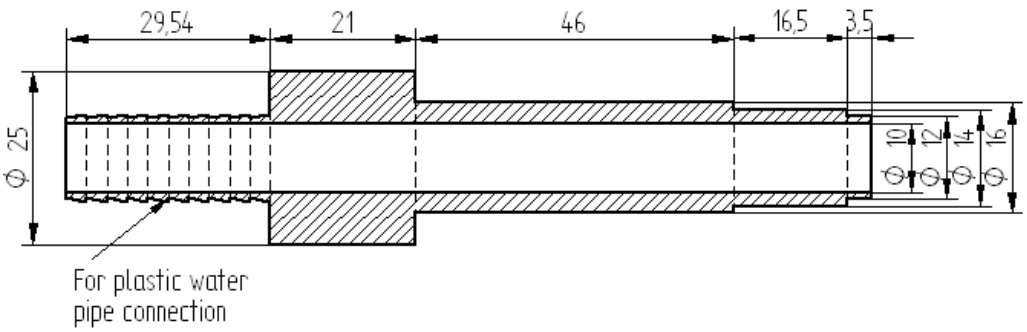

Figure 4.23 Technical Drawing of the Tight Fit Type of Pipe

Figure 4.24 The View of the Tight Fit Type of Pipe.

4.11.2 Threaded Type of Pipe

It was used at the free&forced condensation and annular condensation in concentric spheres experiments. Some modifications were made to the tight fit type of pipe. After free condensation experiment it was seen that some water leakage was taking place. In the free&forced condensation experiments to eliminate the leakage problem instead of tight fit at the tip of the tube 3/8-NPT thread was made. With this method this tube was

connected to the sphere by means of a thread which eliminates cooling water leakage.

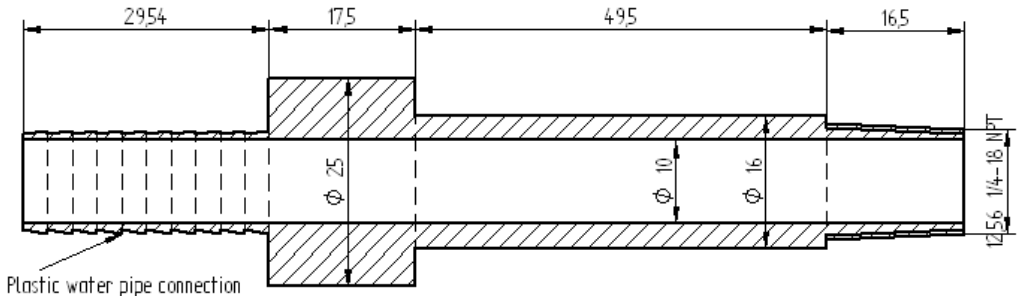

Figure 4.25 Technical Drawing of the Threaded Type of Pipe.

4.12 Cooling Water Distributer Apparatus

The cooling water distributer apparatus was made to distribute the cooling water comign from cooling water tank to three spheres on which condensation is taking place equally.

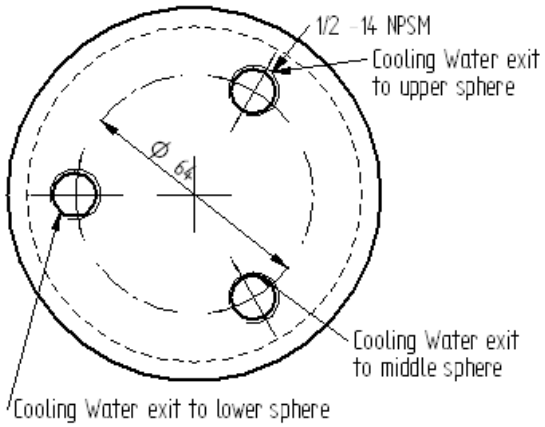

Figure 4.26 Technical Drawing of the Cooling Water Distributer Apparatus, Bottom View.

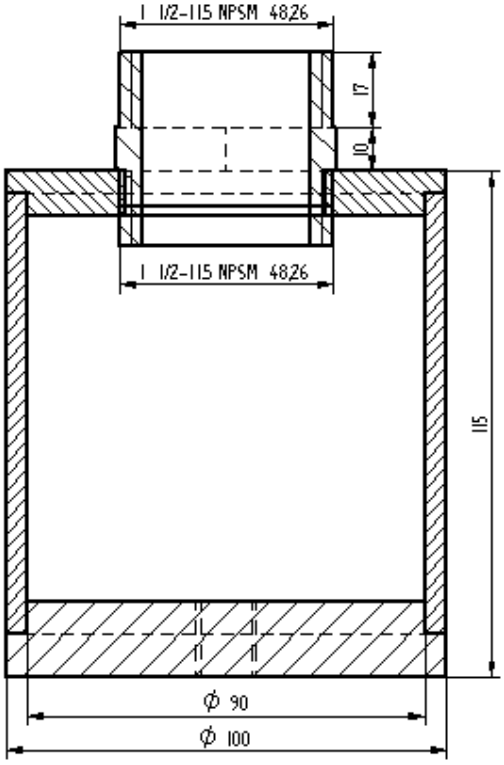

Figure 4.27 Technical Drawing of the Cooling Water Distributer Apparatus, Front View.

This apparatus was made from 316 stainless steel material. It was composed of three parts. They are the tubular body, the upper cap and lower cap which were broght together by welding. The upper cap was connected to the cooling water tank directly with a thread. The lower cap has three holes on it. One ends of three plastic water tubes were connected to each holes and the other ends were connected to steel tubes which were connected to each sphere singly.

Figure 4.28 View of the Cooling Water Distributer Apparatus.

4.13 Pressure Reading System

In forced condensation tests a manometer was placed between test section and vapour valve. The vapour pressure was read from this manometer before starting off the tests. Then this pressure value was used to calculate the vapour velocity. However in this study the vapour velocity caculation could not done. Only the magnitudes were taken as a comparible value.

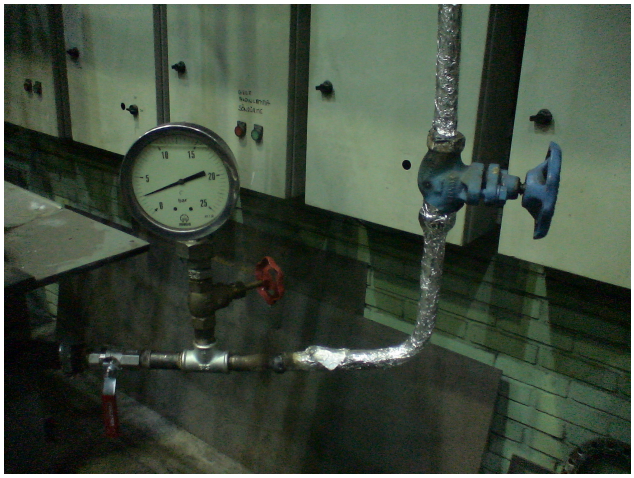

Figure 4.29 View of the Pressure Reading System.

4.14 Temperature Reading System

In all experiments to read the water inlet&exit temperatures and the surface temperatures of spheres two thermometers were used. The thermocouples used are K-Type. On the screen there are 3 digits without any digit after comma. Because one thermometer has 12 channel for thermocouple connection, two thermometers were used. These thermometers have +/-1^{o}C accuracy.

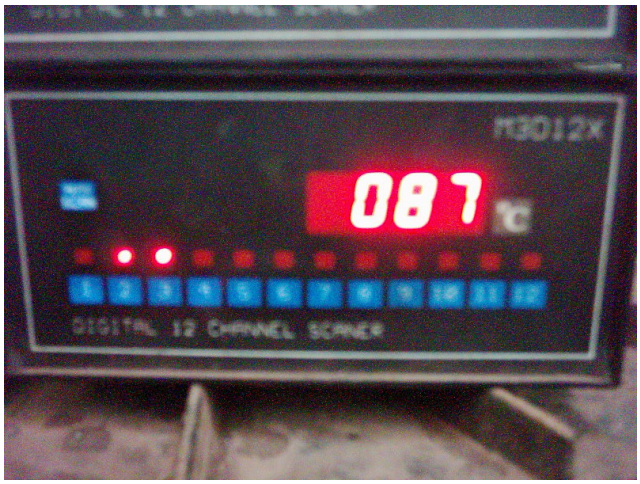

Figure 4.30 View of the Temperature Reading System M3D12x.

4.15 Thermocouple Layout

Three different thermocouple placements were used at experiments.

4.15.1 Case-1:Free Condensation Experiment

At the free condensation experiment 11 K-Type thermocouples were used. On each sphere 2 thermocouples were bonded with Loctite Superior Metal bonder. One at the upper stagnation point and the other at the midle of the sphere, 90 degree from upper point. One thermocouple was placed at the inlet cooling water pipe of the middle sphere. The others were placed at the cooling water exit pipes for each sphere. The inlet and exit pipes connections of thermocouples were made by silver welding.

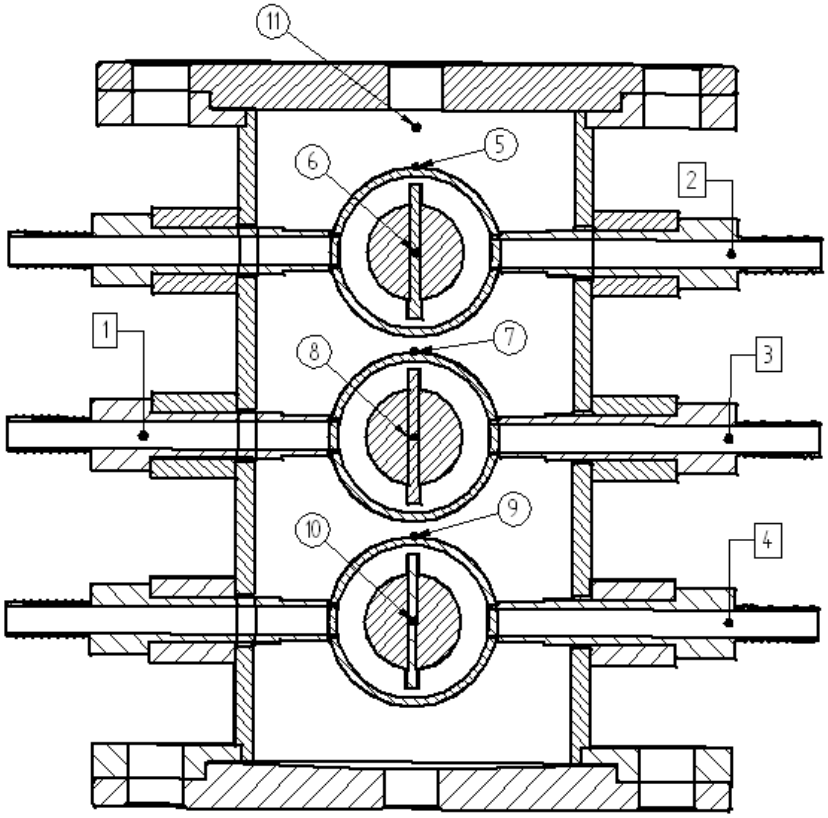

Figure 4.31 The Shematic View of the Thermocouple Layout for Free Condensation Experimental Study.

Number 1 : Cooling water inlet of the middle sphere.
Number 2 : Cooling water exit of the upper sphere.
Number 3 : Cooling water exit of the middle sphere.
Number 4 : Cooling water exit of the bottom sphere.
Number 5 : Upper stagnation point of the upper sphere.
Number 6 : Midpoint of outer surface of the upper sphere.
Number 7 : Upper stagnation point of the middle sphere.
Number 8 : Midpoint of outer surface of the middle sphere.
Number 9 : Upper stagnation point of the bottom sphere.
Number 10 : Midpoint of outer surface of the bottom sphere.
Number 11 : Water vapor inlet to the test section.

4.15.2 Case-2:Free&Forced Condensation Experiments

At the free&forced condensation experiments 20 K-Type thermocouples were used. On each surface of sphere 3 thermocouples were placed by silver welding method. At the inner surface of spheres 2 thermocouples were placed one at the upper and the other at the lower points by silver welding. To do this first thermocouples were welded to the inside surface of spheres and then two hemispheres were welded to each other by silver electrode. The placement of the inlet and exit cooling water pipes were not changed. And the last thermocouple was placed in the test section under the water vapour inlet nozzle.

Number 1 : Cooling water inlet of the middle sphere.
Number 2 : Cooling water exit of the middle sphere.
Number 3 : Cooling water exit of the upper sphere.
Number 4 : Cooling water exit of the bottom sphere.
Number 5 : Upper stagnation point of the upper sphere.
Number 6 : Midpoint of outer surface of the upper sphere.
Number 7 : Bottom point of the upper sphere
Number 14 : Upper point at the inside of the upper sphere

Number 15: Bottom point at the inside of the upper sphere

Number 8 : Upper stagnation point of the middle sphere.

Number 9 : Midpoint of outer surface of the middle sphere..

Number 10: Bottom point of the middle sphere.

Number 16: Upper point at the inside of the middle sphere

Number 17: Bottom point at the inside of the middle sphere

Number 11: Upper stagnation point of the bottom sphere.

Number 12: Midpoint of outer surface of the bottom sphere.

Number 13: Bottom point of the bottom sphere

Number 18: Upper point at the inside of the bottom sphere

Number 19: Bottom point at the inside of the bottom sphere

Number 20: Water vapor inlet to the test section.

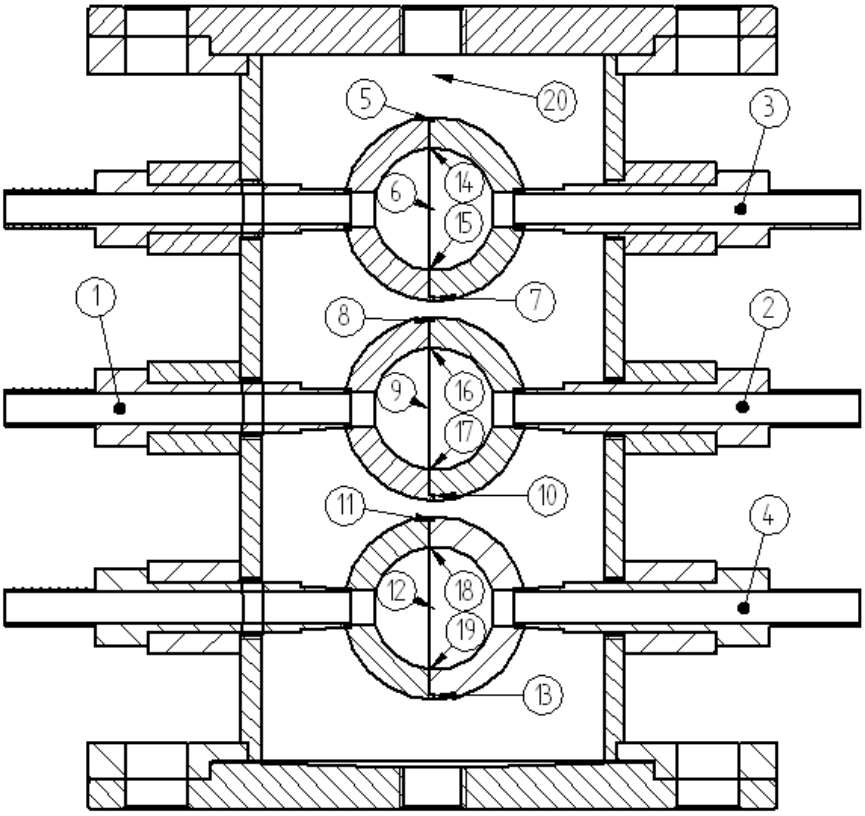

Figure 4.32 The Shematic View of the Thermocouple Layout for Free&Forced Condensation Experimental Study.

4.15.3 Case-3:Annular Condensation in Concentric Spheres Experiment

At the annular condensation in concentric spheres experimental study only one sphere was used. A cylindirical polyamid part was used to accelerate the water vapour flowing around the sphere. Three K-type thermocouples were used on the sphere. One thermocouple was used at the cooling water inlet and one another was used at the cooling water exit. One thermocouple was used to measure the vapour temperature.

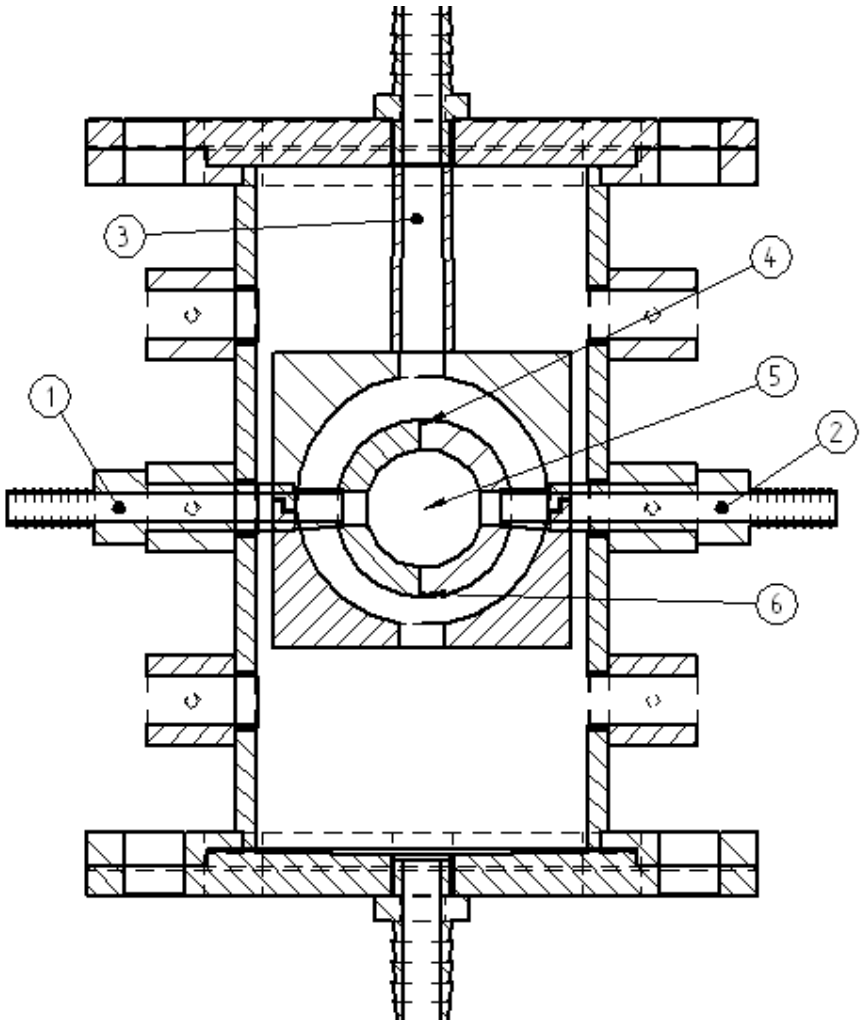

Figure 4.33 The Shematic View of the Thermocouple Layout for Annular Condensation in Concentric Spheres Experimental Study.

Number 1 : Cooling water inlet
Number 2 : Cooling water exit
Number 3 : Vapour inlet
Number 4 : Upper stagnation point
Number 5 : Midpoint of the surface
Number 6 : Lower stagnation point

4.16 Data Collecting Method

The test were done several times by using the same parameters. After obtaining the values, some results were eliminated. The other results were added to each other and the arithmetic averages were calculated as a one value. And these values were used in the heat transfer calculations.

4.17 Thermometer Calibration

Before starting to setup the thermocouples the reader must be checked. To do this a milivolt generator device is used. First of all this device is connected to the reader and then electricity is opened. From the milivolt-temperature graphs milivolt value of the choosen temperature is read. Then this milivolt is given to the reader via the generator and the temperature value is read from the reader screen. In this study this check was made before starting test. It was seen that reader shows temperature values 10^{o}C greather than the real values.

After connecting thermocouples to the readers again temperatures were read from readers and from another thermometer. For this purpose temperature of stationary air was measured by both of them. Also for higher temperature value water was heated to desired value and measured by both of them. It was seen that the readings were 4^{o}C higher than the real values.

So these two temperature differences were added to each other and subtracted from the results as 14^{o}C.

4.18 Experimental Procedure

The aim of these experimental studies is to calculate the heat transfer rate and mean heat transfer coefficient for different diameters, free and forced condensations. There is no heat interactions between the test section and enviroment. So there is no heat transfer to the enviroment and no internal energy generation in the test section. Therefore the steady state condition is available for test section. According to these properties, the heat transfer rate and heat transfer coefficient can be calculated as heat transfered from the vapor to the sphere's surface is equal to the heat transfered from sphere's surface to cooling water flowing in the sphere.

$$Q = mC_p(T_{out} - T_{in}) = h_m A(T_{sat} - T_w) \quad (4.1)$$

4.18.1 Mass Flow Rate Measurements For Case-1,Case-2 & Case-3

At the beginning of the tests, first of all mass flow rate measurements were made. To do this the cooling water tank was filled at the desired level. Then the valves at the exit of the water division aparatus were opened. According to the measured values the adjustment aparatus (valves at the second experiment) at the end of the exit pipes were adjusted for mass flow rates to make them nearly at the same value. Then 3 measurements were made and the values of mass flow rates of each spheres were noted. The time interval was 2 minutes (1.5 minutes at the second experiment).

4.18.2 Case-1 Free Condensation Experiments

The tests were conducted at 0^o,12^o,20^o,30^o inclination angles and at 20^oC-30^oC-40^oC-50^oC-60^oC cooling water inlet temperatures. In the first study the results of Ø50mm and Ø60mm o.d. spheres were obtained and compared for free condensation.

Water vapour was supplied from steam line. The vapour valve is opened. At the same time the air exit valve is opened. Test section is waited about 60 minutes to be completly filled by water vapour. After 60 minutes the air exit valve is closed. The aim of this procedure is to eliminate the air inside the test section to obtain complete condensation. Then the cooling water is heated up to the desired temperature in the tank. When the temperature is reached to the desired point the valves are opened and cooling water runs inside the spheres. About 2 minutes are waited to obtain steady state condition by wacthing the thermocouple reader. When the temperatures are not changed the values are read and noted. The cooling water is collected at the vessels which are placed under each water exit pipes of spheres. The condensation is also collected in another vessel. After readings the valves are closed. The vessels are weighed at the digital heaviness and noted.

4.18.3 Case:2 Free&Forced Condensation Experiments

The tests were conducted at 0^o,5^o,10^o,15^o,20^o inclination angles and at 25^oC-30^oC-40^oC-50^oC cooling water inlet temperatures. In the second study datas are obtained for free and forced condensations.

Water vapour is supplied from boiler which has a 2.5kW heater for free condensation. The heater is plugged. About 60 minutes later the water vapour srarts to occur. At the same time the air exit valve is opened. Test section is waited about 60 minutes to be completly filled by water vapour. After 60 minutes the air exit valve is closed. The aim of this procedure is to

eliminate the air inside the test section to obtain complete condensation. Then the cooling water is heated up to the desired temperature in the tank. When the temperature is reached to the desired point the valves are opened and cooling water runs inside the spheres. About 2 minutes are waited to obtain steady state condition by wacthing the thermocouple reader. When the temperatures are not changed the values are read and noted. The cooling water is collected at the vessels which are placed under each water exit pipes of spheres. The condensation is also collected in another vessel. After readings the valves are closed. The vessels are weighed at the digital heaviness and noted. From 20 termocouples 20 temperature values are read. For forced condensation a manometer is used to read the vapour pressure which is coming from the steamline of workshop.

4.18.4 Case:3 Annular Condensation in the Concentric Spheres

The tests were conducted at 0^{o} inclination angles and at $20^{o}C$-$30^{o}C$-$40^{o}C$-$50^{o}C$ cooling water inlet temperatures. In this study datas are obtained for forced and free condensations.

The aim of third experimental study is to obtain the data for water vapour flowing between to sphere surfaces. To do this a cylindirical part is used. Inside of this part is spherical shaped and has Ø85mm diameter. The steel sphere is placed inside this part. There is 12.5mm space between the surfaces and water vapour flows in this space. Datas are obtained for this situation. At least two measurements are made to obtain the reliable results and then the average of them is taken. For forced condensation steamline is used to obtain high velocity vapour.

CHAPTER 5

5 RESULTS AND DISCUSSION

5.1 Experimental Results

The aim of these experiments is to see the effects of wall temperature, subcooling, inclination angle and vapour velocity over the heat transfer rate and mean heat transfer coefficient. Using the cooling water after some time from starting of the test, the temperature of the surface of the spheres goes to be constant (steady state) but not isothermal because the surface properties can not be same everywere. After the surface temperatures are constant the heat given by the vapor to the surface is equal to the heat taken by water. The heat transfer rate and mean heat transfer coefficients are calculated from the equation below.

$$Q = mC_p(T_{out} - T_{in}) = h_m A(T_{sat} - T_w) \tag{5.1}$$

In free and forced condensation experimental study the local heat transfer values are calculated from this equation.

$$h_{loc} = h_m \frac{T_{sat} - T_{loc}}{T_{sat} - T_w} \tag{5.2}$$

5.1.1 Case 1- Free Condensation Experiments

The tests were conducted at 0^o,12^o,20^o,30^o inclination angles and at 20^oC-30^oC-40^oC-50^oC-60^oC cooling water inlet temperatures. Datas were obtained for Ø50mm and Ø60mm o.d. spheres. In all experiments the effect of mass flow rate of cooling water is considered.

To eliminate the cooling water pressure drop the water tank was placed 200cm above the test section. The mass flow rates were adjusted by using valves. Only the Ø60mm o.d. sphere results are given in the following figures. The Ø50mm o.d. sphere results are given in Appendix-C.

The calculated equations for mass flow rates are as follows.

$$m_1(t)=-0,00458.(t-t1)+m_1 \quad (5.3)$$

$$m_2(t)=-0,00139.(t-t2)+m_2 \quad (5.4)$$

$$m_3(t)=-0,00222.(t-t3)+m_3 \quad (5.5)$$

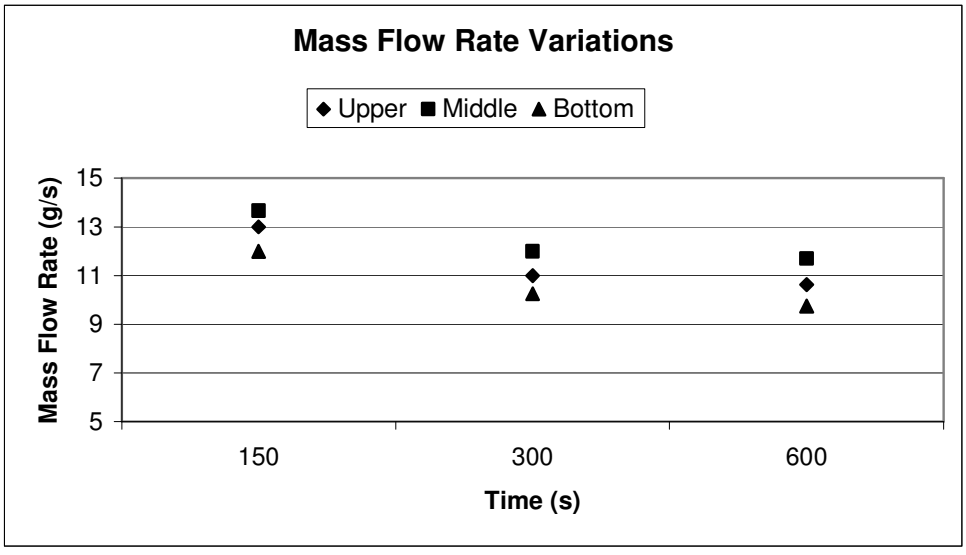

Figure 5.1 Experimental Mass Flow Rate Variation with respect to Time for Case-1, D=Ø60mm.

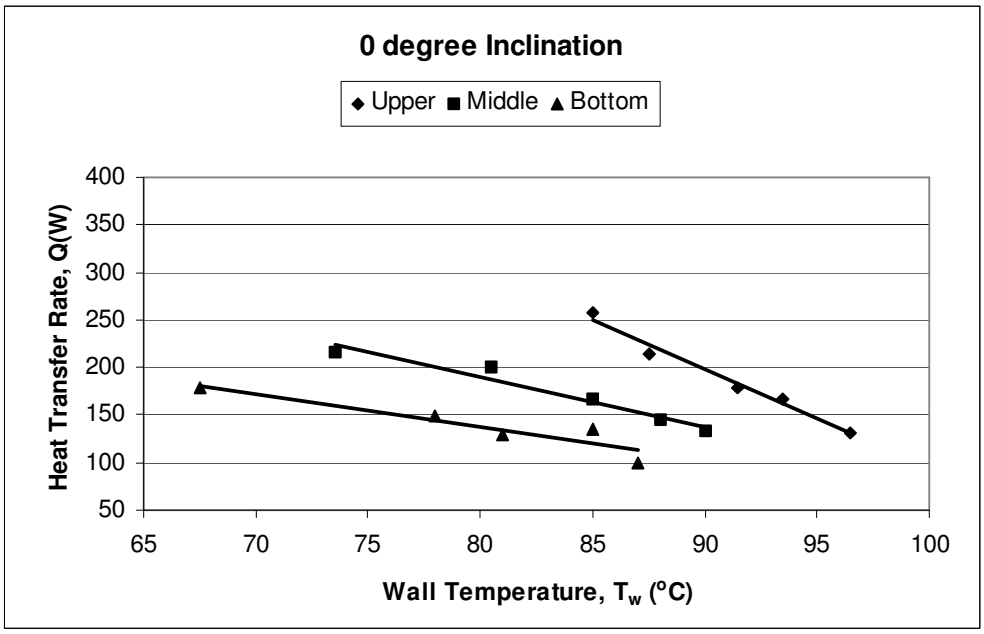

Figure 5.2 Variation of Heat Transfer Rate for 0° of Inclination for Case1, D=Ø60mm.

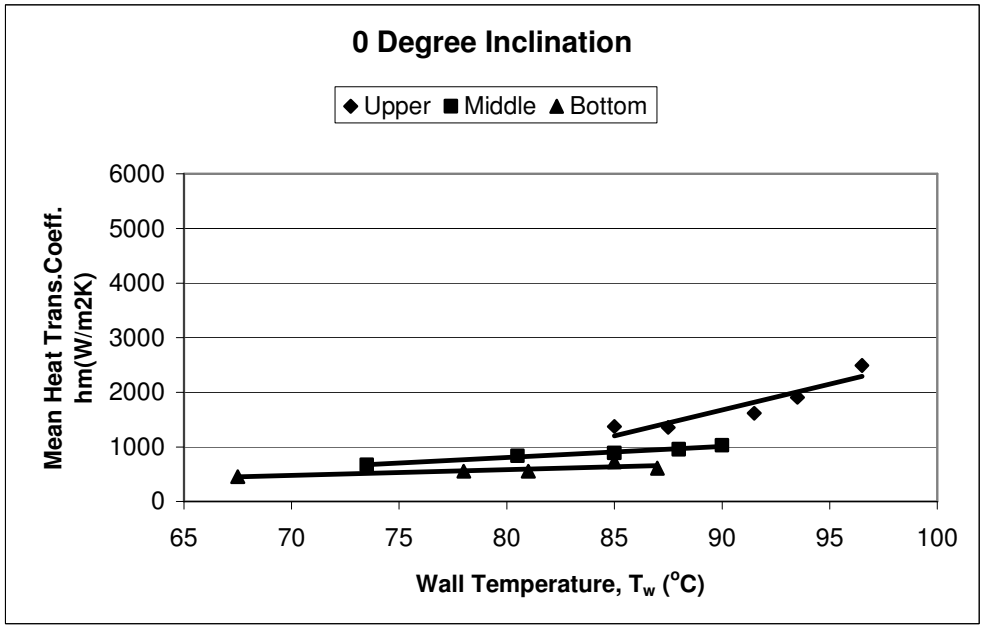

Figure 5.3 Variation of Mean Heat Transfer Coefficient for 0° of Inclination for Case-1, D=Ø60mm.

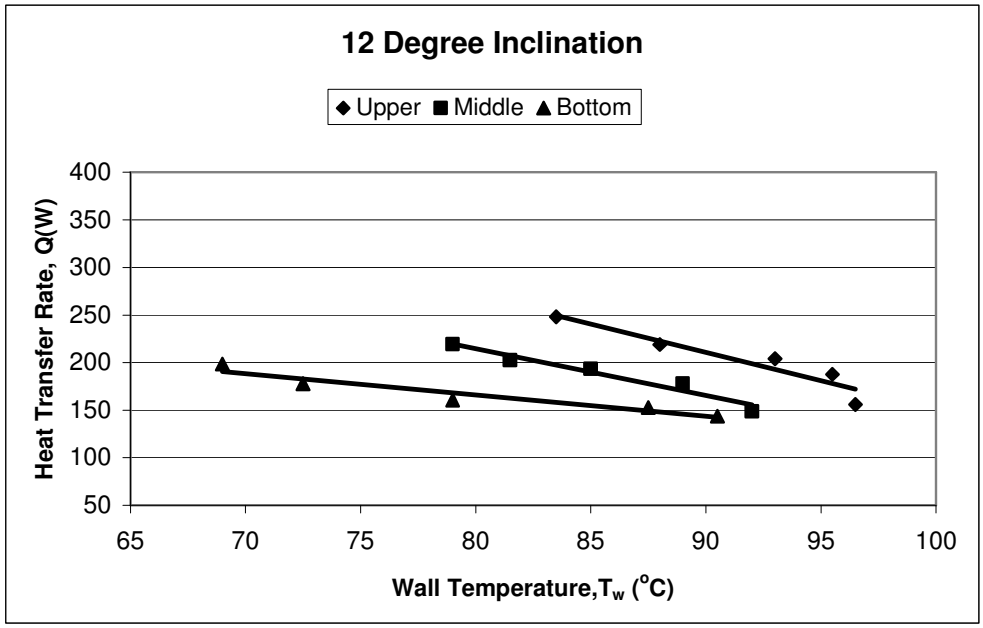

Figure 5.4 Variation of Heat Transfer Rate for 12^o of Inclination for Case-1, D=Ø60mm.

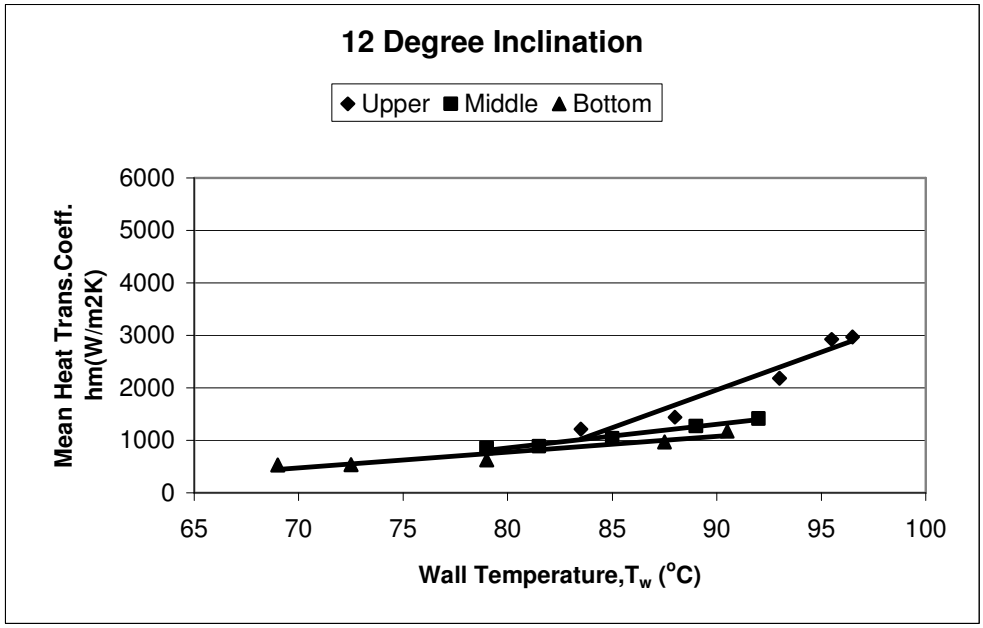

Figure 5.5 Variation of Mean Heat Transfer Coefficient for 12^o of Inclination for Case-1, D=Ø60mm.

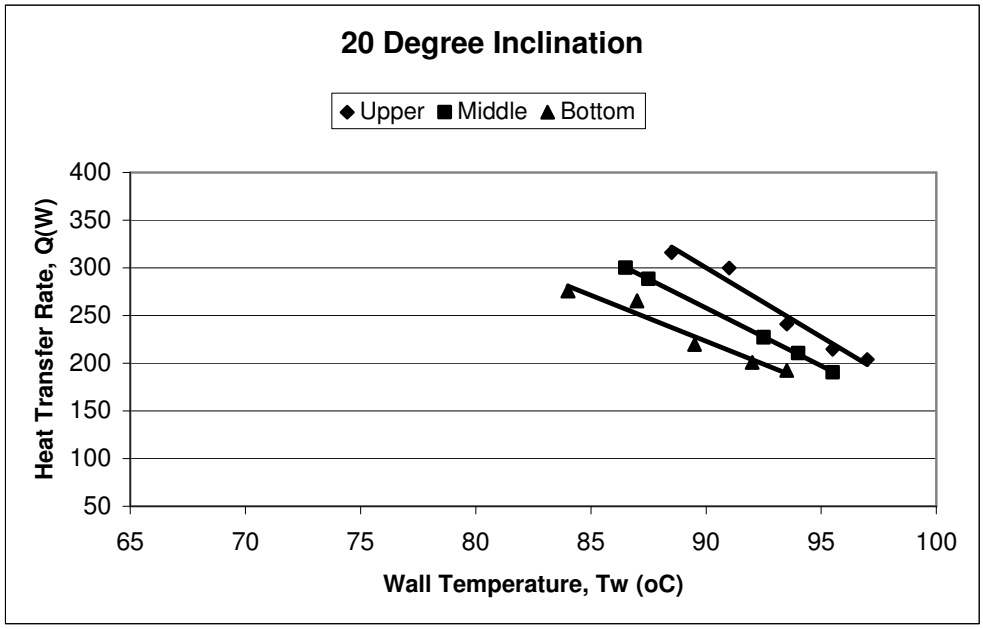

Figure 5.6 Variation of Heat Transfer Rate for 20^{o} of Inclination for Case-1, D=Ø60mm.

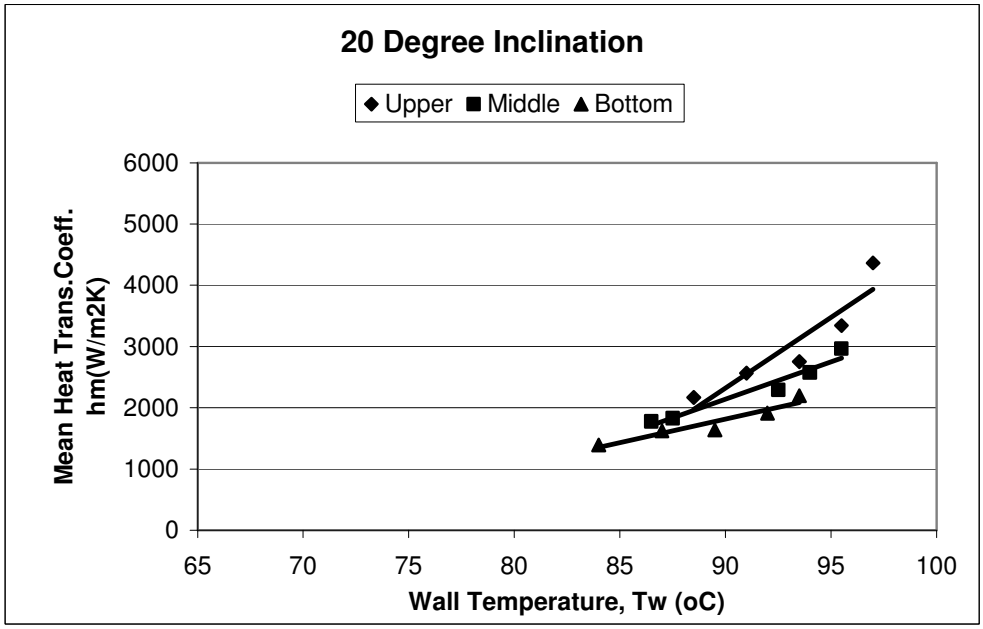

Figure 5.7 Variation of Mean Heat Transfer Coefficient for 20^{o} of Inclination for Case-1, D=Ø60mm.

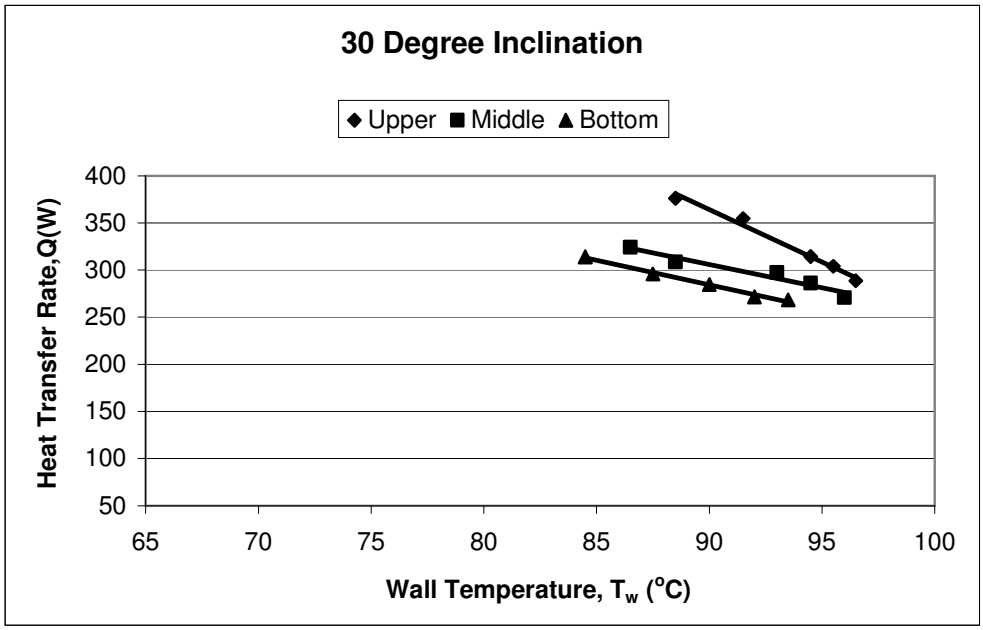

Figure 5.8 Variation of Heat Transfer Rate for 30^o of Inclination for Case-1, D=Ø60mm.

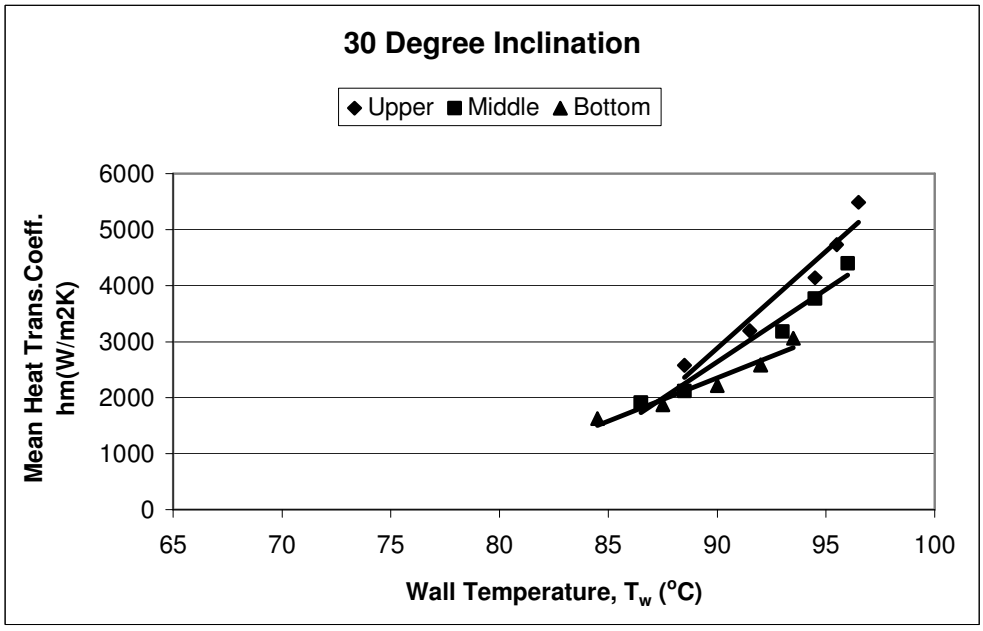

Figure 5.9 Variation of Mean Heat Transfer Coefficient for 30^o of Inclination for Case-1, D=Ø60mm.

5.1.2 Comparison of the Results of Ø50mm and Ø60mm Spheres

Heat flux and mean heat transfer coefficient results were obtained for Ø50mm and Ø60mm o.d. spheres. They are compared at the following figures for 0^o and 12^o inclination angles.

It is seen from these figures that when the diameter gets bigger the heat flux and heat transfer coefficients get smaller because the film thickness gets thicker. And this tchicker film tchikness makes a barrier to resist heat transfer.

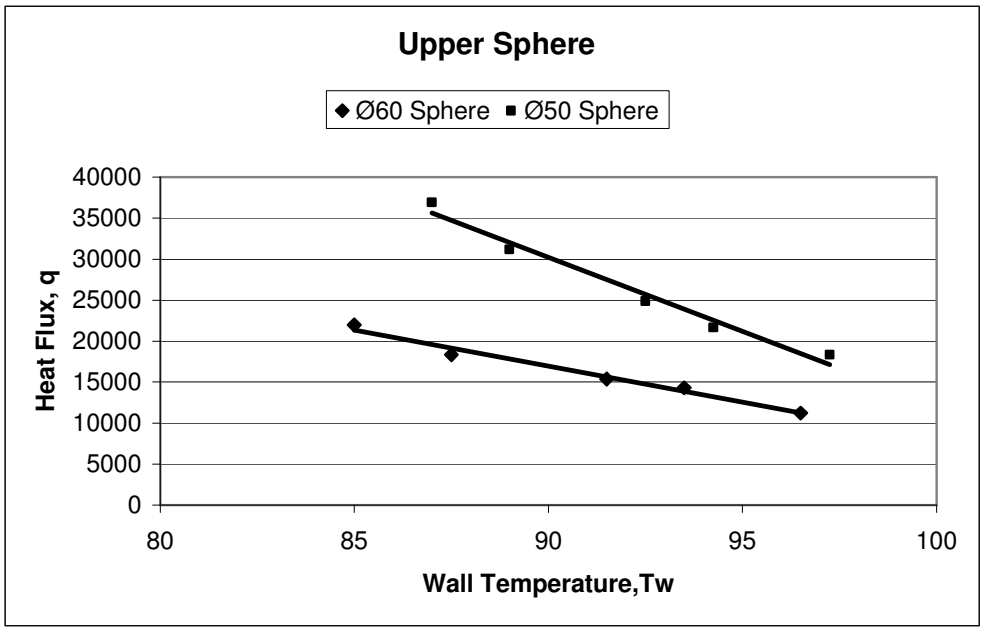

Figure 5.10 Comparison of Heat Flux for 0^o Inclination Angle for Upper Sphere, D=Ø50mm and D=Ø60mm.

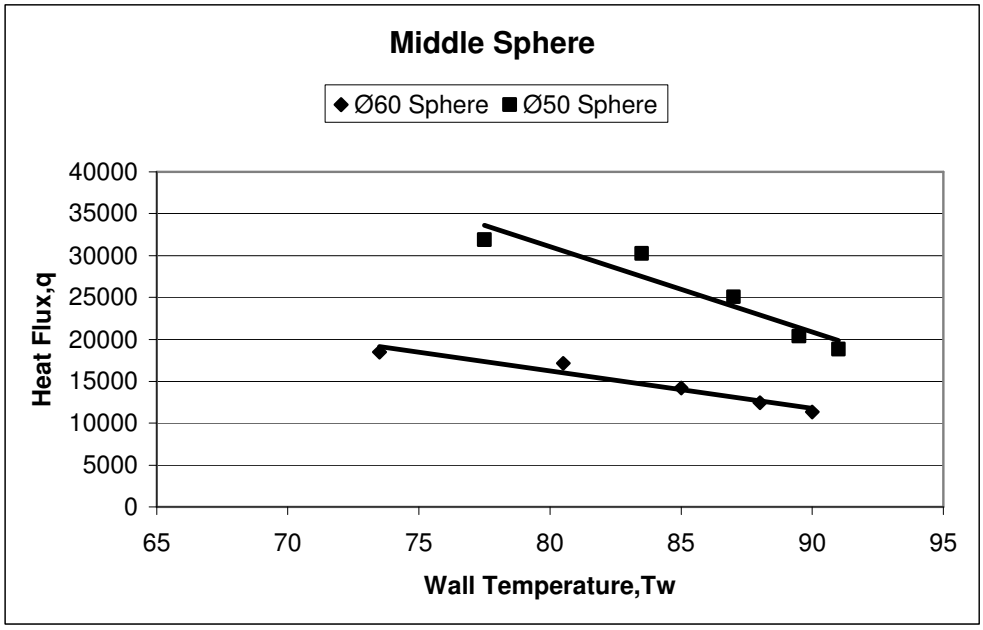

Figure 5.11 Comparison of Heat Flux for 0° Inclination Angle for Middle Sphere, D=Ø50mm and D=Ø60mm.

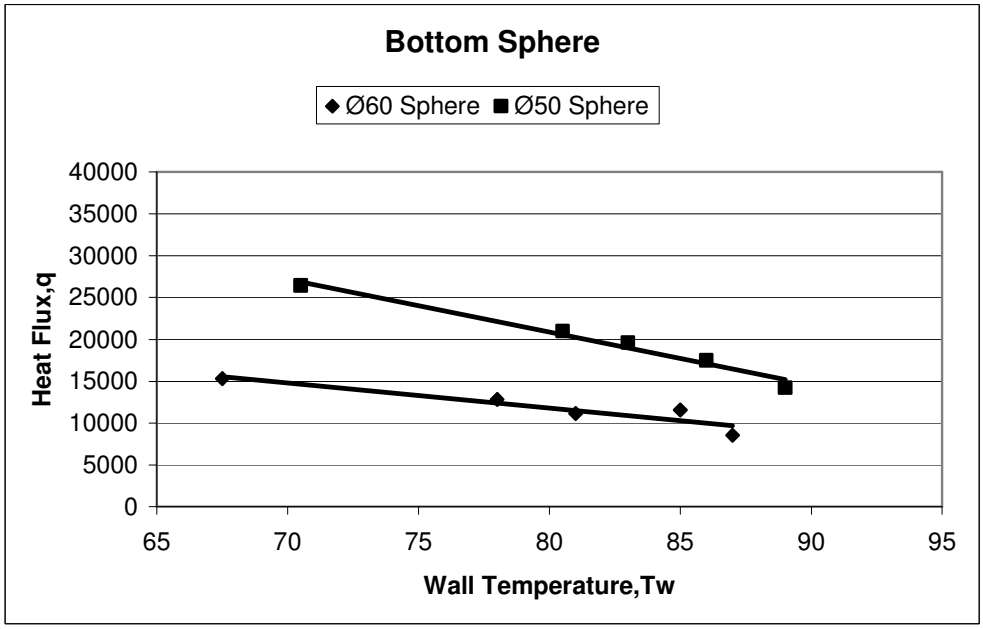

Figure 5.12 Comparison of Heat Flux for 0° Inclination Angle for Bottom Sphere, D=Ø50mm and D=Ø60mm.

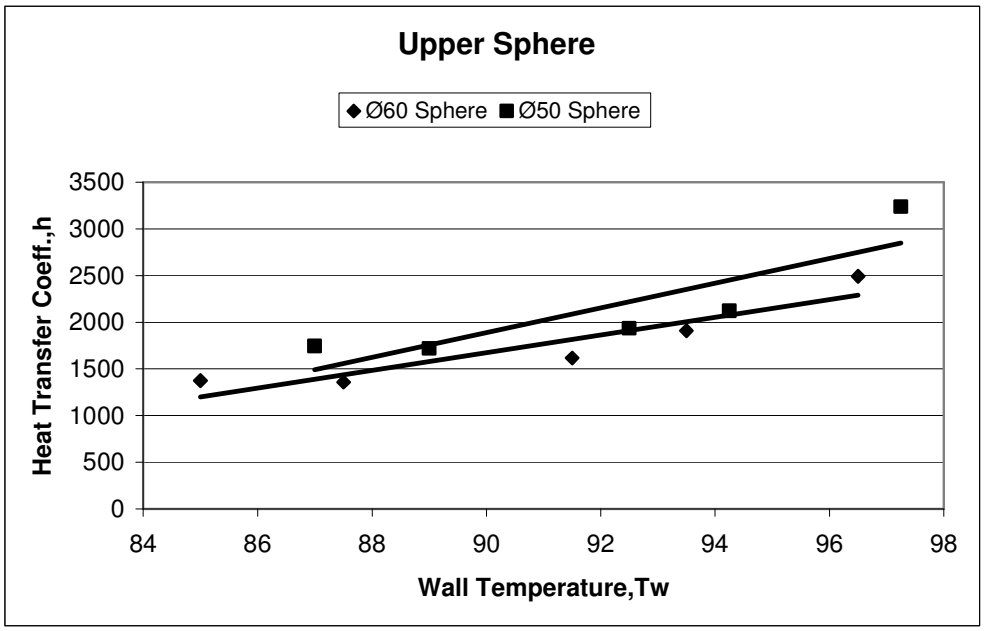

Figure 5.13 Comparison of Mean Heat Transfer Coefficient for 0^{o}Inclination Angle for Upper Sphere, D=Ø50mm and D=Ø60mm.

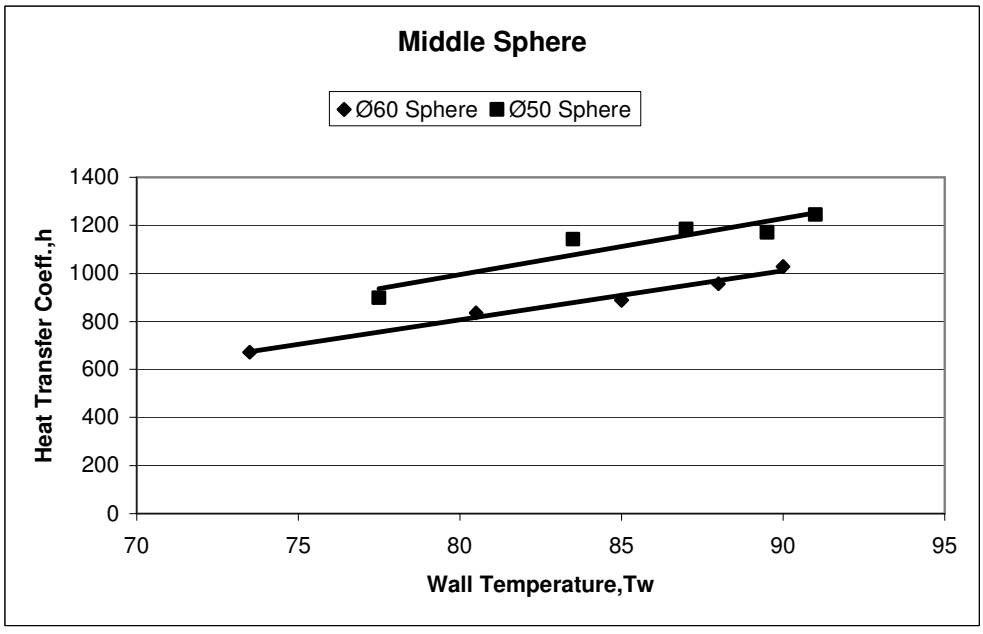

Figure 5.14 Comparison of Mean Heat Transfer Coefficient for 0^{o}Inclination Angle for Middle Sphere, D=Ø50mm and D=Ø60mm.

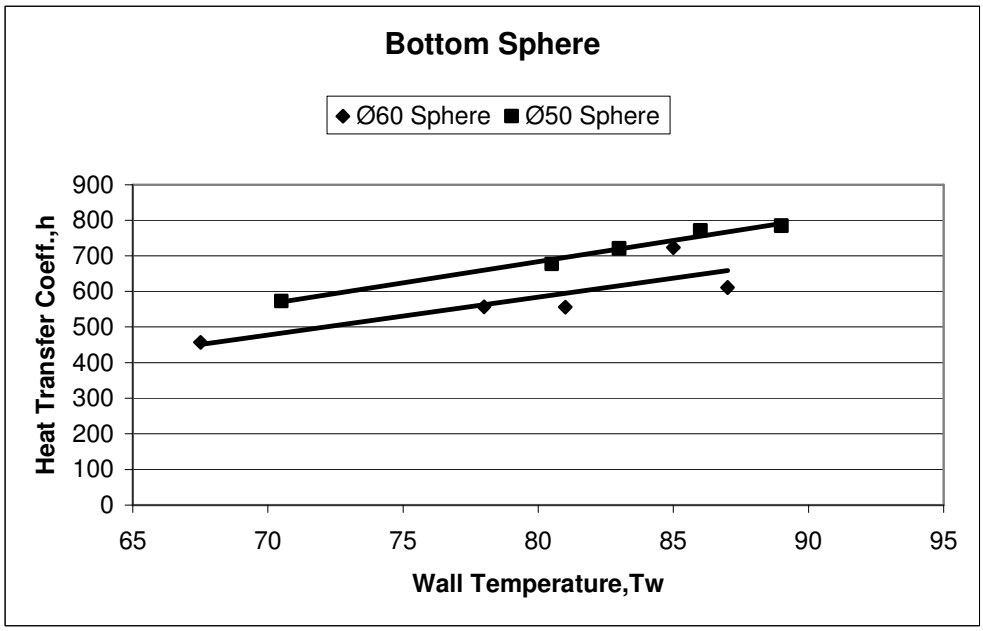

Figure 5.15 Comparison of Mean Heat Transfer Coefficient for 0^{o}Inclination Angle for Bottom Sphere, D=Ø50mm and D=Ø60mm.

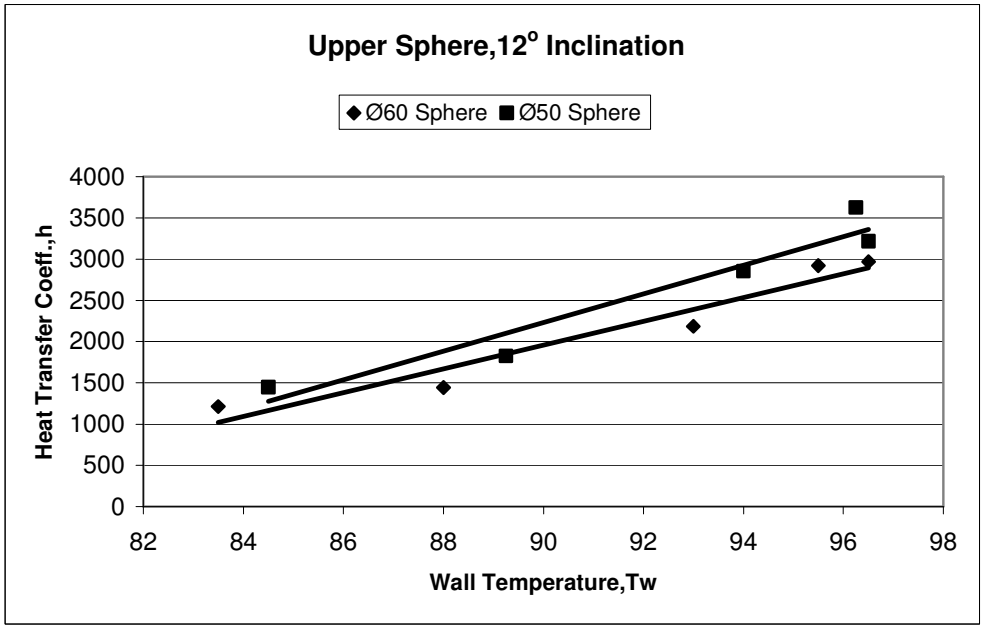

Figure 5.16 Comparison of Mean Heat Transfer Coefficient for 12^{o} Inclination Angle for Upper Sphere, D=Ø50mm and D=Ø60mm.

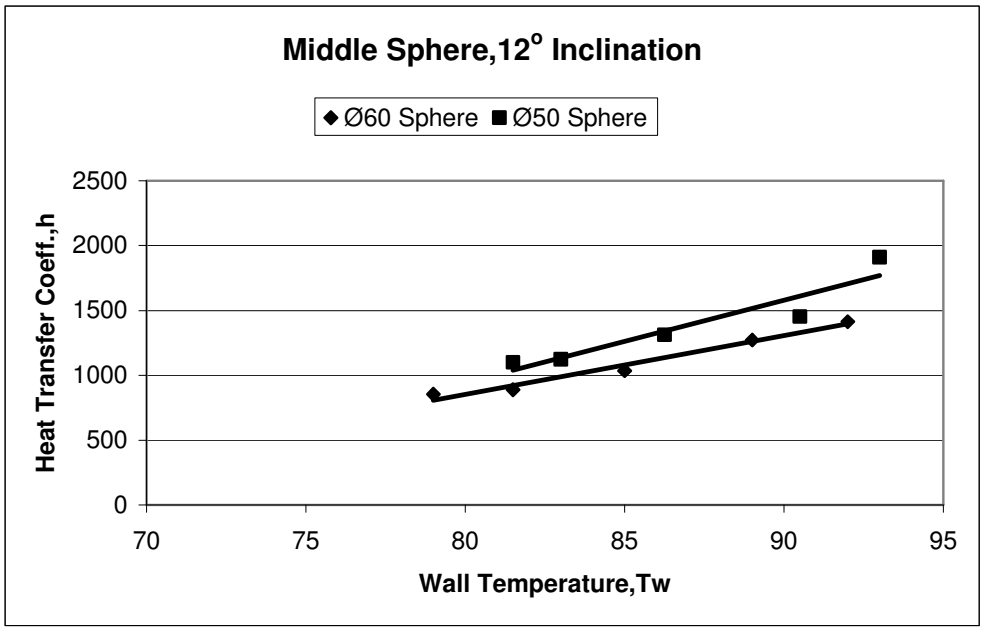

Figure 5.17 Comparison of Mean Heat Transfer Coefficient for 12° Inclination Angle for Middle Sphere, D=Ø50mm and D=Ø60mm.

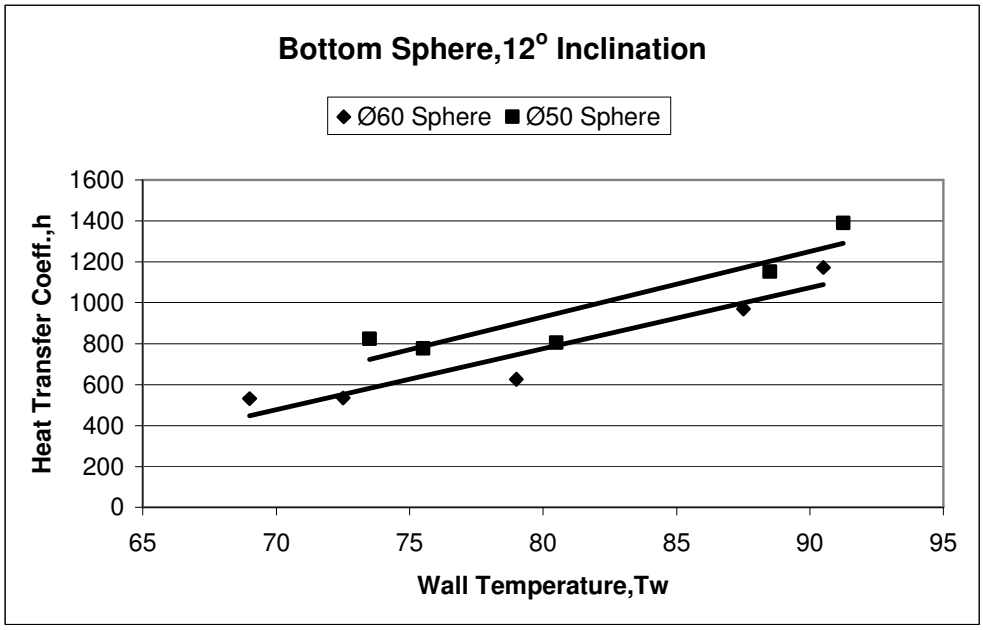

Figure 5.18 Comparison of Mean Heat Transfer Coefficient for 12° Inclination Angle for Bottom Sphere, D=Ø50mm and D=Ø60mm.

5.1.3 Case2 Free&Forced Condensation Experiments

The tests were conducted at 0^o,5^o,10^o,15^o,20^o inclination angles and at 25^oC-30^oC-40^oC-50^oC cooling water inlet temperatures. The test were made for free and forced condensations.

After case1 experiments it was seen that heigth of the water tank was not sufficient to reduce the pressure drop of water. Therefore the heigth was increased to 350cm above the test section and three valves were mounted at the exit of the water pipes. And the mass flow rates were adjusted by using these valves more exactly. The comparison of free and forced condensation is given after free condensation graphs.

The calculated equations for mass flow rates are as follows.

$$m_1(t)=-0,0106635.(t-t1)+m_1 \quad (5.6)$$

$$m_2(t)=-0,0064575.(t-t2)+m_2 \quad (5.7)$$

$$m_3(t)=-0,0067045.(t-t3)+m_3 \quad (5.8)$$

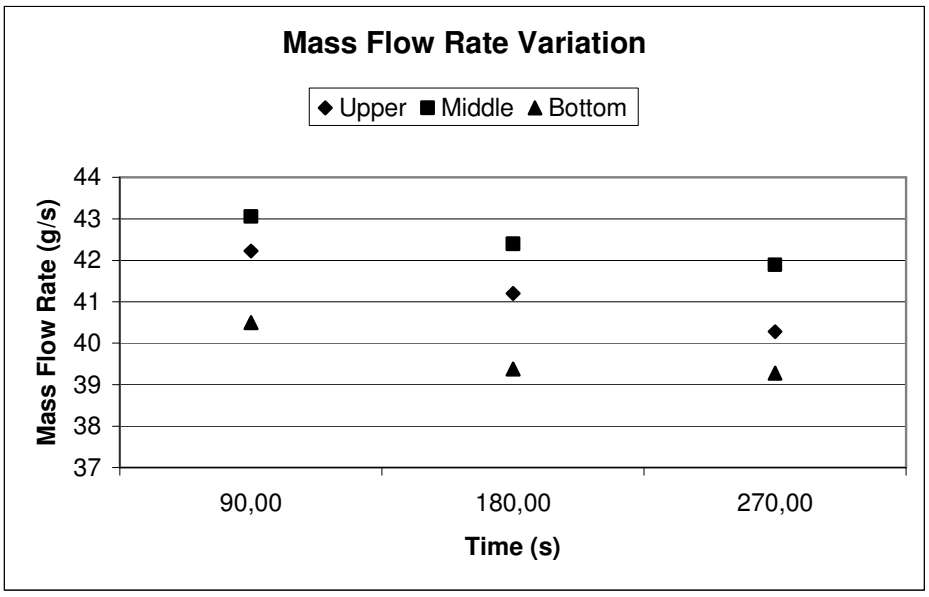

Figure 5.19 Experimental Mass Flow Rate Variation with respect to Time for Free&Forced Condensation Experiments.

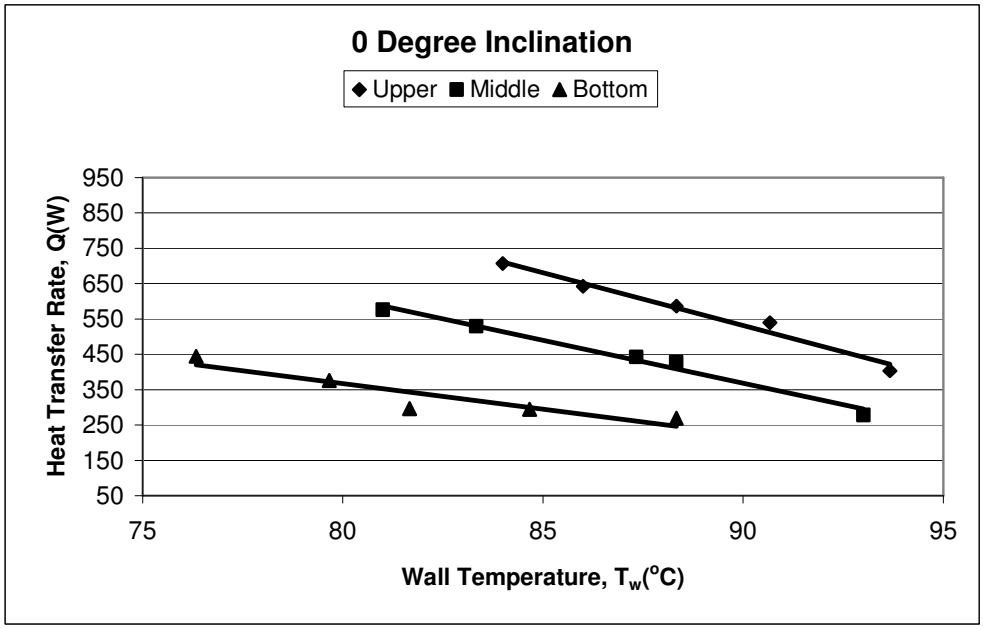

Figure 5.20 Variation of Heat Transfer Rate for 0° of Inclination for Case-2, Free Condensation.

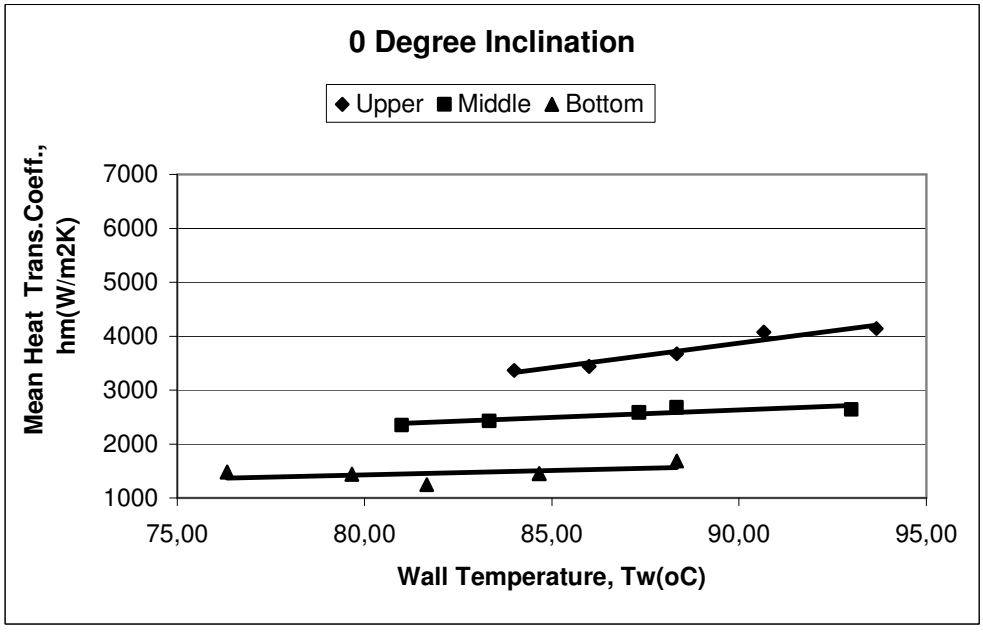

Figure 5.21 Variation of Mean Heat Transfer Coefficient for 0° of Inclination for Case-2, Free Condensation.

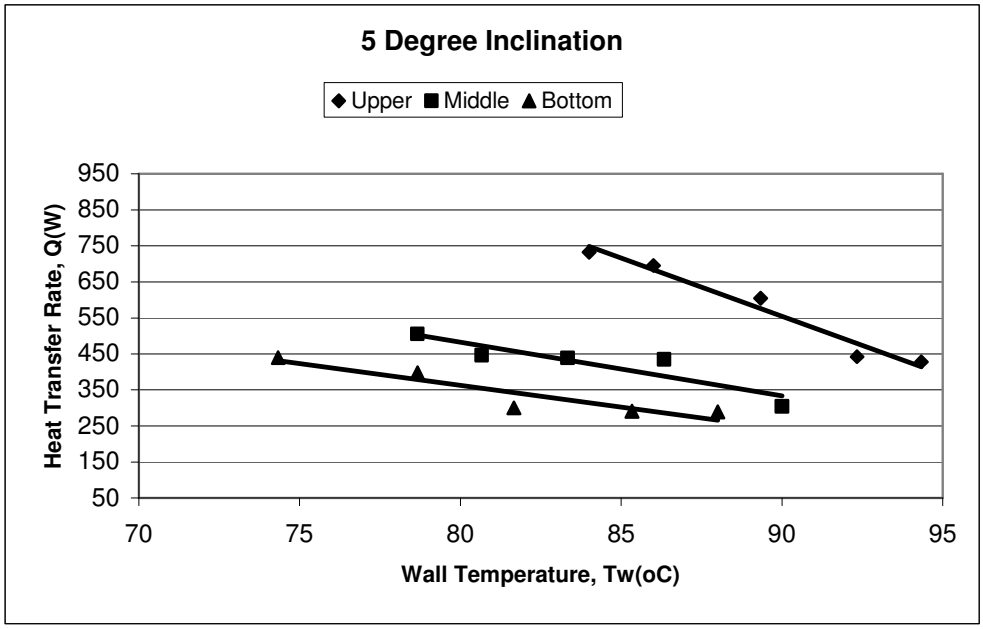

Figure 5.22 Variation of Heat Transfer Rate for 5^{o} of Inclination for Case-2, Free Condensation.

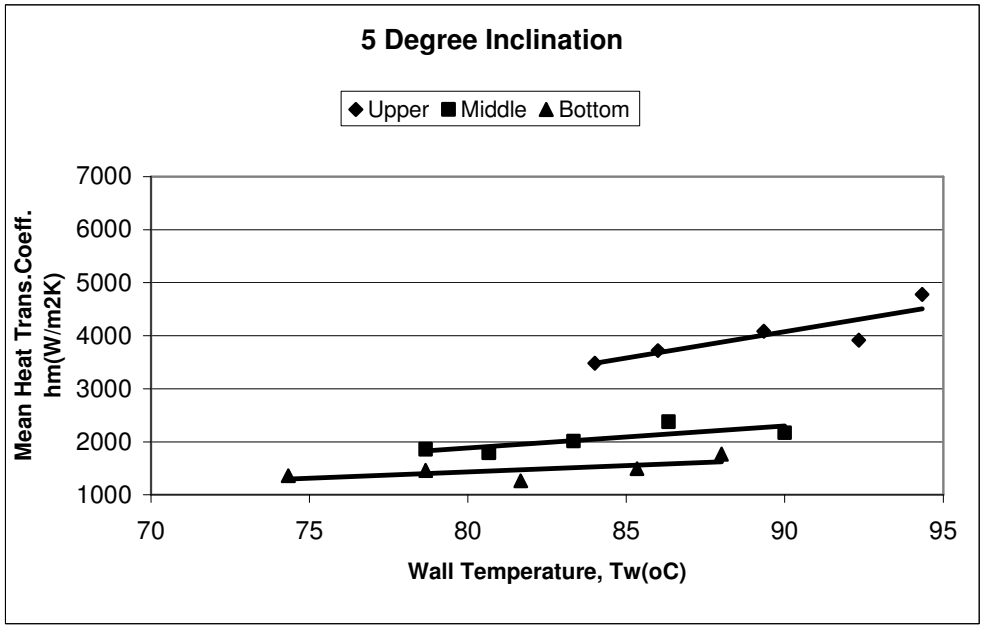

Figure 5.23 Variation of Mean Heat Transfer Coefficient for 5^{o} of Inclination for Case-2, Free Condensation.

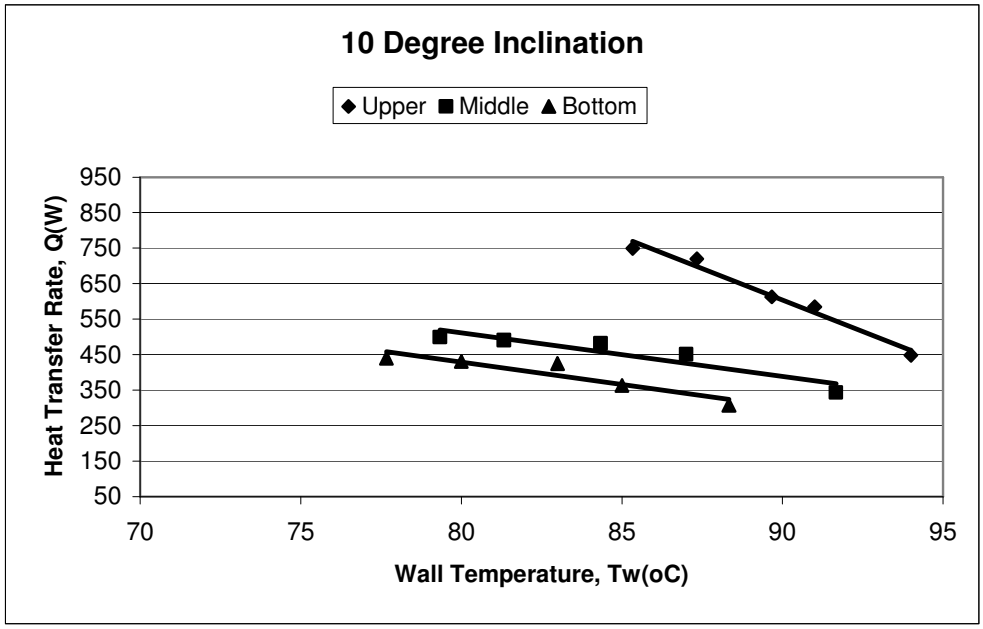

Figure 5.24 Variation of Heat Transfer Rate for 10^{o} of Inclination for Case-2, Free Condensation.

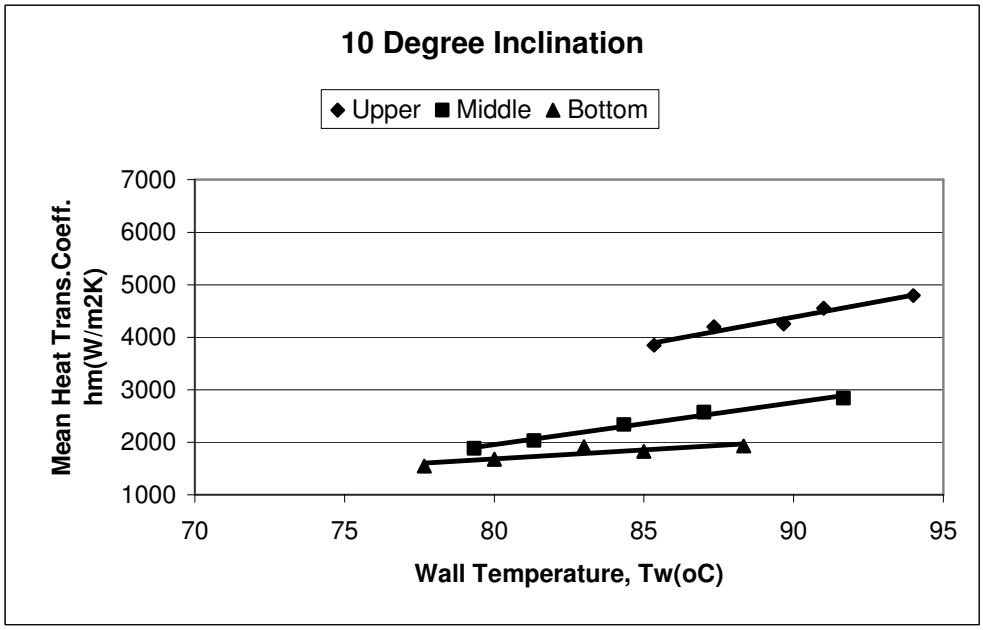

Figure 5.25 Variation of Mean Heat Transfer Coefficient for 10^{o} of Inclination for Case-2, Free Condensation.

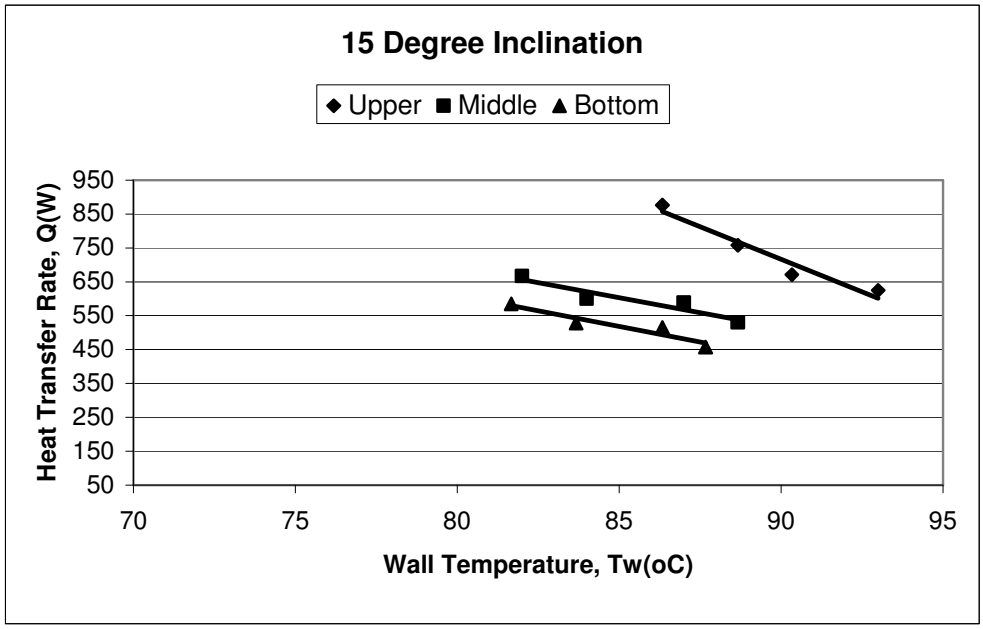

Figure 5.26 Variation of Heat Transfer Rate for 15^{o} of Inclination for Case-2, Free Condensation.

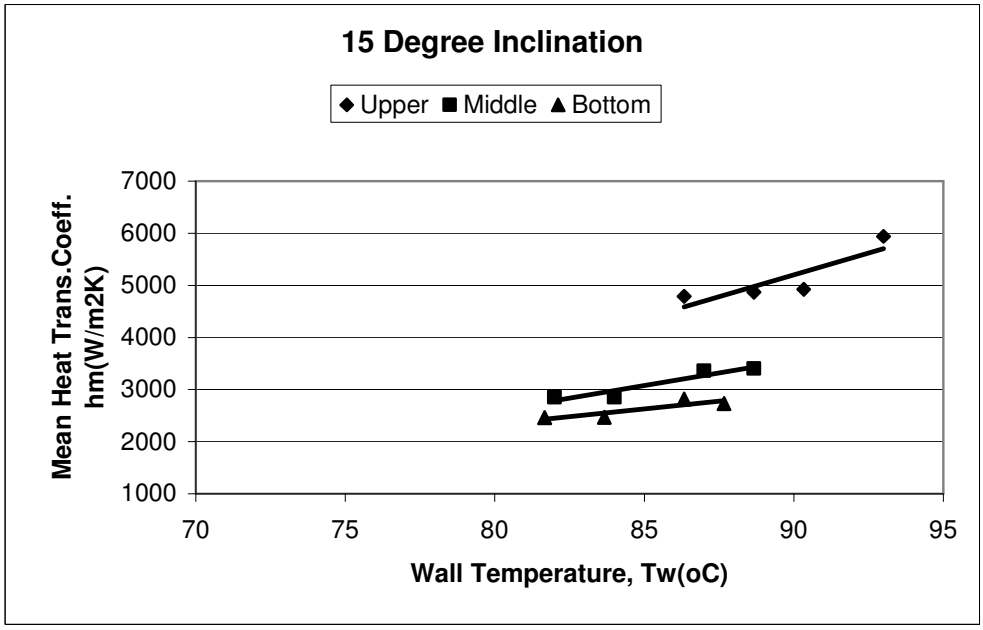

Figure 5.27 Variation of Mean Heat Transfer Coefficient for 15^{o} of Inclination for Case-2, Free Condensation.

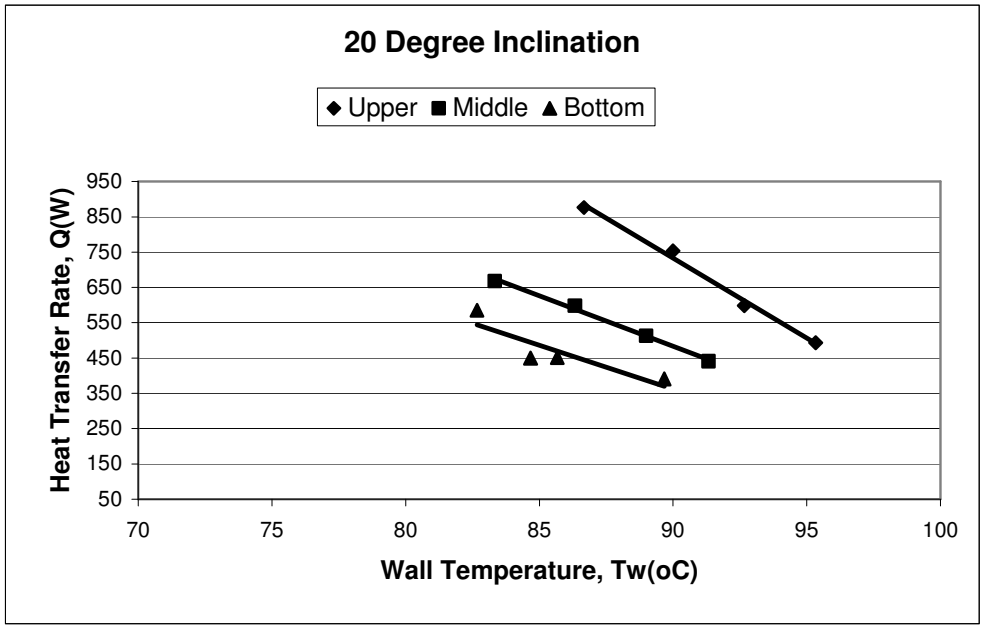

Figure 5.28 Variation of Heat Transfer Rate for 20^{o} of Inclination for Case-2, Free Condensation.

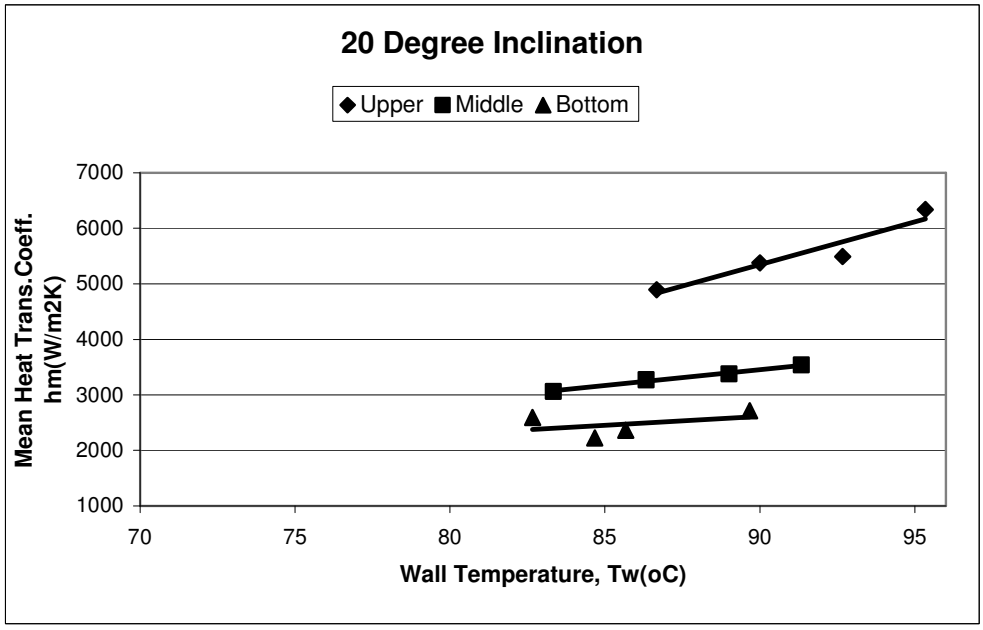

Figure 5.29 Variation of Mean Heat Transfer Coefficient for 20^{o} of Inclination for Case-2, Free Condensation.

5.1.4 Comparison of Free And Forced Condensation for Case-2

It is seen from the following figures that if the vapour velocity increases, the heat transfer rate and mean heat transfer coefficient increases. The film thickness decreases with increasing vapour velocity.

In these figures the results for D=Ø60mm o.d. sphere are shown and compared for free and forced conditions.

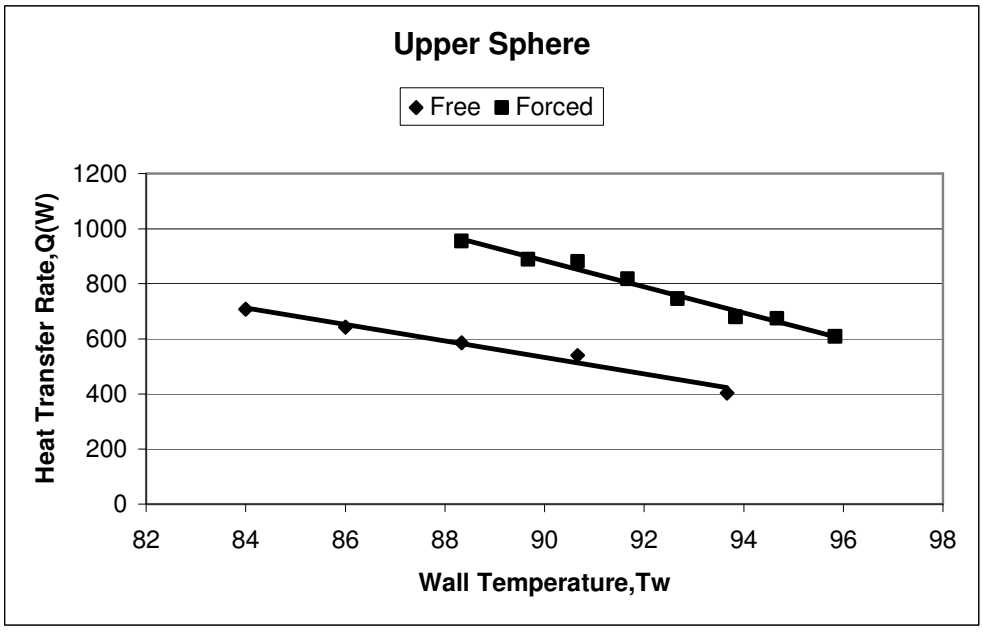

Figure 5.30 Comparison of Heat Transfer Rate for 0^o of Inclination for Case-2, Upper Sphere, Free and Forced Condensation.

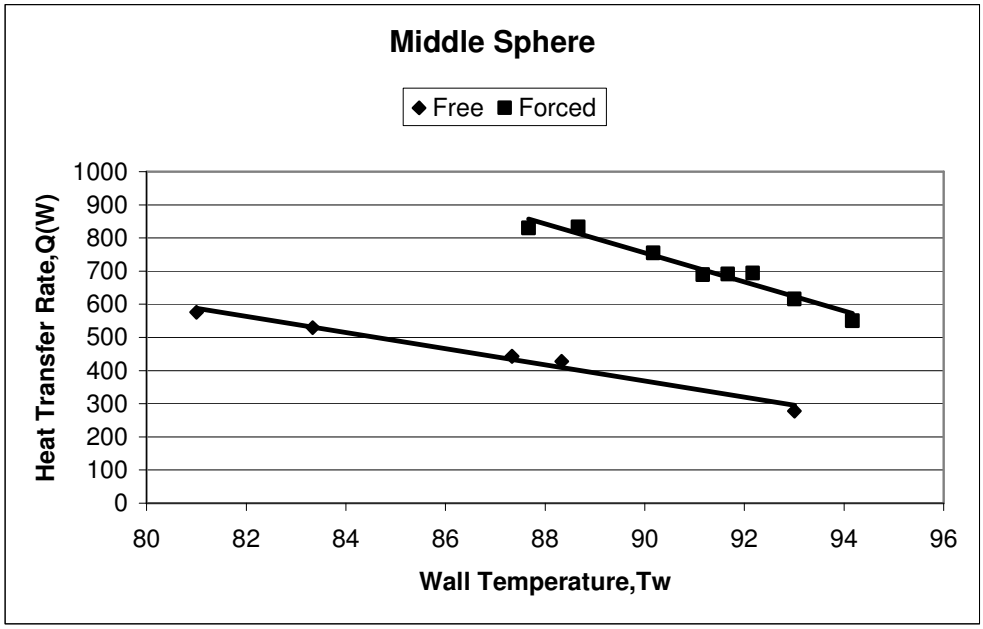

Figure 5.31 Comparison of Heat Transfer Rate for 0^o of Inclination for Case-2, Middle Sphere, Free and Forced Condensation.

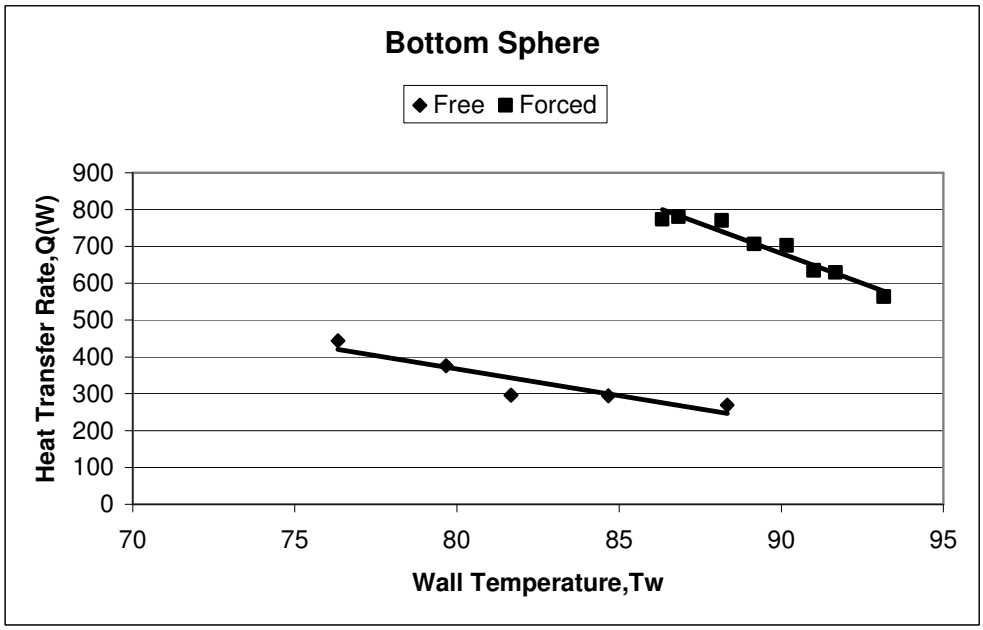

Figure 5.32 Comparison of Heat Transfer Rate for 0^o of Inclination for Case-2, Bottom Sphere, Free and Forced Condensation.

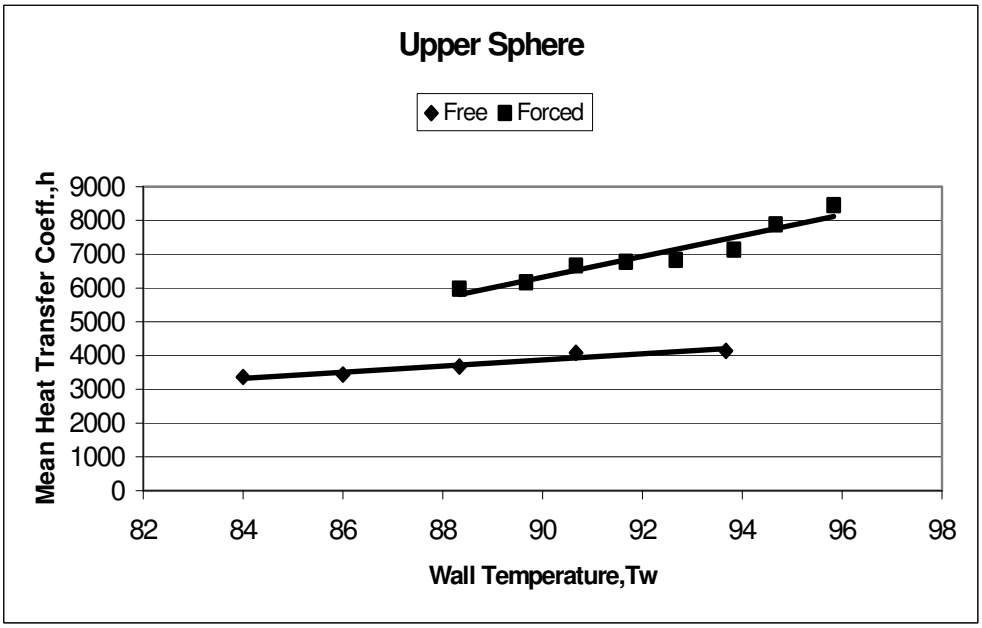

Figure 5.33 Comparison of Mean Heat Transfer Coefficients for 0^o of Inclination for Case-2,Upper Sphere, Free and Forced Condensation.

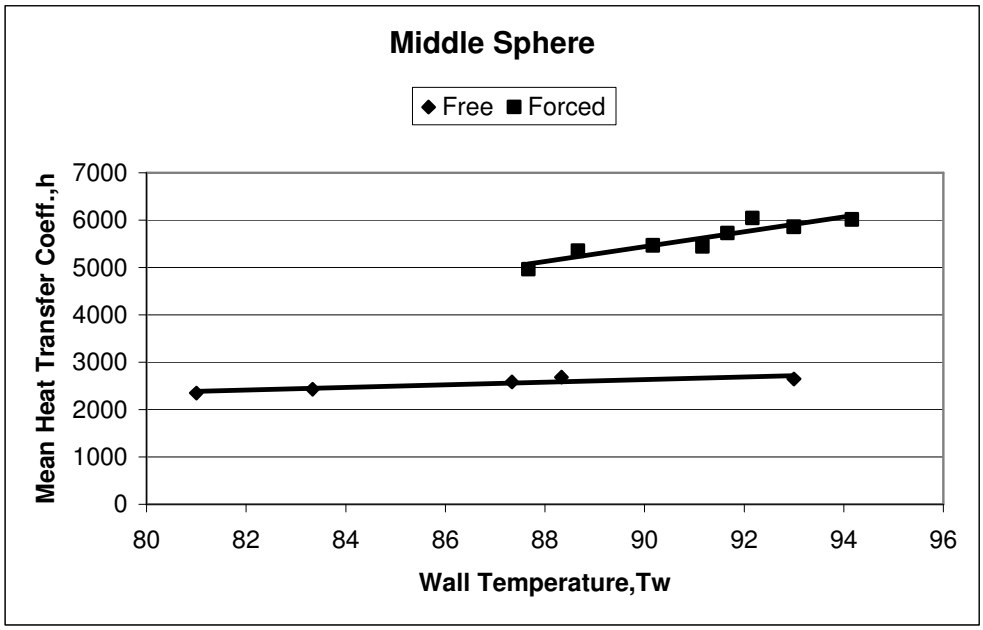

Figure 5.34 Comparison of Mean Heat Transfer Coefficients for 0^o of Inclination for Case-2,Middle Sphere, Free and Forced Condensation.

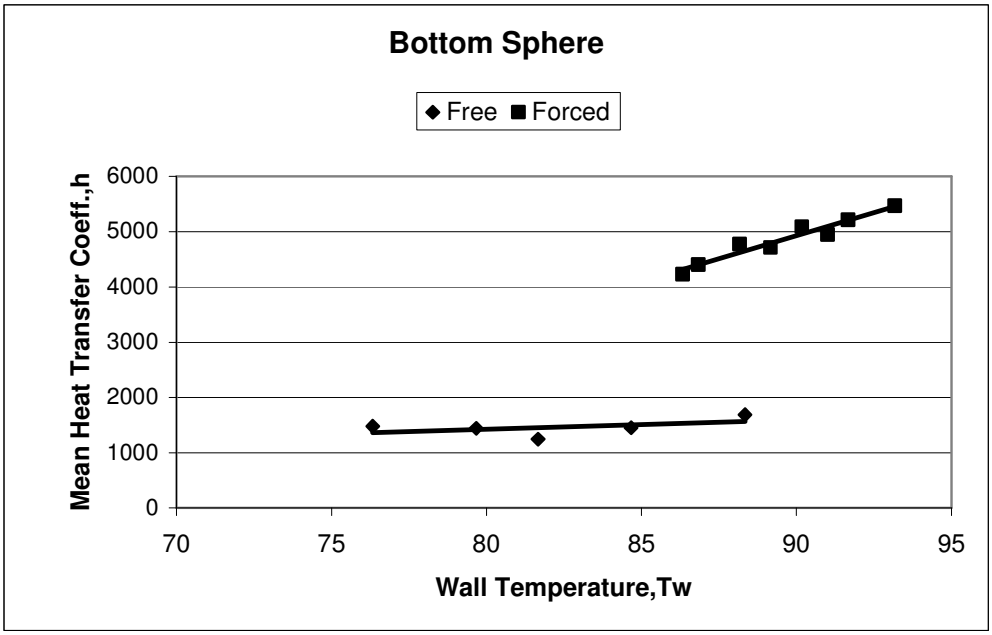

Figure 5.35 Comparison of Mean Heat Transfer Coefficients for 0^o of Inclination for Case-2,Bottom Sphere, Free and Forced Condensation.

5.1.5 Case 3 Annular Condensation in the Concentric Spheres

The tests were conducted at 0^o inclination angle and at 20^oC-30^oC-40^oC-50^oC-60^oC cooling water inlet temperatures for free and forced condensations.

The calculated equation for mass flow rate is as follows.

$$m_1(t)=-001829457.(t-t1)+m_1 \quad (5.9)$$

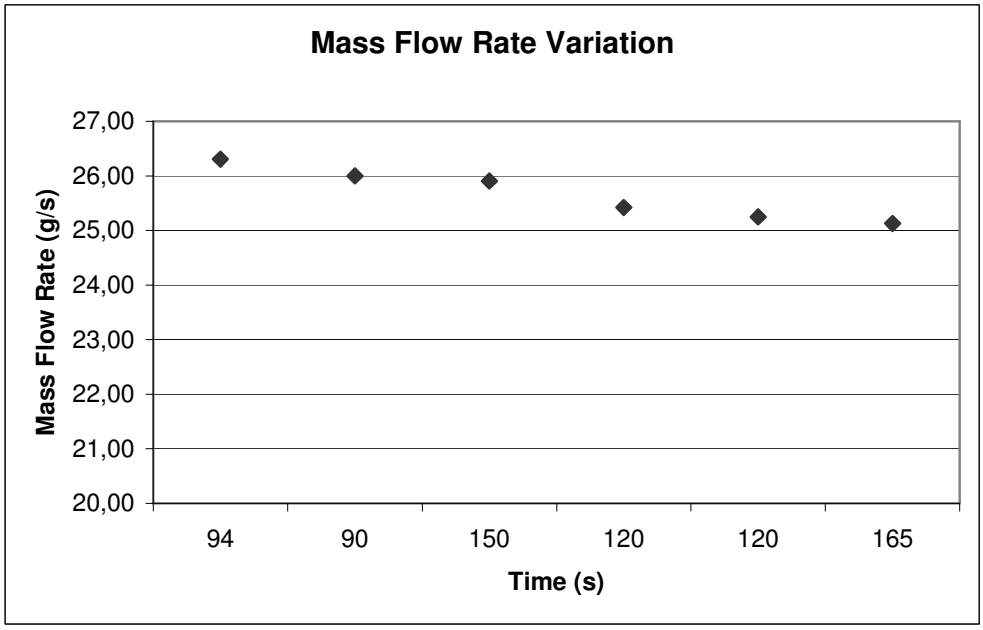

Figure 5.36 Experimental Mass Flow Rate Variation with respect to Time for Annular Condensation in Concentric Spheres.

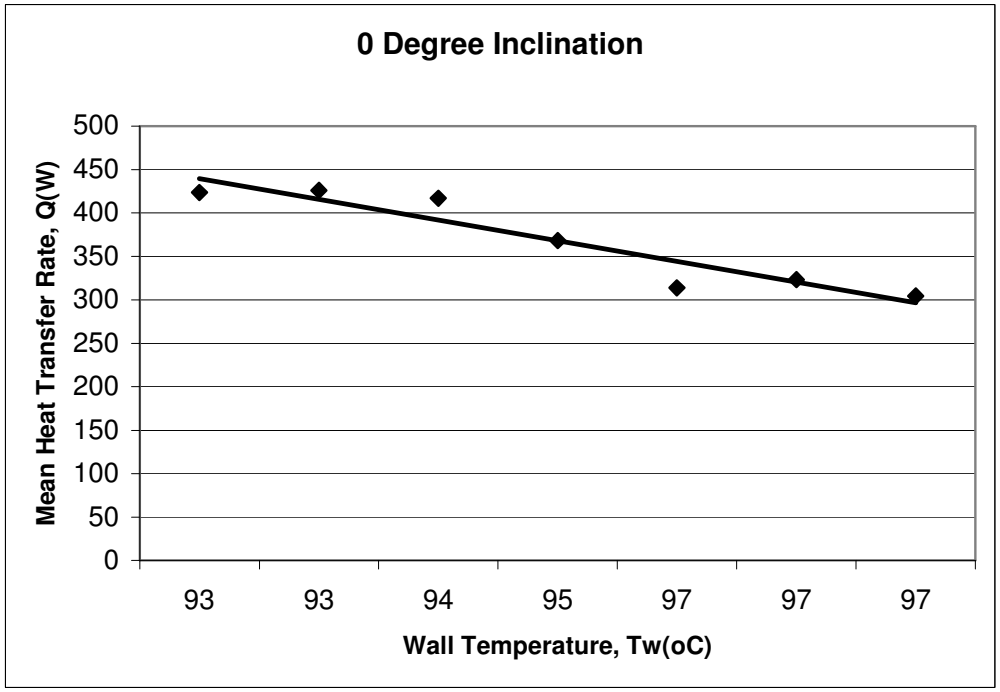

Figure 5.37 Variation of Mean Heat Transfer Rate for 0^o of Inclination for Annular Condensation in Concentric Spheres.

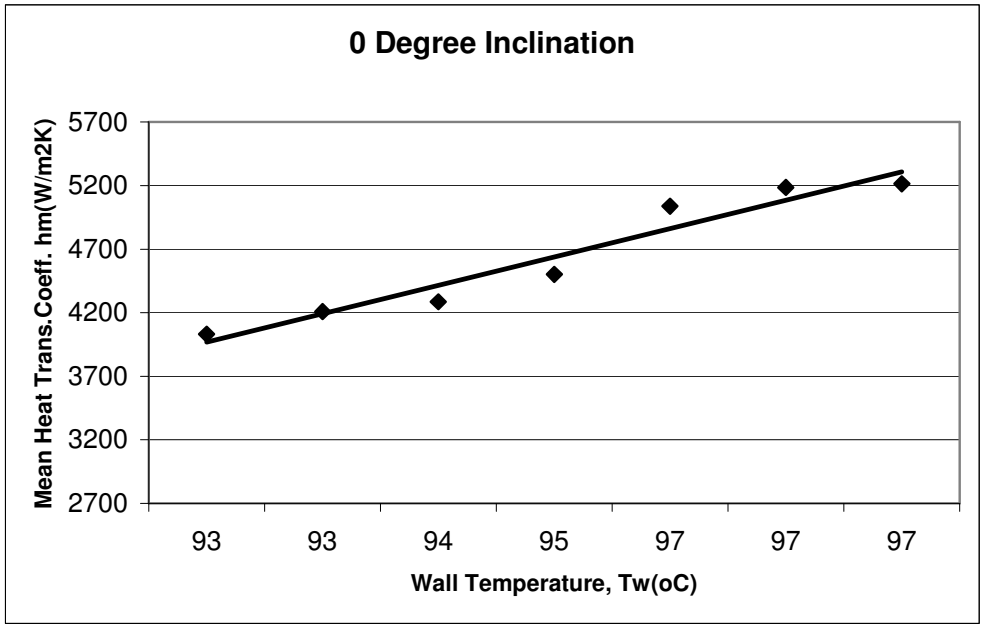

Figure 5.38 Variation of Mean Heat Transfer Coefficient for 0^o of Inclination for Annular Condensation in Concentric Spheres.

It is seen from the above figures that the expected results were obtained. As wall temperature increases heat transfer rate decreases and mean heat transfer coefficient increases. This means when subcooling decreases film thickness decreases. When film thickness decreases heat transfer coefficient increases. When the vapour velocity increases film thickness decreases so heat transfer coefficient increases.

5.1.6 Comparison of Free and Forced Condensation for Case-3

The pressure value was measured as 2.75 bars. This means that the vapour flows 2.75 times greather than the atmospheric pressure. From the following figures it is seen that when vapour velocity increases the heat transfer rate and heat transfer coefficient increase.

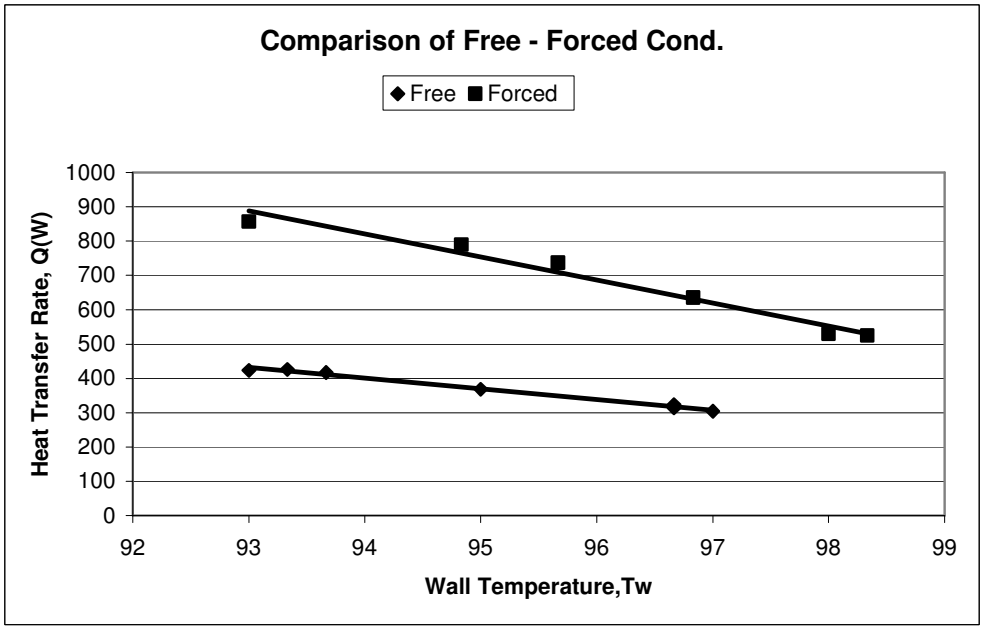

Figure 5.39 Comparison of Heat Transfer Rate for Free and Forced Condensation for Annular Condensation in Concentric Spheres.

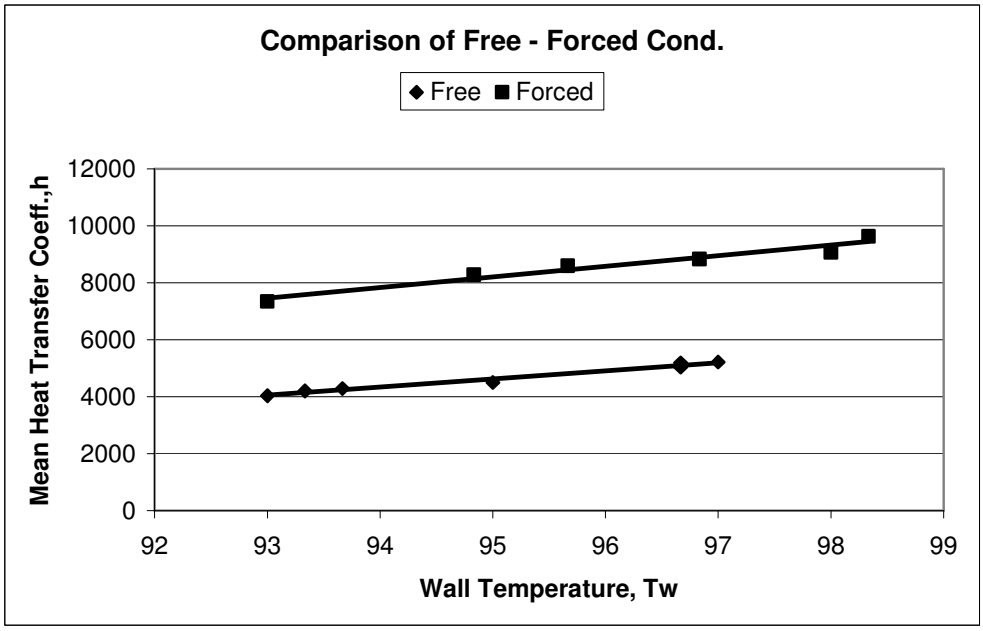

Figure 5.40 Comparison of Mean Heat Transfer Coefficient for Free and Forced Condensation for Annular Condensation in Concentric Spheres.

5.1.7 Effect of Wall Temperature

It is seen from the above figures that when the wall temperature increases near to the saturation temperature the heat transfer rate decreases due to the subcooling. The increase in the wall temperature yields to decrease in subcooling. Also when the heat transfer rate increases the film thickness also increases and it results in lower heat transfer coefficients. So when the wall temperature approaches to the saturation temperature mean heat transfer coefficient increases. Also from these figures it is seen that the upper sphere has higher heat transfer rates and heat transfer coefficients then the middle and bottom spheres. The cause is the condensation flow. The condensation coming from the upper sphere to the middle sphere and from it to the bottom sphere results in thicker condensation thickness and it prevents the heat transfer and the heat transfer rate and mean heat transfer coefficient decrase.

5.1.8 Effect of Subcooling

It is seen from the above figures that when the subcooling decreases heat transfer rate decreases but the mean heat transfer coefficient increases. The reason for decrease of subcooling is the decrease of condensate film thickness. It means the heat transfer coefficient increases. Also the subcooling decreases at the bottom spheres because of the cooling effect of the condensate coming from upper sphere.

5.1.9 Effect of Inclination Angle

It is shown from the above figures that when the inclination angle increases the heat transfer rate and heat transfer coefficient increase at the middle and bottom spheres. Because of the inclination angle the cooling effect of the condesate falling from upper sphere to lower sphere reduces and also subcooling reduces. So when the degree is 30 the condenaste coming from

upper sphere does not touch the lower sphere. This means that as the inclination angle increases the condensate film thickness reduces at the upper stagnation point of the lower spheres and these result in increase of heat transfer coefficient and heat transfer rate.

5.1.10 Effect of Sphere Diameter

It is seen from the above figures for case-1 that if the diameter of the sphere gets bigger, the heat transfer rate and mean heat transfer coefficients get smaller. It confirms that the film tchickness gets bigger and makes a barrier to heat transfer.

5.1.11 Effect of Vapour Velocity

It seen the figures for case2 and case3 that if the vapour velocity increases the heat transfer rate and mean heat transfer coefficient increase. So at higher vapour velocity the condensate film is to be sweeping to down in a high velocity. And it makes the film thickness to decrease. In case-2 and case-3 experimentes the vapour velocity was measured as 2.75 bar. It means that the vapour flows 2.75 times faster than atmospheric pressure. The exact velocity could not measured because the copper selenoid did not work properly.

5.2 Analytical Results

The analytical model was established based on the Nusselt type of analysis. In analytical study the Newton-Raphson Method was used. To do this the equations were obtained by using an integral control volume. From integral conservation of mass and conservation of momentum principles two equations were obtained. Then these two equations were transformed into finete difference equations. By using these equations velocity at the interface (where $y=\delta$) and film thickness at the condensate layer were obtained.

To make these calculations by numerically a computer program MathCad V11 was used.

In this chapter the film thickness, the velocity at the interface, the heat transfer coefficient are analyzed.

Since linear temperature distribution and only conduction type of heat transfer through the condensate are assumed at the beginning of the analysis, heat fluxes can be calculated by Fourier's law of conduction:

$$q = k\frac{(T_{sat} - T_w)}{\delta} \tag{5.10}$$

Heat transfer coefficients for the condensate can be calculated by the convection heat transfer formula:

$$h_{cond} = \frac{q}{(T_{sat} - T_w)} \tag{5.11}$$

The analytical results were obtained for Ø60mm o.d. sphere and ΔT=8K. The other properties used are given in Appendix D.

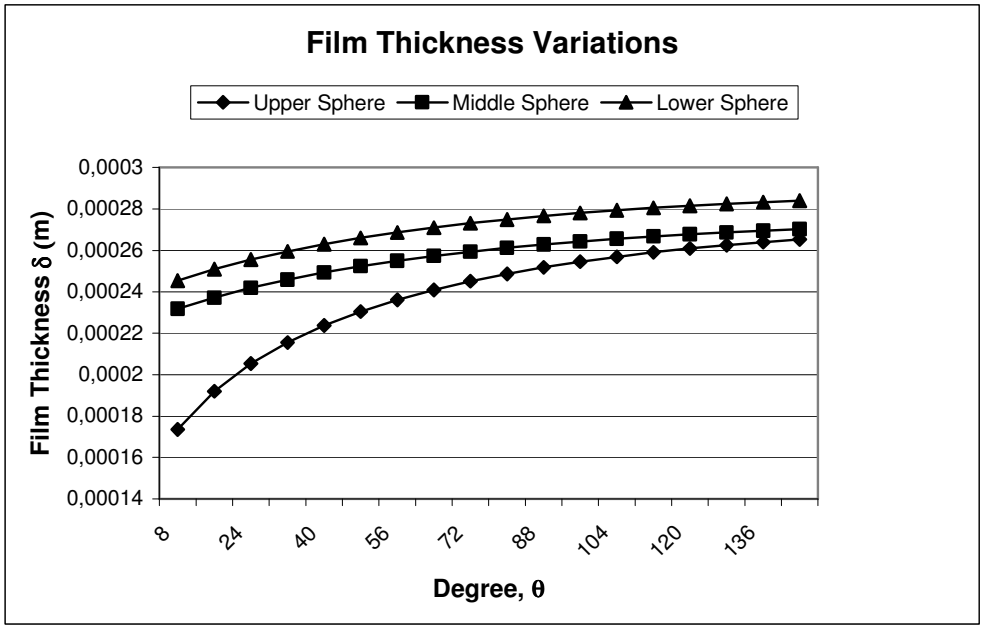

Figure 5.41 Variation of Film Thickness with Angular Position at D=60mm and ΔT=8K

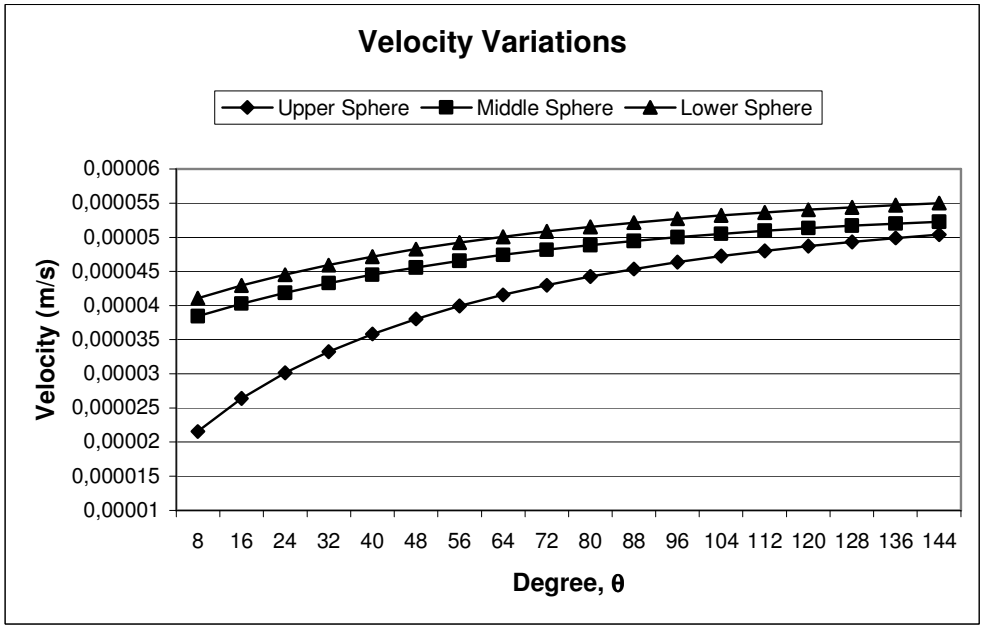

Figure 5.42 Variation of Velocity of the Condensate with Angular Position at D=60mm and ΔT=8K

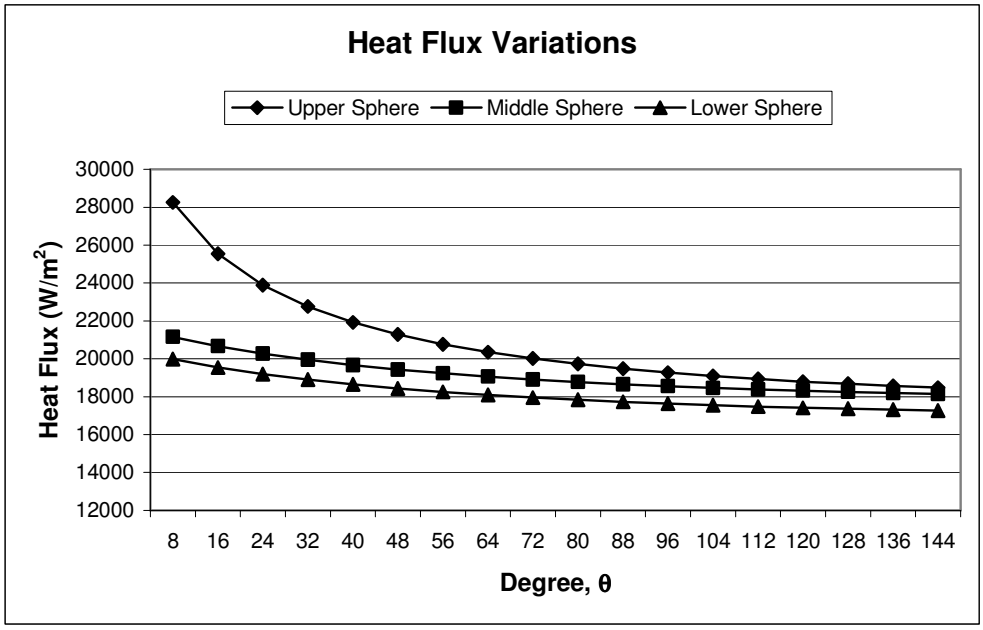

Figure 5.43 Variation of Heat Flux with Angular Position at D=60mm and ΔT=8K

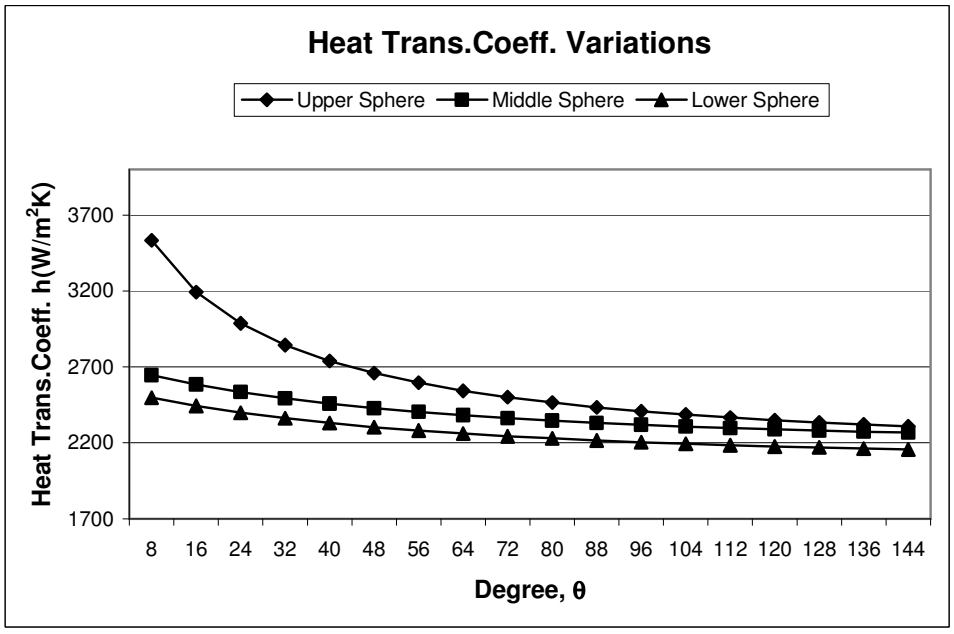

Figure 5.44 Variation of Heat Transfer Coefficient with Angular Position at D=60mm and ΔT=8K

5.3 Comparison of the Analytical and Experimental Studies

After obtaining the analytical and experimental results for Ø60mm o.d. spheres, the heat transfer rate and mean heat transfer coefficients are compared. The mean heat transfer coefficinets for analytical study were calculated by taking the arithmetic average of the local heat transfer coefficients.

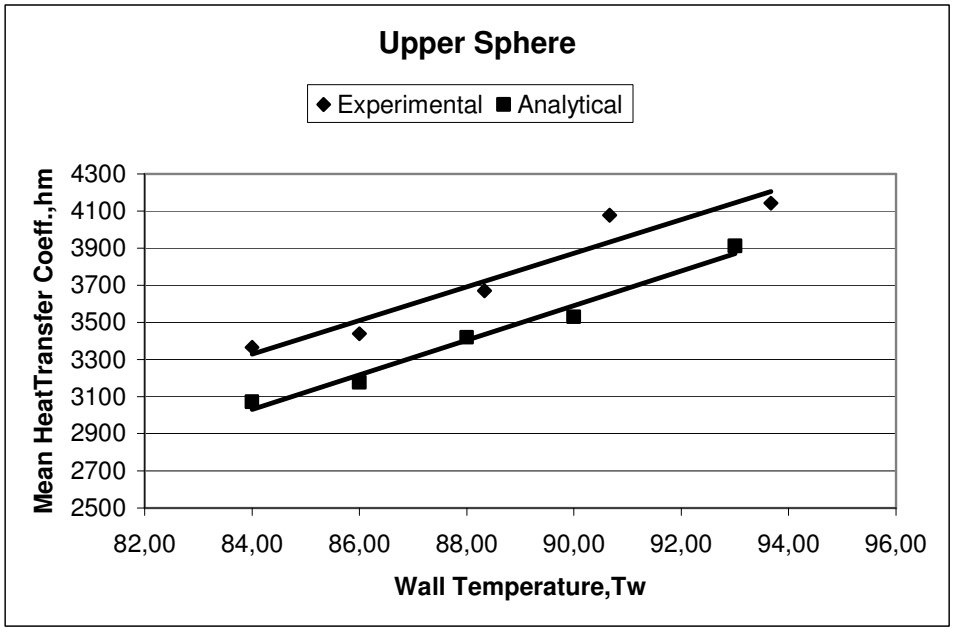

Figure 5.45 Comparison of Mean Heat Transfer Coefficients for Analytical and Experimental Studies for Upper Sphere.

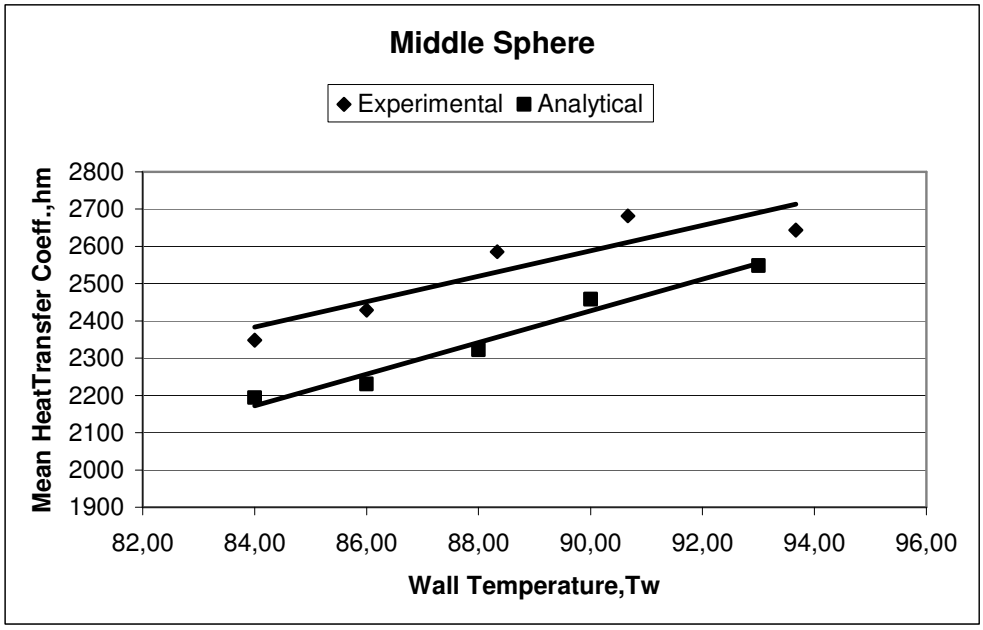

Figure 5.46 Comparison of Mean Heat Transfer Coefficients for Analytical and Experimental Studies for Middle Sphere.

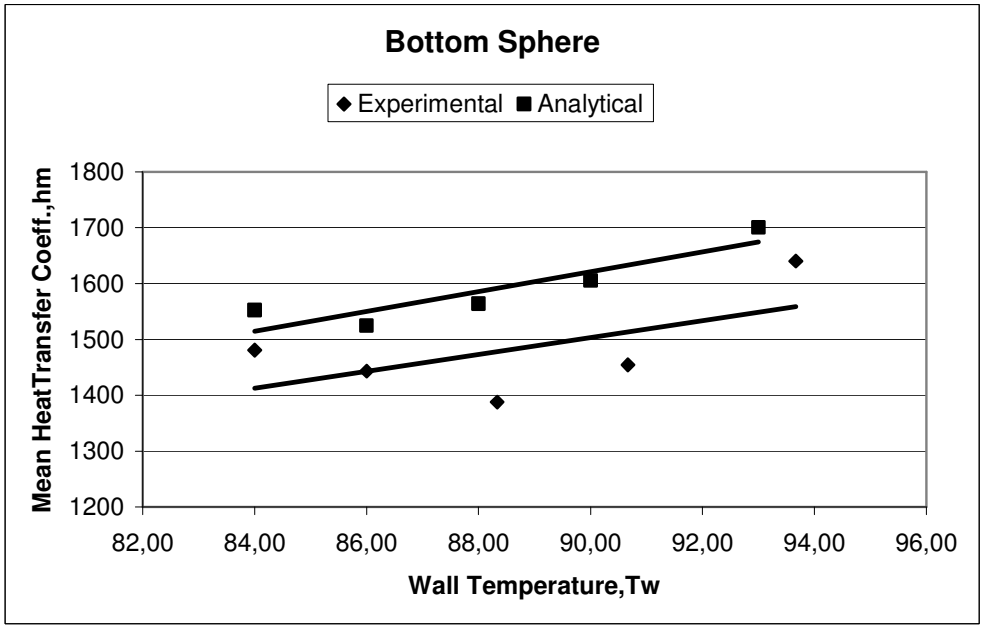

Figure 5.47 Comparison of Mean Heat Transfer Coefficients for Analytical and Experimental Studies for Bottom Sphere.

5.4 Comparison of the Experimental Results with Literature

The heat transfer coefficient for a sphere can be calculated from the Nusselt's original formula for the radial systems. In order to compare Nusselt's analysis with the present study, mean heat transfer coefficient values of the upper sphere are compared with the following formula:

$$\bar{h}_{m,sph} = 0.815\left[\frac{g\rho_f(\rho_f-\rho_v)k_f^3 h_{fg}}{\mu_f(T_{sat}-T_w)D}\right]^{1/4} \tag{5.12}$$

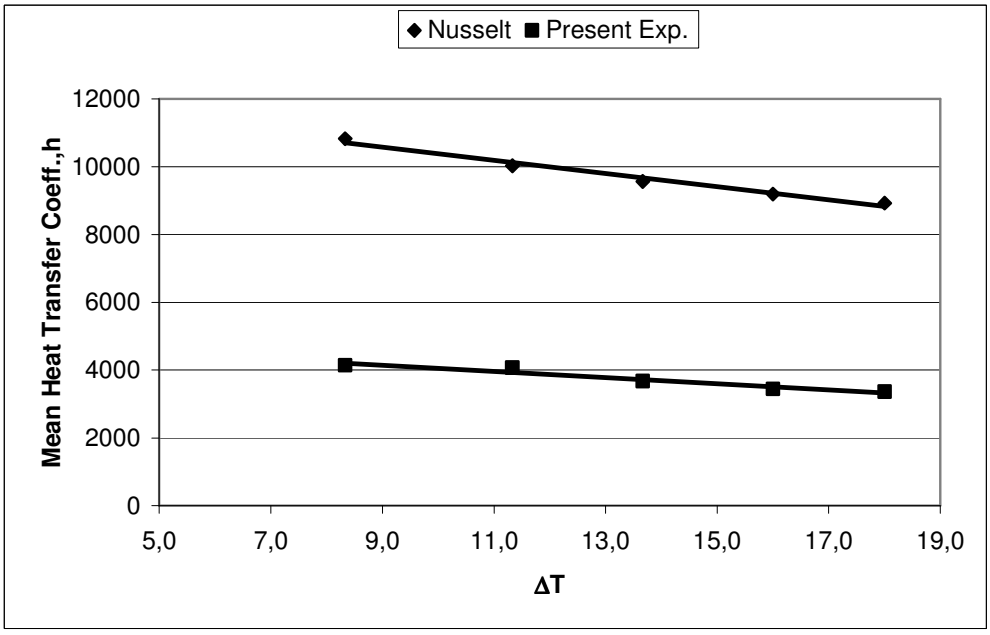

Figure 5.48 Comparison of Mean Heat Transfer Coefficients Between the Present Experimental Study and the Nusselt Analysis for Sphere.

5.5 Comparison of Sphere and Cylinder Results

The heat transfer coefficient for a horizontal tube can be calculated from the Nusselt's original formula for the radial systems. In order to compare Nusselt's analysis with the present study, heat transfer coefficient values of the upper sphere are compared with the following formula.

$$h_{m,cyl} = 0.729\left[\frac{\rho_l(\rho_l - \rho_v)gk^3h_{fg}}{\mu(T_{sat} - T_w)D}\right] \tag{5.13}$$

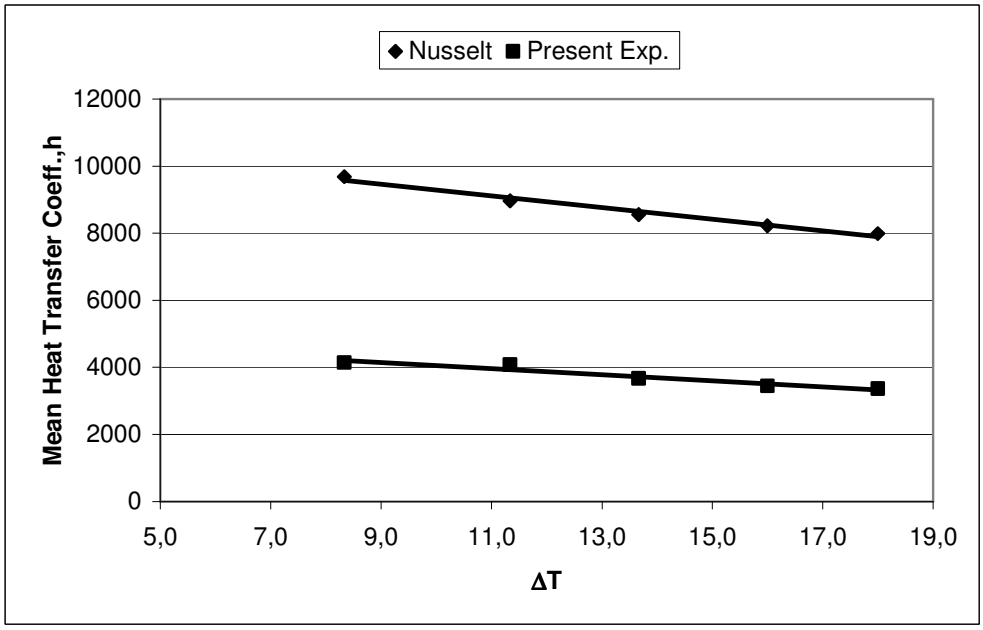

Figure 5.49 Comparison of Mean Heat Transfer Coefficients Between the Present Experimental Study and the Nusselt Analysis for Cylinder.

CHAPTER 6

6 CONCLUSIONS

6.1 Discussion

- The diameter of sphere affects heat flux and mean heat transfer coefficient. It is seen fron free condensation experiment that heat flux and mean heat transfer coefficient are bigger in Ø50mm sphere than Ø60mm sphere.
- The increase in wall temperature results in a decrease in heat transfer rate and subcooling but an increase in mean heat transfer coefficient.
- The increasing of the subcooling increases heat transfer rate and condensate thickness but decreases heat transfer coefficient.
- The increasing of the inclination angle makes the heat transfer rate and heat transfer coefficient higher than the lower angles for middle and bottom spheres.
- At the first experimental study Ø60 mm o.d and Ø57mm i.d. spheres were used. At second experiment Ø60mm o.d. and Ø40mm i.d. spheres were used. According to the results when the wall thickness of the sphere increases the heat transfer from condensate to water by conduction reduces.
- The pressure was 2.75 bar in forced condensation tests. In high pressure value the heat transfer rate and heat transfer coefficients increase. The sweeping effect plays an important role for higher velocity. It makes the condensate thickness smaller.

- The height of the cooling water tank was increased from 200cm to 300cm at the second experimental study. This revision makes the water pressure higher and eliminates the mass flow rate decrease when the water level in the tank reduces.
- At the first experimental study 2 thermocouples were used per each sphere. But at the second experimental study 3 thermocouples were used per each sphere. So when the number of thermocouples increases the wall temperature measurement could be more exact. So at the first experimental study the wall temperatures were somewhat bigger than the real values.
- The constant called as “axis” assumed in the Mathcad program to obtain the film thickness for lower spheres at the upper stagnation point. The reason of thin film thickness for bottom sphere may be this constant. For cylinder it can be used. But in sphere it can not run right.

6.2 Observations

- The bonding of hemispheres to each other is very important. The only way to make a sphere whose inside is empty is machining two hemisphere and bonding them to each other. The bonding operation is very sensitive at first experimental study because no welding material was used, only metal bonder was used.
- The polishing of these spheres was taken 5 hours per sphere. So the polishing process is important to obtain uniform boundary layer over the sphere surface. The rough surface may effect the heat transfer rate and coefficient.
- The air discharge valve to eliminate the air inside the test section was used. This operation made the condensation well.
- At least 4 thermocouple must be placed over one sphere to obtain more accurate wall temperature results. But in these studies it was not possible because of the narrow area in the test section.

- At first experimental study the used thermocouples are very stiff because they have a protective case. So the mounting of spheres was very hard. To do this these thermocouples were pull out and elastic covered thermocouples were bonded on the surface.
- A thermostat was used to heat the cooling water to desired value. But a digital thermostat is more suitable for these purpose. Because by the analog thermostat the temperature can not be adjusted to desired value exactly. So the readings for inlet water temperature were $2^{o}C$ or $3^{o}C$ different from the desired value.
- The placing of the thermocouples on the spheres are important. If the degree between the thermocouples was different for each sphere the temperature readings are different for each sphere from the real values.
- Also the inclination direction is important. In these studies the inclination direction was to the thermocouple direction. So the intense condensation affects the temperature readings.
- To give an inclination angle to the test section a mechanism can be used. In these studies 5 different block of metal were used to give an inclination to the test section.
- To obtain more accurate temperature readings the bonding of thermocouples to the surface of sphere is important.

REFERENCES

1. Michael Ming Chen, An Analytical Study of Laminar Film Condensation: Part 2 –Single and Multiple Horizontal Tubes, *Journal of Heat Transfer-Transactıon of the Asme*, pp. 55-60, 1961

2. E. M. Sparrow and J. L. Gregg, A Boundary – Layer Treatment of Laminar – Film Condensation, Journal of Heat Transfer-*Transactıon of the Asme*, pp. 13 -18, 1959.

3. Cz. O. Popıel and L. Boguslawskı, Heat Transfer by Laminar Film Condensation on Sphere Surfaces, *Int. J. Heat Mass Transfer*, pp.1486-1488, 1975.

4. S. B. Memory and V. H. Adams and P. J. Marto, Free and Forced Convection Laminar Film Condensation on Horizontal Elliptical Tubes, *Int. J. Heat Mass Transfer*, Vol. 40, pp. 3395-3406, 1997.

5. Ravi Kumar, H. K. Varma, Bikash Mohanty, K. N. Agrawal, Augmentatıon of Outside Tube Heat Transfer Coefficent During Condensation of Steam Over Horızontal Copper Tubes, *Int. Comm. Heat Mass Transfer*, Vol. 25, pp. 81-91, 1998.

6. M. Mosaad, Combined Free and Forced Convection Laminar Film Condensatıon On An İnclined Circular Tube With Isothermal Surface, *Internatıonal Journal of Heat and Mass Transfer*, Vol. 42, pp. 4017-4025, 1999.

7. C.H.Hsu and S.A.Yang, Pressure Gradient and Variable Wall Temperature Effects During Filmwise Condensation From Downward Flowing Vapors Onto a Horizontal Tube, *Internatıonal Journal of Heat and Mass Transfer*, Vol. 42, pp. 2419-2426, 1999.

8. S. S. Kutateladze and I. I. Gogonın, Investigation of Heat Transfer in Film Condensation of Flowing Vapour on Horizontal Tube Banks, *Int. J. Heat Mass Transfer*, Vol. 28, pp.1831-1836, 1985.

9. Georg Peter Fıeg and Wılfrıed Roetzel, Calculatıon of Laminar Film Condensation ın/on Inclined Elliptical Tubes, *Int. J. Heat Mass Transfer*, Vol. 37, pp. 619-624, 1994.

10. Stuart W. Churchıll, Laminar Film Condensatıon, *Int. J. Heat Mass Transfer,* Vol. 29, pp.1219-1226, 1986.

11. T. Fujıı, H. Uehara, K. Hırata and K. Oda, Heat Transfer and Flow Resıstance ın Condensatıon of Low Pressure Steam Flowıng Through Tube Banks, *Int. J. Heat Mass Transfer*, Vol. 15, pp.247-260, 1972.

12. E. S. Gaddıs, Solutıon Of The Two Phase Boundary-Layer Equatıons For Lamınar Film Condensatıon of Vapour Flowıng Perpendıcular To a Horızontal Cylınder*, Int. J. Heat Mass Transfer*, Vol. 22, pp.371-382, 1979.

13. Tetsu Fujıı, Haruo Uehara and Chıkatoshı Kurata, Lamınar Filmwıse Condensatıon of Flowıng Vapour on a Horızontal Cylınder*, Int. J. Heat Mass Transfer,* Vol. 15, pp. 235-246, 1972.

14. J. W. Rose, Effect of Pressure Gradıent ın Forced Convectıon Fılm Condensatıon on a Horızontal Tube, *Int. J. Heat Mass Transfer*, Vol. 27, pp. 39-47, 1984.

15. Nusselt, W., Die Oberflachen-Kondensation des Wasserdampfes, *Zeitschrift des Vereines deutscher Ingenieure*, 60, pp.541-546, 569-575, 1916.

16. Karabulut, H. and Ataer, Ö.E., Numerical Analysis of Laminar Filmwise Condensation, *International Journal of Refrigeration*, Vol.19, No.2, pp.117-123, 1996.

17. Kakaç, S. and Yener, Y., Convective Heat Transfer Second Edition, pp.81-90, 1995.

APPENDIX A

RESULTS OF THE FREE CONDENSATION EXPERIMENT

Table A.1 Experimental Results for 0^o Inclination Angle, D=Ø60mm.

EXPERIMENTAL RESULTS FOR D=Ø60mm AND 0^O OF INCLINATION					
T1 (^{o}C)	23	29	39	51	60
T2 (^{o}C)	32	37	46	58	66
T3 (^{o}C)	30	35	45	57	65
T4 (^{o}C)	30	35	45	57	65
T5 (^{o}C)	90	93	95	97	97
T6 (^{o}C)	80	82	88	90	96
T7 (^{o}C)	85	87	90	91	92
T8 (^{o}C)	62	74	80	85	88
T9 (^{o}C)	78	83	86	88	89
T10 (^{o}C)	57	73	76	82	85
Tw1 (^{o}C)	85	87,5	91,5	93,5	96,5
Tw2 (^{o}C)	73,5	80,5	85	88	90
Tw3 (^{o}C)	67,5	78	81	85	87
Q1(W)	256,8	214,24	179,42	167,32	130,99
Q2(W)	215,73	200,23	166,06	145,24	132,2
Q3(W)	178,8	149,72	129,96	135,25	100,01
h1(W/m^{2}K)	1374,2	1358,7	1617	1910	2492,3
h2(W/m^{2}K)	671,63	836,26	888,6	956,54	1029
h3(W/m^{2}K)	456,96	557,31	556,35	723,73	611,63

Table A.2 Experimental Results for 12^{o} Inclination Angle, D=Ø60mm.

EXPERIMENTAL RESULTS FOR D=Ø60mm AND 12^{O} OF INCLINATION					
T1 (^{o}C)	25	30	40	50	59
T2 (^{o}C)	33	37	47	57	65
T3 (^{o}C)	32	36	46	56	64
T4 (^{o}C)	31	35	45	55	64
T5 (^{o}C)	90	94	96	96	97
T6 (^{o}C)	77	82	90	95	96
T7 (^{o}C)	88	90	92	93	94
T8 (^{o}C)	70	73	78	85	90
T9 (^{o}C)	81	83	88	90	92
T10 (^{o}C)	57	62	70	85	89
Tw1 (^{o}C)	83,5	88	93	95,5	96,5
Tw2 (^{o}C)	79	81,5	85	89	92
Tw3 (^{o}C)	69	72,5	79	87,5	90,5
Q1(W)	248,02	219,03	204,08	187,78	156,05
Q2(W)	219,38	202,62	193,59	178,15	148,72
Q3(W)	198,54	177,94	160,67	152,87	143,86
h1(W/m^{2}K)	1213,4	1442,5	2184	2923	2969
h2(W/m^{2}K)	853,74	889,62	1035,9	1271,1	1414,8
h3(W/m^{2}K)	531,19	534,53	625,28	969,49	1173

Table A.3 Experimental Results for 20° Inclination Angle, D=Ø60mm.

EXPERIMENTAL RESULTS FOR D=Ø60mm AND 20° OF INCLINATION					
T1 (°C)	24	30	40	51	59
T2 (°C)	34	40	49	59	66
T3 (°C)	33	39	48	58	65
T4 (°C)	33	39	48	58	65
T5 (°C)	92	93	95	96	98
T6 (°C)	85	89	92	95	96
T7 (°C)	90	90	95	95	96
T8 (°C)	83	85	90	93	95
T9 (°C)	88	89	92	93	95
T10 (°C)	80	85	87	91	92
Tw1 (°C)	88,5	91	93,5	95,5	97
Tw2 (°C)	86,5	87,5	92,5	94	95,5
Tw3 (°C)	84	87	89,5	92	93,5
Q1(W)	316,13	299,84	241,02	214,62	203,78
Q2(W)	300,12	288,26	227,19	210,5	190,32
Q3(W)	275,73	265,45	219,52	200,78	192,43
h1(W/m^{2}K)	2165,3	2567,1	2751,4	3340,9	4361,6
h2(W/m^{2}K)	1772,1	1828,1	2288,4	2574,6	2962,6
h3(W/m^{2}K)	1388,6	1623,3	1634,3	1910	2196,7

Table A.4 Experimental Results for 30° Inclination Angle,D=Ø60mm.

EXPERIMENTAL RESULTS FOR D=Ø60mm AND 30° OF INCLINATION					
T1 (°C)	25	29	40	49	59
T2 (°C)	35	39	49	58	67
T3 (°C)	34	38	48	57	66
T4 (°C)	34	38	47	56	66
T5 (°C)	92	93	96	97	98
T6 (°C)	85	90	93	94	95
T7 (°C)	90	91	95	96	97
T8 (°C)	83	86	91	93	95
T9 (°C)	89	90	92	93	94
T10 (°C)	80	85	88	91	93
Tw1 (°C)	88,5	91,5	94,5	95,5	96,5
Tw2 (°C)	86,5	88,5	93	94,5	96
Tw3 (°C)	84,5	87,5	90	92	93,5
Q1(W)	376,24	354,63	314,37	304,09	288,66
Q2(W)	324,12	308,73	297,36	286,17	270,84
Q3(W)	314,13	295,94	284,73	271,66	268,43
h1(W/m^{2}K)	2577	3196	4140,8	4733,7	5492
h2(W/m^{2}K)	1913,8	2114,6	3182,3	3769,4	4400
h3(W/m^{2}K)	1630	1876,8	2216,1	2584,3	3064,3

Table A.5 Experimental Results for 0^o of Inclination Angle,D=Ø50mm.

EXPERIMENTAL RESULTS FOR D=Ø50mm AND 0^O OF INCLINATION					
T1 (^{o}C)	23	29	39	51	60
T2 (^{o}C)	33	38	46,5	58	66,5
T3 (^{o}C)	31	36	46	57,5	65,5
T4 (^{o}C)	31	35,5	46	57	65,5
T5 (^{o}C)	92	94	96	97,5	98
T6 (^{o}C)	82	84	89	91	96,5
T7 (^{o}C)	87	89	91	92	93
T8 (^{o}C)	68	78	83	87	89
T9 (^{o}C)	81	85	88	89	91
T10 (^{o}C)	60	76	78	83	87
Tw1 (^{o}C)	87	89	92,5	94,25	97,25
Tw2 (^{o}C)	77,5	83,5	87	89,5	91
Tw3 (^{o}C)	70,5	80,5	83	86	89
q1(W/m^2)	36920	31185	24874	21649	18362
q2(W/m^2)	31900	30226	25068	20359	18816
q3(W/m^2)	26440	20986	19619	17500	14235
h1(W/m^{2}K)	2637,1	2598,8	2926,3	3207,3	4896,4
h2(W/m^{2}K)	1357,5	1727,2	1790,6	1770,3	1881,6
h3(W/m^{2}K)	866,87	1023,7	1089,9	1166,7	1186,2

Table A.6 Experimental Results for 12^o of Inclination Angle,D=Ø50mm.

EXPERIMENTAL RESULTS FOR D=Ø50mm AND 12^O OF INCLINATION					
T1 (^{o}C)	25	30	40	50	59
T2 (^{o}C)	34	38	48	57,5	65,5
T3 (^{o}C)	33	37	47	56	65
T4 (^{o}C)	33	36,5	46	55,5	64,5
T5 (^{o}C)	91	94,5	96	96,5	97
T6 (^{o}C)	78	84	92	96	96
T7 (^{o}C)	90	91	92,5	94	95
T8 (^{o}C)	73	75	80	87	91
T9 (^{o}C)	84	86	88	91	92,5
T10 (^{o}C)	63	65	73	86	90
Tw1 (^{o}C)	84,5	89,25	94	96,25	96,5
Tw2 (^{o}C)	81,5	83	86,25	90,5	93
Tw3 (^{o}C)	73,5	75,5	80,5	88,5	91,25
q1(W/m^2)	36103	32388	30178	26032	21874
q2(W/m^2)	32440	30586	29223	23051	23092
q3(W/m^2)	34251	29930	24947	21758	20476
h1(W/m^{2}K)	2188,1	2756,5	4311,1	5480,4	4860,9
h2(W/m^{2}K)	1663,6	1699,2	1981,2	2195,4	2886,5
h3(W/m^{2}K)	1245,5	1173,7	1216,9	1740,6	2100,1

Table A.7 Experimental Results for 20^o of Inclination Angle,D=Ø50mm.

EXPERIMENTAL RESULTS FOR D=Ø50mm AND 20^O OF INCLINATION					
T1 (^{o}C)	24	30	42	50	59
T2 (^{o}C)	34,5	40	51	58,5	66,5
T3 (^{o}C)	33	39	50	57,5	66
T4 (^{o}C)	33	38	50	57	65,5
T5 (^{o}C)	93	94	95,5	96	98,5
T6 (^{o}C)	87	91	92,5	95	96
T7 (^{o}C)	92	92,5	95	96	97,5
T8 (^{o}C)	86	87	91	92	95
T9 (^{o}C)	90	90	92,5	93,5	95,5
T10 (^{o}C)	83	84	88	91	92,5
Tw1 (^{o}C)	90	92,5	94	95,5	97,25
Tw2 (^{o}C)	89	89,75	93	94	96,25
Tw3 (^{o}C)	86,5	87	90,25	92,25	94
q1(W/m^2)	42950	38796	31185	29505	28250
q2(W/m^2)	38833	37298	29396	29182	28729
q3(W/m^2)	35677	30530	28403	25979	26974
h1(W/m^{2}K)	3904,5	4564,2	4455,1	5364,5	7533,3
h2(W/m^{2}K)	3236,1	3315,4	3674,5	4168,8	6048,3
h3(W/m^{2}K)	2460,5	2180,7	2642,2	2969,1	3853,4

Table A.8 Experimental Results for 30^o of Inclination Angle,D=Ø50mm.

EXPERIMENTAL RESULTS FOR D=Ø50mm AND 30^O OF INCLINATION					
T1 (^{o}C)	23	31	41	50	58
T2 (^{o}C)	33	40	50	58	65
T3 (^{o}C)	32	39	49	57	65
T4 (^{o}C)	32	38,5	48	57	65
T5 (^{o}C)	93	94	97	97,5	98,5
T6 (^{o}C)	87	91	94	94,5	96
T7 (^{o}C)	92	93	95,5	96	97
T8 (^{o}C)	85	89	92	93,5	95
T9 (^{o}C)	91	91	94	94	96
T10 (^{o}C)	84	87	90	92	93,5
Tw1 (^{o}C)	90	92,5	95,5	96	97,25
Tw2 (^{o}C)	88,5	91	93,75	94,75	96
Tw3 (^{o}C)	87,5	89	92	93	94,75
q1(W/m^2)	48682	41297	40676	34975	32681
q2(W/m^2)	41938	35509	38475	32400	35044
q3(W/m^2)	40645	31910	36841	35150	34732
h1(W/m^{2}K)	4425,6	4858,5	7395,7	6995	8715
h2(W/m^{2}K)	3355	3550,9	5306,9	5183,9	7008,8
h3(W/m^{2}K)	3010,8	2659,1	4093,4	4393,8	5557,1

APPENDIX B

RESULTS OF THE FREE&FORCED CONDENSATION EXPERIMENTS

Table B.1 Experimental Results for 0^o Inclination Angle,D=Ø60mm.

EXPERIMENTAL RESULTS OF FREE CONDENSATİON 0^O OF INCLINATION					
T1 (^{o}C)	25	30	36	48	56
T3 (^{o}C)	30	35	40	52	59
T2 (^{o}C)	29	34	39	51	58
T4 (^{o}C)	28	33	38	50	58
T5 (^{o}C)	93	94	95	95	97
T6 (^{o}C)	85	87	90	92	95
T7 (^{o}C)	74	77	80	85	89
T8 (^{o}C)	92	93	94	95	96
T9 (^{o}C)	81	83	86	87	94
T10 (^{o}C)	70	74	82	83	89
T11 (^{o}C)	87	90	92	94	94
T12 (^{o}C)	75	77	80	83	88
T13 (^{o}C)	67	72	73	77	83
T14 (^{o}C)	76	81	82	83	84
T15 (^{o}C)	56	60	63	69	75
T16(^{o}C)	72	78	80	82	85
T17(^{o}C)	48	51	55	61	61
T18(^{o}C)	67	70	75	77	80
T19(^{o}C)	41	44	47	50	55
T20(^{o}C)	102	102	102	102	102
Tw1(^{o}C)	84	86	88,333333	90,666667	93,666667
Tw2(^{o}C)	81	83,333333	87,333333	88,333333	93
Tw3(^{o}C)	76,333333	79,666667	81,666667	84,666667	88,333333
Q1(W)	707,65723	642,80626	586,06553	539,70381	403,23122
Q2(W)	576,00829	529,54764	442,87073	428,09162	277,89916
Q3(W)	443,92389	376,46434	296,18443	294,45984	269,09731
h1(W/m^{2}K)	3365,9496	3439,6739	3671,4764	4077,1339	4142,7865
h2(W/m^{2}K)	2348,3704	2428,8205	2585,251	2681,8302	2643,6374
h3(W/m^{2}K)	1480,7993	1443,2031	1247,1273	1454,4578	1685,7917

Table B.2 Experimental Results for 5° Inclination Angle,D=Ø60mm.

EXPERIMENTAL RESULTS OF FREE CONDENSATİON 5° OF INCLINATION					
T1(°C)	25	31	39	48	56
T3(°C)	30	36	43	51	59
T2 (°C)	29	35	42	51	58
T4(°C)	28	34	41	50	58
T5(°C)	92	93	95	97	98
T6(°C)	86	88	91	93	95
T7(°C)	74	77	82	87	90
T8(°C)	90	91	92	93	95
T9(°C)	75	78	83	85	89
T10(°C)	71	73	75	81	86
T11(°C)	86	88	89	91	93
T12(°C)	72	76	80	84	87
T13(°C)	65	72	76	81	84
T14(°C)	73	76	80	83	85
T15(°C)	56	58	63	69	75
T16(°C)	71	73	76	78	80
T17(°C)	44	45	48	54	60
T18(°C)	67	69	72	75	77
T19(°C)	40	42	45	48	51
T20(°C)	102	102	102	102	102
Tw1(°C)	84	86	89,3333	92,3333	94,3333
Tw2(°C)	78,6667	80,6667	83,3333	86,3333	90
Tw3(°C)	74,3333	78,6667	81,6667	85,3333	88
Q1(W)	732,294	695,327	604,346	442,125	427,892
Q2(W)	505,672	446,571	438,96	434,932	304,113
Q3(W)	439,949	398,04	300,163	291,026	289,105
h1(W/m^{2}K)	3483,13	3720,72	4084,89	3915,85	4778,42
h2(W/m^{2}K)	1855,45	1792,21	2013,33	2376,85	2169,75
h3(W/m^{2}K)	1361,45	1460,52	1263,88	1495	1768,01
h1loc up	5611,72	6046,16	7094,81	7696,67	10595,6
h1loc down	1362,97	1352,99	1326,72	1147,07	1356,84
h2loc up	2465,1	2436,28	2804,29	3641,14	3977,88
h2loc down	746,446	670,768	695,967	775,778	619,929
h3loc up	1722,32	2065,59	1864,74	2421,9	3157,16
h3loc down	607,53	567,98	450,857	461,419	485,335

Table B.3 Experimental Results for 10° Inclination Angle,D=Ø60mm.

EXPERIMENTAL RESULTS OF FREE CONDENSATİON 10° OF INCLINATION					
T1(°C)	25	32	37	46	49
T3(°C)	30	37	41	50	52
T2 (°C)	28	35	40	49	51
T4(°C)	28	35	40	48,5	51
T5(°C)	92	93	97	97	98
T6(°C)	87	90	91	94	95
T7(°C)	77	79	81	82	89
T8(°C)	90	91	92	93	95
T9(°C)	76	79	84	86	92
T10(°C)	72	74	77	82	88
T11(°C)	87	88	88	90	92
T12(°C)	75	79	83	85	87
T13(°C)	71	73	78	80	86
T14(°C)	75	78	81	82	84
T15(°C)	56	61	63	68	73
T16(°C)	72	75	77	78	79
T17(°C)	43	48	49	58	60
T18(°C)	68	72	73	75	75
T19(°C)	42	45	47	53	58
T20(°C)	102	102	102	102	102
Tw1(°C)	85,3333	87,3333	89,6667	91	94
Tw2(°C)	79,3333	81,3333	84,3333	87	91,6667
Tw3(°C)	77,6667	80	83	85	88,3333
Q1(W)	749,209	719,187	612,928	584,626	448,062
Q2(W)	499,105	490,332	481,305	450,6	342,818
Q3(W)	439,651	430,891	424,837	362,695	307,574
h1(W/m^{2}K)	3848,68	4198,24	4254,87	4550,33	4795,18
h2(W/m^{2}K)	1885,22	2031,31	2332,51	2571,92	2840,41
h3(W/m^{2}K)	1546,9	1676,88	1914,37	1826,63	1926,83
h1loc up	6234,86	6869,85	7244,77	8273,33	10789,2
h1loc down	1394,45	1501,81	1345,56	1472,17	1322,81
h2loc up	2495,14	2653,81	3300,72	4115,07	6322,2
h2loc down	724,265	777,416	777,502	876,79	698,831
h3loc up	2161,43	2286,65	2921,94	2901,11	3806,66
h3loc down	627,355	647,217	661,329	633,727	598,485

Table B.4 Experimental Results for 15° Inclination Angle,D=Ø60mm.

EXPERIMENTAL RESULTS OF FREE CONDENSATİON 15° OF INCLINATION				
T1(°C)	25	33	39	49
T3(°C)	31	38	43,5	53
T2 (°C)	29	36,5	42,5	52
T4(°C)	29	36,5	42,5	52
T5(°C)	93	94	96	97
T6(°C)	88	91	92	95
T7(°C)	78	81	83	87
T8(°C)	91	92	94	94
T9(°C)	80	83	86	88
T10(°C)	75	77	81	84
T11(°C)	89	90	92	93
T12(°C)	80	83	86	88
T13(°C)	76	78	81	82
T14(°C)	74	75	76	77
T15(°C)	58	61	63	67
T16(°C)	70	71	73	74
T17(°C)	43	48	53	54
T18(°C)	67	68	70	72
T19(°C)	40	44	50	52
T20(°C)	102	102	102	102
Tw1(°C)	86,333333	88,666667	90,333333	93
Tw2(°C)	82	84	87	88,666667
Tw3(°C)	81,666667	83,666667	86,333333	87,666667
Q1(W)	876,36491	758,05788	671,05093	624,48232
Q2(W)	666,66785	599,81796	588,70005	529,98139
Q3(W)	584,60879	528,39691	515,22824	457,29171
h1(W/m^{2}K)	4789,2283	4867,6662	4924,5421	5940,6613
h2(W/m^{2}K)	2853,8863	2853,0154	3360,1601	3403,1339
h3(W/m^{2}K)	2461,5798	2467,607	2815,66	2731,5131
h1loc up	8559,4718	9857,0241	10974,694	16501,837
h1loc down	1705,2555	1582,9809	1473,1536	1527,5986
h2loc up	4566,2182	4913,5266	6496,3095	7146,5812
h2loc down	967,4191	951,00514	1028,6204	945,31498
h3loc up	4237,1456	4576,2893	5751,1354	5717,1204
h3loc down	807,2923	779,99071	848,30783	783,03375

Table B.5 Experimental Results for 20° Inclination Angle,D=Ø60mm.

EXPERIMENTAL RESULTS OF FREE CONDENSATİON 20° OF INCLINATION				
T1(°C)	24	34	40	50
T3(°C)	30	39	44	53
T2 (°C)	28	37,5	43	52,5
T4(°C)	28	37	43	52,5
T5(°C)	93	94	97	98
T6(°C)	89	91	95	96
T7(°C)	78	85	86	92
T8(°C)	92	94	95	97
T9(°C)	80	83	87	90
T10(°C)	78	82	85	87
T11(°C)	90	91	92	94
T12(°C)	80	84	85	90
T13(°C)	78	79	80	85
T14(°C)	72	76	77	82
T15(°C)	57	64	72	78
T16(°C)	69	73	78	83
T17(°C)	46	53	60	62
T18(°C)	67	67	70	73
T19(°C)	44	50	50	56
T20(°C)	102	102	102	102
Tw1(°C)	86,666667	90	92,666667	95,333333
Tw2(°C)	83,333333	86,333333	89	91,333333
Tw3(°C)	82,666667	84,666667	85,666667	89,666667
Q1(W)	876,36491	753,69445	598,42804	493,42974
Q2(W)	667,46385	598,14875	512,41524	440,60666
Q3(W)	585,40479	450,1004	451,48253	390,73805
h1(W/m^{2}K)	4893,3419	5377,3862	5489,494	6336,8545
h2(W/m^{2}K)	3061,3863	3268,8106	3374,7052	3536,5474
h3(W/m^{2}K)	2592,4279	2223,2304	2366,5914	2712,4541
h1loc up	9573,9298	11651,003	14704,002	19010,564
h1loc down	1667,3609	1698,122	1707,8426	1760,2374
h2loc up	5412,0936	6050,7771	6230,225	6299,4751
h2loc down	1020,4621	1045,1299	1044,5516	943,07932
h3loc up	4693,1885	4489,2151	4636,5872	6377,9325
h3loc down	864,14264	741,07679	743,35243	727,25218

Table B.6 Experimental Results of Forced Condensation for 0^o Inclination Angle, D=Ø60mm.

EXPERIMENTAL RESULTS OF FORCED CONDENSATION 0^O OF INCLINATION								
T1(^{o}C)	25	29	39	43	47	51	55	57,5
T3(^{o}C)	32	35,5	45,5	49	52,5	56	60	62
T2(^{o}C)	31	35	44,5	48	52	56	59,5	61,5
T4(^{o}C)	30,5	34,5	44,5	48	52	55,5	59,5	61,5
T5(^{o}C)	96	97	98	99	99	99	99,5	100
T6(^{o}C)	88	89,5	90,5	91,5	92,5	94	95	96
T7(^{o}C)	81	82,5	83,5	84,5	86,5	88,5	89,5	91,5
T8(^{o}C)	94	96	97	98	98	98	98,5	99
T9(^{o}C)	89	90	91,5	92,5	93	94	94,5	95,5
T10(^{o}C)	80	80	82	83	84	84,5	86	88
T11(^{o}C)	93	93	94	95	95	96	97	98
T12(^{o}C)	88	89	90	91	92	93	93,5	94,5
T13(^{o}C)	78	78,5	80,5	81,5	83,5	84	84,5	87
T14(^{o}C)	103	103	103	103	103	103	103	103
Tw1(^{o}C)	88,33	89,67	90,67	91,67	92,67	93,83	94,67	95,83
Tw2(^{o}C)	87,67	88,67	90,17	91,17	91,67	92,17	93	94,17
Tw3(^{o}C)	86,33	86,83	88,17	89,17	90,17	91	91,67	93,17
Q1(W)	954,3	888,8	881,5	817,5	745,3	680,3	674,7	608,5
Q2(W)	830,4	833,5	754,9	689,4	691,3	694	615,9	550,1
Q3(W)	773,8	779,8	770,6	706,4	702,8	635	628,7	564,2
h1(W/m^{2}K)	5978	6170	6659	6773	6837	7132	7877	8448
h2(W/m^{2}K)	4960	5352	5462	5448	5727	6043	5859	6012
h3(W/m^{2}K)	4229	4402	4769	4713	5085	4942	5209	5469

APPENDIX C

RESULTS OF THE ANNULAR CONDENSATION IN THE CONCENTRIC SPHERES EXPERIMENT

Table C.1 Experimental Results of Free Condensation for 0^o Inclination Angle, D=Ø60mm.

EXPERIMENTAL RESULTS OF FREE CONDENSATİON FOR 2 SPHERES ONE WITHIN THE OTHER							
T1(^{o}C)	22	29	33	37,5	41	48	51
T2(^{o}C)	26	33	37	41	44	51	54
T3(^{o}C)	100	100	100	100	101	101	101
T4(^{o}C)	91	92	92	93	95	95	96
T5(^{o}C)	88	88	89	92	94	94	94
T6(^{o}C)	102	102	102	102	102	102	102
Tw1(^{o}C)	93	93,333	93,667	95	96,667	96,667	97
Q1(W)	423,69	426,07	417,11	368,14	313,86	323,01	304,55
h1(W/m^{2}K)	4030,5	4209,1	4285,4	4502,7	5038,5	5185,4	5214,9

Table C.2 Experimental Results of Forced Condensation for 0^o Inclination Angle, D=Ø60mm.

EXPERIMENTAL RESULTS OF FORCED CONDENSATİON FOR 2 SPHERES ONE WITHIN THE OTHER						
T1(^{o}C)	20	27	32,0	37	43	45
T2(^{o}C)	28	34,5	39,0	43	48	50
T3(^{o}C)	100	101,5	102,0	102,5	103	103
T4(^{o}C)	90	93	94,0	95	97	97
T5(^{o}C)	89	90	91,0	93	94	95
T6(^{o}C)	103	103	103,0	103	103	103
Tw1(^{o}C)	93	94,833	95,667	96,833	98	98,333
Q1(W)	856,94	789,74	736,66	635,82	529,54	525,07
h1(W/m^{2}K)	7336,8	8279,4	8600,5	8827,6	9067,5	9633,1

APPENDIX D

MATHCAD PROGRAM SOURCE

Tablo D.1 Values of Properties for Mathcad Program

$r \equiv 30 \cdot 10^{-3}$	$\rho_f \equiv 963$	$k_f \equiv 613 \cdot 10^{-3}$	$T_w \equiv 365$
$g \equiv 9.81$	$\rho_g \equiv 0.596$	$C_{pw} \equiv 4180$	$T_s \equiv 373$
$\mu \equiv 3.062 \cdot 10^{-4}$	$\nu \equiv 0.318 \cdot 10^{-6}$	$h \equiv 5 \cdot 10^{-3}$	$\Delta T \equiv 8$
$h_g \equiv 2676 \cdot 10^{3}$	$h_{fg} \equiv 2278 \cdot 10^{3}$	$axis2 := 0.4$	

result :=

$neq \leftarrow 18$

$\Delta x \leftarrow \frac{\pi \cdot r}{40}$

$xloc \leftarrow \Delta x$

for $i \in 0 .. neq$

$\delta_i \leftarrow \left[\frac{\nu \cdot r \cdot (3 \cdot k_f \cdot \Delta T)}{g \cdot \rho_f \cdot h_{fg}}\right]^{\frac{1}{4}}$

$U\omega_i \leftarrow \frac{g \cdot \rho_f \cdot (\delta_i)^2 \cdot \sin\left(\frac{xloc}{r}\right)}{2 \cdot \mu}$

$xloc \leftarrow xloc + \Delta x$

$\delta inc \leftarrow \frac{\delta_{18}}{1000}$

$Uinc \leftarrow \frac{U\omega_{18}}{1000}$

for $iter \in 1 .. 20$

$C_0 \leftarrow \frac{5}{4\,r} \cdot \cos\left(\frac{\Delta x}{r}\right) \cdot \delta_0 \cdot U\omega_0 + \frac{5}{4} \cdot \frac{\delta_0 \cdot U\omega_0 - 0}{\Delta x} - \frac{k_f \cdot \Delta T}{\rho_f \cdot h_{fg} \cdot \delta_0} \cdot \sin\left(\frac{\Delta x}{r}\right)$

$C_1 \leftarrow \frac{34}{35} \cdot \pi \cdot \rho_f \cdot \cos\left(\frac{\Delta x}{r}\right) \cdot \delta_0 \cdot (U\omega_0)^2 + \frac{34}{35} \cdot \pi \cdot r \cdot \rho_f \cdot \left[\frac{\delta_0 \cdot (U\omega_0)^2 - 0}{\Delta x}\right] - 2 \cdot \pi \cdot r^2 \cdot \delta_0 \cdot \rho_f \cdot g \cdot \left(\sin\left(\frac{\Delta x}{r}\right)\right)^2 + \frac{3}{2} \cdot \mu \cdot \frac{U\omega_0}{\delta_0}$

$\psi(0,0) \leftarrow \frac{\left[\frac{5}{4 \cdot r} \cdot \cos\left(\frac{\Delta x}{r}\right) \cdot (\delta_0 + \delta inc) \cdot U\omega_0 + \frac{5}{4} \cdot \frac{(\delta_0 + \delta inc) \cdot U\omega_0 - 0}{\Delta x} - \frac{k_f \cdot \Delta T}{\rho_f \cdot h_{fg} \cdot (\delta_0 + \delta inc)} \cdot \sin\left(\frac{\Delta x}{r}\right)\right] - \left(\frac{5}{4\,r} \cdot \cos\left(\frac{\Delta x}{r}\right) \cdot \delta_0 \cdot U\omega_0 + \frac{5}{4} \cdot \frac{\delta_0 \cdot U\omega_0 - 0}{\Delta x} - \frac{k_f \cdot \Delta T}{\rho_f \cdot h_{fg} \cdot \delta_0} \cdot \sin\left(\frac{\Delta x}{r}\right)\right)}{\delta inc}$

$\psi(0,1) \leftarrow \frac{\left[\frac{5}{4\,r} \cdot \cos\left(\frac{\Delta x}{r}\right) \cdot \delta_0 \cdot (U\omega_0 + Uinc) + \frac{5}{4} \cdot \frac{\delta_0 \cdot (U\omega_0 + Uinc) - 0}{\Delta x}\right] - \left(\frac{5}{4 \cdot r} \cdot \cos\left(\frac{\Delta x}{r}\right) \cdot \delta_0 \cdot U\omega_0 + \frac{5}{4} \cdot \frac{\delta_0 \cdot U\omega_0 - 0}{\Delta x}\right)}{Uinc}$

$$\psi(1,0) \leftarrow \frac{\left[\frac{34}{35}\cdot\pi\cdot\rho_f\cdot\cos\left(\frac{\Delta x}{r}\right)\cdot(\delta_0+\delta inc)\cdot(U\omega_0)^2+\frac{34}{35}\cdot\pi\cdot r\cdot\rho_f\cdot\left[\frac{(\delta_0+\delta inc)\cdot(U\omega_0)^2-0}{\Delta x}\right]-(\delta_0+\delta inc)\cdot 2\cdot\pi\cdot r^2\cdot\rho_f\cdot g\cdot\left(\sin\left(\frac{\Delta x}{r}\right)\right)^2+\frac{3}{2}\cdot\mu\cdot\frac{U\omega_0}{(\delta_0+\delta inc)}\right]-\blacksquare\ldots}{+\left[\frac{34}{35}\cdot\pi\cdot\rho_f\cdot\cos\left(\frac{\Delta x}{r}\right)\cdot\delta_0\cdot(U\omega_0)^2+\frac{34}{35}\cdot\pi\cdot r\cdot\rho_f\cdot\left[\frac{\delta_0\cdot(U\omega_0)^2-0}{\Delta x}\right]-\delta_0\cdot 2\cdot\pi\cdot r^2\cdot\rho_f\cdot g\cdot\left(\sin\left(\frac{\Delta x}{r}\right)\right)^2+\frac{3}{2}\cdot\mu\cdot\frac{U\omega_0}{\delta_0}\right]}{\delta inc}$$

$$\psi(1,1) \leftarrow \frac{\left[\frac{34}{35}\cdot\pi\cdot\rho_f\cdot\cos\left(\frac{\Delta x}{r}\right)\cdot\delta_0\cdot(U\omega_0+Uinc)^2+\frac{34}{35}\cdot\pi\cdot r\cdot\rho_f\cdot\left[\frac{\delta_0\cdot(U\omega_0+Uinc)^2-0}{\Delta x}\right]-\delta_0\cdot 2\cdot\pi\cdot r^2\cdot\rho_f\cdot g\cdot\left(\sin\left(\frac{\Delta x}{r}\right)\right)^2+\frac{3}{2}\cdot\mu\cdot\frac{(U\omega_0+Uinc)}{\delta_0}\right]-\blacksquare\ldots}{+\left[\frac{34}{35}\cdot\pi\cdot\rho_f\cdot\cos\left(\frac{\Delta x}{r}\right)\cdot\delta_0\cdot(U\omega_0)^2+\frac{34}{35}\cdot\pi\cdot r\cdot\rho_f\cdot\left[\frac{\delta_0\cdot(U\omega_0)^2-0}{\Delta x}\right]-\delta_0\cdot 2\cdot\pi\cdot r^2\cdot\rho_f\cdot g\cdot\left(\sin\left(\frac{\Delta x}{r}\right)\right)^2+\frac{3}{2}\cdot\mu\cdot\frac{U\omega_0}{\delta_0}\right]}{Uinc}$$

$$del \leftarrow -\left(\psi^{-1}\cdot C\right)$$

$$\delta_0 \leftarrow \delta_0 + del_0$$

$$U\omega_0 \leftarrow U\omega_0 + del_1$$

for $ie \in 1..neq$

for $iter \in 1..20$

$$C_0 \leftarrow \frac{5}{8\cdot r}\cdot\cos\left(\frac{\Delta x}{r}\right)\cdot\delta_{ie}\cdot U\omega_{ie}+\frac{5}{8}\cdot\frac{\delta_{ie}\cdot U\omega_{ie}-\delta_{ie-1}\cdot U\omega_{ie-1}}{\Delta x}-\frac{k_f\cdot\Delta T}{\rho_f\cdot h_{fg}\cdot\delta_{ie}}\cdot\sin\left(\frac{\Delta x}{r}\right)$$

$$C_1 \leftarrow \frac{34}{35}\cdot\pi\cdot\rho_f\cdot\cos\left(\frac{\Delta x}{r}\right)\cdot\delta_{ie}\cdot(U\omega_{ie})^2+\frac{34}{35}\cdot\pi\cdot r\cdot\rho_f\cdot\frac{\left[(\delta_{ie})\cdot(U\omega_{ie})^2-\delta_{ie-1}\cdot(U\omega_{ie-1})^2\right]}{\Delta x}-\delta_{ie}\cdot 2\cdot\pi\cdot r^2\cdot\rho_f\cdot g\cdot\left(\sin\left(\frac{\Delta x}{r}\right)\right)^2+\frac{3}{2}\cdot\mu\cdot\frac{U\omega_{ie}}{\delta_{ie}}$$

$$\psi(0,0) \leftarrow \frac{\left[\frac{5}{4\cdot r}\cdot\cos\left(\frac{\Delta x}{r}\right)\cdot(\delta_{ie}+\delta inc)\cdot U\omega_{ie}+\frac{5}{4}\cdot\frac{(\delta_{ie}+\delta inc)\cdot U\omega_{ie}-\delta_{ie-1}\cdot U\omega_{ie-1}}{\Delta x}-\frac{k_f\cdot\Delta T}{\rho_f\cdot h_{fg}\cdot(\delta_{ie}+\delta inc)}\cdot\sin\left(\frac{\Delta x}{r}\right)\right]-\blacksquare\ldots}{+\left(\frac{5}{4\cdot r}\cdot\cos\left(\frac{\Delta x}{r}\right)\cdot\delta_{ie}\cdot U\omega_{ie}+\frac{5}{4}\cdot\frac{\delta_{ie}\cdot U\omega_{ie}-\delta_{ie-1}\cdot U\omega_{ie-1}}{\Delta x}-\frac{k_f\cdot\Delta T}{\rho_f\cdot h_{fg}\cdot\delta_{ie}}\cdot\sin\left(\frac{\Delta x}{r}\right)\right)}{\delta inc}$$

$$\psi_{0,1} \leftarrow \frac{\left[\frac{5}{4\cdot r}\cdot\cos\left(\frac{\Delta x}{r}\right)\cdot\delta_{ie}\cdot\left(U\omega_{ie}+Uinc\right)+\frac{5}{4}\cdot\frac{\delta_{ie}\cdot\left(U\omega_{ie}+Uinc\right)-\delta_{ie-1}\cdot U\omega_{ie-1}}{\Delta x}\right]-\left(\frac{5}{4\cdot r}\cdot\cos\left(\frac{\Delta x}{r}\right)\cdot\delta_{ie}\cdot U\omega_{ie}+\frac{5}{4}\cdot\frac{\delta_{ie}\cdot U\omega_{ie}-\delta_{ie-1}\cdot U\omega_{ie-1}}{\Delta x}\right)}{Uinc}$$

$$\psi_{1,0} \leftarrow \frac{\left[\frac{34}{35}\cdot\pi\cdot\rho_f\cdot\cos\left(\frac{\Delta x}{r}\right)\cdot\left(\delta_{ie}+\delta inc\right)\cdot\left(U\omega_{ie}\right)^2+\frac{34}{35}\cdot\pi\cdot r\cdot\rho_f\cdot\frac{\left[\left(\delta_{ie}+\delta inc\right)\cdot\left(U\omega_{ie}\right)^2-\delta_{ie-1}\cdot\left(U\omega_{ie-1}\right)^2\right]}{\Delta x}-\left(\delta_{ie}+\delta inc\right)\cdot 2\cdot\pi\cdot r^2\cdot\rho_f\cdot g\cdot\left(\sin\left(\frac{\Delta x}{r}\right)\right)^2+\frac{3}{2}\cdot\mu\cdot\frac{U\omega_{ie}}{\left(\delta_{ie}+\delta inc\right)}\right]-\blacksquare\ldots}{\delta inc}$$
$$+\left[\frac{34}{35}\cdot\pi\cdot\rho_f\cdot\cos\left(\frac{\Delta x}{r}\right)\cdot\delta_{ie}\cdot\left(U\omega_{ie}\right)^2+\frac{34}{35}\cdot\pi\cdot r\cdot\rho_f\cdot\frac{\left[\delta_{ie}\cdot\left(U\omega_{ie}\right)^2-\delta_{ie-1}\cdot\left(U\omega_{ie-1}\right)^2\right]}{\Delta x}-\delta_{ie}\cdot 2\cdot\pi\cdot r^2\cdot\rho_f\cdot g\cdot\left(\sin\left(\frac{\Delta x}{r}\right)\right)^2+\frac{3}{2}\cdot\mu\cdot\frac{U\omega_{ie}}{\delta_{ie}}\right]$$

$$\psi_{1,1} \leftarrow \frac{\left[\frac{34}{35}\cdot\pi\cdot\rho_f\cdot\cos\left(\frac{\Delta x}{r}\right)\cdot\delta_{ie}\cdot\left(U\omega_{ie}+Uinc\right)^2+\frac{34}{35}\cdot\pi\cdot r\cdot\rho_f\cdot\frac{\left[\delta_{ie}\cdot\left(U\omega_{ie}+Uinc\right)^2-\delta_{ie-1}\cdot\left(U\omega_{ie-1}\right)^2\right]}{\Delta x}-\delta_{ie}\cdot 2\cdot\pi\cdot r^2\cdot\rho_f\cdot g\cdot\left(\sin\left(\frac{\Delta x}{r}\right)\right)^2+\frac{3}{2}\cdot\mu\cdot\frac{\left(U\omega_{ie}+Uinc\right)}{\delta_{ie}}\right]-\blacksquare\ldots}{Uinc}$$
$$+\left[\frac{34}{35}\cdot\pi\cdot\rho_f\cdot\cos\left(\frac{\Delta x}{r}\right)\cdot\delta_{ie}\cdot\left(U\omega_{ie}\right)^2+\frac{34}{35}\cdot\pi\cdot r\cdot\rho_f\cdot\frac{\left[\delta_{ie}\cdot\left(U\omega_{ie}\right)^2-\delta_{ie-1}\cdot\left(U\omega_{ie-1}\right)^2\right]}{\Delta x}-\delta_{ie}\cdot 2\cdot\pi\cdot r^2\cdot\rho_f\cdot g\cdot\left(\sin\left(\frac{\Delta x}{r}\right)\right)^2+\frac{3}{2}\cdot\mu\cdot\frac{U\omega_{ie}}{\delta_{ie}}\right]$$

$$del \leftarrow -\left(\psi^{-1}\cdot C\right)$$

$$\delta_{ie} \leftarrow \delta_{ie} + del_0$$

$$U\omega_{ie} \leftarrow U\omega_{ie} + del_1$$

$$result1 \leftarrow augment(\delta, U\omega)$$

$$Um \leftarrow result1_{18,1}$$

$$v1 \leftarrow Um$$

$$\delta 1 \leftarrow result1_{18,0}$$

$$v2 \leftarrow \sqrt{v1^2 + 2\cdot g\cdot h}$$

$$\delta 2 \leftarrow \frac{\delta 1\cdot v1}{v2}$$

for $i \in 0 .. neq$

$$\delta_i \leftarrow \left[\frac{\nu \cdot (3 \cdot k_f \cdot \Delta T) \cdot r}{g \cdot \rho_f \cdot h_{fg}}\right]^{\frac{1}{4}}$$

$$U\omega_i \leftarrow \frac{g \cdot \rho_f \cdot (\delta_i)^2 \cdot \sin\left(\frac{xloc}{r}\right)}{2 \cdot \mu}$$

$xloc \leftarrow xloc + \Delta x$

$U\omega_0 \leftarrow v2$

$\Delta_0 \leftarrow \delta 2 \cdot axis2$

$\delta inc \leftarrow \frac{\delta_{18}}{1000}$

$Uinc \leftarrow \frac{U\omega_{18}}{1000}$

$h \leftarrow r \cdot \left(1 - \cos\left(\frac{\Delta x}{r}\right)\right)$

$U\omega_0 \leftarrow \sqrt{(v2)^2 + 2 \cdot g \cdot h}$

$\Delta_0 \leftarrow \frac{v2 \cdot \Delta_0}{U\omega_0}$

for $iter \in 1 .. 10$

$$C_0 \leftarrow \frac{5}{4 \cdot r} \cdot \cos\left(\frac{\Delta x}{r}\right) \cdot \delta_0 \cdot U\omega_0 + \frac{5}{4} \cdot \frac{\delta_0 \cdot U\omega_0 - 0}{\Delta x} - \frac{k_f \cdot \Delta T}{\rho_f \cdot h_{fg} \cdot (\delta_0 + \Delta_0)} \cdot \sin\left(\frac{\Delta x}{r}\right) + \frac{\Delta_0 \cdot U\omega_0 - \delta 2 \cdot axis2 \cdot v2}{\Delta x}$$

$$C_1 \leftarrow \frac{34}{35} \cdot \pi \cdot \rho_f \cdot \cos\left(\frac{\Delta x}{r}\right) \cdot \delta_0 \cdot (U\omega_0)^2 + \frac{34}{35} \cdot \pi \cdot r \cdot \rho_f \cdot \left[\frac{\delta_0 \cdot (U\omega_0)^2 - 0}{\Delta x}\right] - 2 \cdot \pi \cdot r^2 \cdot \delta_0 \cdot \rho_f \cdot g \cdot \left(\sin\left(\frac{\Delta x}{r}\right)\right)^2 + \frac{3}{2} \cdot \mu \cdot \frac{U\omega_0}{\delta_0} + \rho_f \cdot \left[\frac{\Delta_0 \cdot (U\omega_0)^2 - \delta 2 \cdot axis2 \cdot v2^2}{\Delta x}\right]$$

$$\psi(0,0) \leftarrow \frac{\left[\frac{5}{4\,r}\cdot\cos\left(\frac{\Delta x}{r}\right)\cdot(\delta_0+\delta inc)\cdot U\omega_0+\frac{5}{4}\cdot\frac{(\delta_0+\delta inc)\cdot U\omega_0-0}{\Delta x}-\frac{k_f\cdot\Delta T}{\rho_f\cdot h_{fg}\cdot(\delta_0+\delta inc+\Delta_0)}\cdot\sin\left(\frac{\Delta x}{r}\right)+\frac{\Delta_0\cdot U\omega_0-0}{\Delta x}\right]-\blacksquare\ldots}{+\left[\frac{5}{4\cdot r}\cdot\cos\left(\frac{\Delta x}{r}\right)\cdot\delta_0\cdot U\omega_0+\frac{5}{4}\cdot\frac{\delta_0\cdot U\omega_0-0}{\Delta x}-\frac{k_f\cdot\Delta T}{\rho_f\cdot h_{fg}\cdot(\delta_0+\Delta_0)}\cdot\sin\left(\frac{\Delta x}{r}\right)+\frac{\Delta_0\cdot U\omega_0-0}{\Delta x}\right]}{\delta inc}$$

$$\psi(0,1) \leftarrow \frac{\left[\frac{5}{4\cdot r}\cdot\cos\left(\frac{\Delta x}{r}\right)\cdot\delta_0\cdot(U\omega_0+Uinc)+\frac{5}{4}\cdot\frac{\delta_0\cdot(U\omega_0+Uinc)-0}{\Delta x}\right]-\left(\frac{5}{4\cdot r}\cdot\cos\left(\frac{\Delta x}{r}\right)\cdot\delta_0\cdot U\omega_0+\frac{5}{4}\cdot\frac{\delta_0\cdot U\omega_0-0}{\Delta x}\right)}{Uinc}$$

$$\psi(1,0) \leftarrow \frac{\left[\frac{34}{35}\cdot\pi\cdot\rho_f\cdot\cos\left(\frac{\Delta x}{r}\right)\cdot(\delta_0+\delta inc)\cdot(U\omega_0)^2+\frac{34}{35}\cdot\pi\cdot r\cdot\rho_f\cdot\left[\frac{(\delta_0+\delta inc)\cdot(U\omega_0)^2-0}{\Delta x}\right]-(\delta_0+\delta inc)\cdot 2\cdot\pi\cdot r^2\cdot\rho_f\cdot g\cdot\left(\sin\left(\frac{\Delta x}{r}\right)\right)^2+\frac{3}{2}\cdot\mu\cdot\frac{U\omega_0}{(\delta_0+\delta inc)}\right]-\blacksquare\ldots}{+\left[\frac{34}{35}\cdot\pi\cdot\rho_f\cdot\cos\left(\frac{\Delta x}{r}\right)\cdot\delta_0\cdot(U\omega_0)^2+\frac{34}{35}\cdot\pi\cdot r\cdot\rho_f\cdot\left[\frac{\delta_0\cdot(U\omega_0)^2-0}{\Delta x}\right]-\delta_0\cdot 2\cdot\pi\cdot r^2\cdot\rho_f\cdot g\cdot\left(\sin\left(\frac{\Delta x}{r}\right)\right)^2+\frac{3}{2}\cdot\mu\cdot\frac{U\omega_0}{\delta_0}\right]}{\delta inc}$$

$$\psi(1,1) \leftarrow \frac{\left[\frac{34}{35}\cdot\pi\cdot\rho_f\cdot\cos\left(\frac{\Delta x}{r}\right)\cdot\delta_0\cdot(U\omega_0+Uinc)^2+\frac{34}{35}\cdot\pi\cdot r\cdot\rho_f\cdot\left[\frac{\delta_0\cdot(U\omega_0+Uinc)^2-0}{\Delta x}\right]-\delta_0\cdot 2\cdot\pi\cdot r^2\cdot\rho_f\cdot g\cdot\left(\sin\left(\frac{\Delta x}{r}\right)\right)^2+\frac{3}{2}\cdot\mu\cdot\frac{(U\omega_0+Uinc)}{\delta_0}\right]-\blacksquare\ldots}{+\left[\frac{34}{35}\cdot\pi\cdot\rho_f\cdot\cos\left(\frac{\Delta x}{r}\right)\cdot\delta_0\cdot(U\omega_0)^2+\frac{34}{35}\cdot\pi\cdot r\cdot\rho_f\cdot\left[\frac{\delta_0\cdot(U\omega_0)^2-0}{\Delta x}\right]-\delta_0\cdot 2\cdot\pi\cdot r^2\cdot\rho_f\cdot g\cdot\left(\sin\left(\frac{\Delta x}{r}\right)\right)^2+\frac{3}{2}\cdot\mu\cdot\frac{U\omega_0}{\delta_0}\right]}{Uinc}$$

$$del \leftarrow -\left(\psi^{-1}\cdot C\right)$$

$$\delta_0 \leftarrow \delta_0 + del_0$$

$$U\omega_0 \leftarrow U\omega_0 + del_1$$

for $ie \in 1..neq$

$$\Delta_{ie} \leftarrow \frac{U\omega_{ie-1}\cdot\Delta_{ie-1}}{U\omega_{ie}}$$

$$h \leftarrow r\cdot\left(1-\cos\left(\frac{\Delta x}{r}\right)\right)$$

$$U\omega_{ie} \leftarrow \sqrt{(U\omega_{ie-1})^2 + 2 \cdot g \cdot h}$$

for $iter \in 1..10$

$$C_0 \leftarrow \frac{5}{4 \cdot r} \cdot \cos\left(\frac{\Delta x}{r}\right) \cdot \delta_{ie} \cdot U\omega_{ie} + \frac{5}{4} \cdot \frac{\delta_{ie} \cdot U\omega_{ie} - \delta_{ie-1} \cdot U\omega_{ie-1}}{\Delta x} - \frac{k_f \cdot \Delta T}{\rho_f \cdot h_{fg} \cdot (\delta_{ie} + \Delta_{ie})} \cdot \sin\left(\frac{\Delta x}{r}\right) + \frac{\Delta_{ie} \cdot U\omega_{ie} - \Delta_{ie-1} \cdot U\omega_{ie-1}}{\Delta x}$$

$$C_1 \leftarrow \frac{34}{35} \cdot \pi \cdot \rho_f \cdot \cos\left(\frac{\Delta x}{r}\right) \cdot \delta_{ie} \cdot (U\omega_{ie})^2 + \frac{34}{35} \cdot \pi \cdot r \cdot \rho_f \cdot \frac{\left[(\delta_{ie}) \cdot (U\omega_{ie})^2 - \delta_{ie-1} \cdot (U\omega_{ie-1})^2\right]}{\Delta x} - \delta_{ie} \cdot 2 \cdot \pi \cdot r^2 \cdot \rho_f \cdot g \cdot \left(\sin\left(\frac{\Delta x}{r}\right)\right)^2 + \left(\frac{3}{2} \cdot \mu \cdot \frac{U\omega_{ie}}{\delta_{ie}}\right) + \rho_f \cdot \left[\frac{\Delta_{ie} \cdot (U\omega_{ie})^2 - \Delta_{ie-1} \cdot (U\omega_{ie-1})^2}{\Delta x}\right]$$

$$\psi(0,0) \leftarrow \frac{\left[\frac{5}{4 \cdot r} \cdot \cos\left(\frac{\Delta x}{r}\right) \cdot (\delta_{ie} + \delta inc) \cdot U\omega_{ie} + \frac{5}{4} \cdot \frac{(\delta_{ie} + \delta inc) \cdot U\omega_{ie} - \delta_{ie-1} \cdot U\omega_{ie-1}}{\Delta x} - \frac{k_f \cdot \Delta T}{\rho_f \cdot h_{fg} \cdot (\delta_{ie} + \delta inc + \Delta_{ie})} \cdot \sin\left(\frac{\Delta x}{r}\right)\right] - \blacksquare \ldots + \left[\frac{5}{4 \cdot r} \cdot \cos\left(\frac{\Delta x}{r}\right) \cdot \delta_{ie} \cdot U\omega_{ie} + \frac{5}{4} \cdot \frac{\delta_{ie} \cdot U\omega_{ie} - \delta_{ie-1} \cdot U\omega_{ie-1}}{\Delta x} - \frac{k_f \cdot \Delta T}{\rho_f \cdot h_{fg} \cdot (\delta_{ie} + \Delta_{ie})} \cdot \sin\left(\frac{\Delta x}{r}\right)\right]}{\delta inc}$$

$$\psi(0,1) \leftarrow \frac{\left[\frac{5}{4 \cdot r} \cdot \cos\left(\frac{\Delta x}{r}\right) \cdot \delta_{ie} \cdot (U\omega_{ie} + Uinc) + \frac{5}{4} \cdot \frac{\delta_{ie} \cdot (U\omega_{ie} + Uinc) - \delta_{ie-1} \cdot U\omega_{ie-1}}{\Delta x}\right] - \left(\frac{5}{4 \cdot r} \cdot \cos\left(\frac{\Delta x}{r}\right) \cdot \delta_{ie} \cdot U\omega_{ie} + \frac{5}{4} \cdot \frac{\delta_{ie} \cdot U\omega_{ie} - \delta_{ie-1} \cdot U\omega_{ie-1}}{\Delta x}\right)}{Uinc}$$

$$\psi(1,0) \leftarrow \frac{\left[\frac{34}{35} \cdot \pi \cdot \rho_f \cdot \cos\left(\frac{\Delta x}{r}\right) \cdot (\delta_{ie} + \delta inc) \cdot (U\omega_{ie})^2 + \frac{34}{35} \cdot \pi \cdot r \cdot \rho_f \cdot \frac{\left[(\delta_{ie} + \delta inc) \cdot (U\omega_{ie})^2 - \delta_{ie-1} \cdot (U\omega_{ie-1})^2\right]}{\Delta x} - (\delta_{ie} + \delta inc) \cdot 2 \cdot \pi \cdot r^2 \cdot \rho_f \cdot g \cdot \left(\sin\left(\frac{\Delta x}{r}\right)\right)^2 + \frac{3}{2} \cdot \mu \cdot \frac{U\omega_{ie}}{(\delta_{ie} + \delta inc)}\right] - \blacksquare \ldots + \left[\frac{34}{35} \cdot \pi \cdot \rho_f \cdot \cos\left(\frac{\Delta x}{r}\right) \cdot \delta_{ie} \cdot (U\omega_{ie})^2 + \frac{34}{35} \cdot \pi \cdot r \cdot \rho_f \cdot \frac{\left[\delta_{ie} \cdot (U\omega_{ie})^2 - \delta_{ie-1} \cdot (U\omega_{ie-1})^2\right]}{\Delta x} - \delta_{ie} \cdot 2 \cdot \pi \cdot r^2 \cdot \rho_f \cdot g \cdot \left(\sin\left(\frac{\Delta x}{r}\right)\right)^2 + \frac{3}{2} \cdot \mu \cdot \frac{U\omega_{ie}}{\delta_{ie}}\right]}{\delta inc}$$

$$\psi(1,1) \leftarrow \frac{\left[\frac{34}{35} \cdot \pi \cdot \rho_f \cdot \cos\left(\frac{\Delta x}{r}\right) \cdot \delta_{ie} \cdot (U\omega_{ie} + Uinc)^2 + \frac{34}{35} \cdot \pi \cdot r \cdot \rho_f \cdot \frac{\left[\delta_{ie} \cdot (U\omega_{ie} + Uinc)^2 - \delta_{ie-1} \cdot (U\omega_{ie-1})^2\right]}{\Delta x} - \delta_{ie} \cdot 2 \cdot \pi \cdot r^2 \cdot \rho_f \cdot g \cdot \left(\sin\left(\frac{\Delta x}{r}\right)\right)^2 + \frac{3}{2} \cdot \mu \cdot \frac{(U\omega_{ie} + Uinc)}{\delta_{ie}}\right] - \blacksquare \ldots + \left[\frac{34}{35} \cdot \pi \cdot \rho_f \cdot \cos\left(\frac{\Delta x}{r}\right) \cdot \delta_{ie} \cdot (U\omega_{ie})^2 + \frac{34}{35} \cdot \pi \cdot r \cdot \rho_f \cdot \frac{\left[\delta_{ie} \cdot (U\omega_{ie})^2 - \delta_{ie-1} \cdot (U\omega_{ie-1})^2\right]}{\Delta x} - \delta_{ie} \cdot 2 \cdot \pi \cdot r^2 \cdot \rho_f \cdot g \cdot \left(\sin\left(\frac{\Delta x}{r}\right)\right)^2 + \frac{3}{2} \cdot \mu \cdot \frac{U\omega_{ie}}{\delta_{ie}}\right]}{Uinc}$$

$$\text{del} \leftarrow -\left(\psi^{-1} \cdot C\right)$$

$$\delta_{ie} \leftarrow \delta_{ie} + \text{del}_0$$

$$U\omega_{ie} \leftarrow U\omega_{ie} + \text{del}_1$$

for $\text{iter} \in 1 .. 10$

$$C_0 \leftarrow \frac{5}{4 \cdot r} \cdot \cos\left(\frac{\Delta x}{r}\right) \cdot \delta_{ie} \cdot U\omega_{ie} + \frac{5}{4} \cdot \frac{\delta_{ie} \cdot U\omega_{ie} - \delta_{ie-1} \cdot U\omega_{ie-1}}{\Delta x} - \frac{k_f \cdot \Delta T}{\rho_f \cdot h_{fg} \cdot \delta_{ie}} \cdot \sin\left(\frac{\Delta x}{r}\right)$$

$$C_1 \leftarrow \frac{34}{35} \cdot \pi \cdot \rho_f \cdot \cos\left(\frac{\Delta x}{r}\right) \cdot \delta_{ie} \cdot \left(U\omega_{ie}\right)^2 + \frac{34}{35} \cdot \pi \cdot r \cdot \rho_f \cdot \frac{\left[\left(\delta_{ie}\right) \cdot \left(U\omega_{ie}\right)^2 - \delta_{ie-1} \cdot \left(U\omega_{ie-1}\right)^2\right]}{\Delta x} - \delta_{ie} \cdot 2 \cdot \pi \cdot r^2 \cdot \rho_f \cdot g \cdot \left(\sin\left(\frac{\Delta x}{r}\right)\right)^2 + \left(\frac{3}{2} \cdot \mu \cdot \frac{U\omega_{ie}}{\delta_{ie}}\right)$$

$$\psi(0,0) \leftarrow \frac{\left[\frac{5}{4 \cdot r} \cdot \cos\left(\frac{\Delta x}{r}\right) \cdot \left(\delta_{ie} + \delta inc\right) \cdot U\omega_{ie} + \frac{5}{4} \cdot \frac{\left(\delta_{ie} + \delta inc\right) \cdot U\omega_{ie} - \delta_{ie-1} \cdot U\omega_{ie-1}}{\Delta x} - \frac{k_f \cdot \Delta T}{\rho_f \cdot h_{fg} \cdot \left(\delta_{ie} + \delta inc\right)} \cdot \sin\left(\frac{\Delta x}{r}\right)\right] - \blacksquare \ldots + \left(\frac{5}{4 \cdot r} \cdot \cos\left(\frac{\Delta x}{r}\right) \cdot \delta_{ie} \cdot U\omega_{ie} + \frac{5}{4} \cdot \frac{\delta_{ie} \cdot U\omega_{ie} - \delta_{ie-1} \cdot U\omega_{ie-1}}{\Delta x} - \frac{k_f \cdot \Delta T}{\rho_f \cdot h_{fg} \cdot \delta_{ie}} \cdot \sin\left(\frac{\Delta x}{r}\right)\right)}{\delta inc}$$

$$\psi(0,1) \leftarrow \frac{\left[\frac{5}{4 \cdot r} \cdot \cos\left(\frac{\Delta x}{r}\right) \cdot \delta_{ie} \cdot \left(U\omega_{ie} + U inc\right) + \frac{5}{4} \cdot \frac{\delta_{ie} \cdot \left(U\omega_{ie} + U inc\right) - \delta_{ie-1} \cdot U\omega_{ie-1}}{\Delta x}\right] - \left(\frac{5}{4 \cdot r} \cdot \cos\left(\frac{\Delta x}{r}\right) \cdot \delta_{ie} \cdot U\omega_{ie} + \frac{5}{4} \cdot \frac{\delta_{ie} \cdot U\omega_{ie} - \delta_{ie-1} \cdot U\omega_{ie-1}}{\Delta x}\right)}{U inc}$$

$$\psi(1,0) \leftarrow \frac{\left[\frac{34}{35} \cdot \pi \cdot \rho_f \cdot \cos\left(\frac{\Delta x}{r}\right) \cdot \left(\delta_{ie} + \delta inc\right) \cdot \left(U\omega_{ie}\right)^2 + \frac{34}{35} \cdot \pi \cdot r \cdot \rho_f \cdot \frac{\left[\left(\delta_{ie} + \delta inc\right) \cdot \left(U\omega_{ie}\right)^2 - \delta_{ie-1} \cdot \left(U\omega_{ie-1}\right)^2\right]}{\Delta x} - \left(\delta_{ie} + \delta inc\right) \cdot 2 \cdot \pi \cdot r^2 \cdot \rho_f \cdot g \cdot \left(\sin\left(\frac{\Delta x}{r}\right)\right)^2 + \frac{3}{2} \cdot \mu \cdot \frac{U\omega_{ie}}{\left(\delta_{ie} + \delta inc\right)}\right] - \blacksquare \ldots + \left[\frac{34}{35} \cdot \pi \cdot \rho_f \cdot \cos\left(\frac{\Delta x}{r}\right) \cdot \delta_{ie} \cdot \left(U\omega_{ie}\right)^2 + \frac{34}{35} \cdot \pi \cdot r \cdot \rho_f \cdot \frac{\left[\delta_{ie} \cdot \left(U\omega_{ie}\right)^2 - \delta_{ie-1} \cdot \left(U\omega_{ie-1}\right)^2\right]}{\Delta x} - \delta_{ie} \cdot 2 \cdot \pi \cdot r^2 \cdot \rho_f \cdot g \cdot \left(\sin\left(\frac{\Delta x}{r}\right)\right)^2 + \frac{3}{2} \cdot \mu \cdot \frac{U\omega_{ie}}{\delta_{ie}}\right]}{\delta inc}$$

$$\psi(1,1) \leftarrow \frac{\left[\frac{34}{35} \cdot \pi \cdot \rho_f \cdot \cos\left(\frac{\Delta x}{r}\right) \cdot \delta_{ie} \cdot \left(U\omega_{ie} + U inc\right)^2 + \frac{34}{35} \cdot \pi \cdot r \cdot \rho_f \cdot \frac{\left[\delta_{ie} \cdot \left(U\omega_{ie} + U inc\right)^2 - \delta_{ie-1} \cdot \left(U\omega_{ie-1}\right)^2\right]}{\Delta x} - \delta_{ie} \cdot 2 \cdot \pi \cdot r^2 \cdot \rho_f \cdot g \cdot \left(\sin\left(\frac{\Delta x}{r}\right)\right)^2 + \frac{3}{2} \cdot \mu \cdot \frac{\left(U\omega_{ie} + U inc\right)}{\delta_{ie}}\right] - \blacksquare \ldots + \left[\frac{34}{35} \cdot \pi \cdot \rho_f \cdot \cos\left(\frac{\Delta x}{r}\right) \cdot \delta_{ie} \cdot \left(U\omega_{ie}\right)^2 + \frac{34}{35} \cdot \pi \cdot r \cdot \rho_f \cdot \frac{\left[\delta_{ie} \cdot \left(U\omega_{ie}\right)^2 - \delta_{ie-1} \cdot \left(U\omega_{ie-1}\right)^2\right]}{\Delta x} - \delta_{ie} \cdot 2 \cdot \pi \cdot r^2 \cdot \rho_f \cdot g \cdot \left(\sin\left(\frac{\Delta x}{r}\right)\right)^2 + \frac{3}{2} \cdot \mu \cdot \frac{U\omega_{ie}}{\delta_{ie}}\right]}{U inc}$$

$$\text{del} \leftarrow -\left(\psi^{-1} \cdot C\right)$$

$$\delta_{ie} \leftarrow \delta_{ie} + \text{del}_0$$

$$U\omega_{ie} \leftarrow U\omega_{ie} + \text{del}_1$$

$$\delta \leftarrow \delta + \Delta$$

$$\text{result2} \leftarrow \text{augment}(\delta, U\omega)$$

$$\text{result2} \leftarrow \text{augment}(\text{result1}, \text{result2})$$

$$Um \leftarrow \text{result2}_{18,3}$$

$$v1 \leftarrow Um$$

$$\delta 1 \leftarrow \text{result2}_{18,2}$$

$$h \leftarrow 5 \cdot 10^{-3}$$

$$xloc \leftarrow \Delta x$$

$$v2 \leftarrow \sqrt{v1^2 + 2 \cdot g \cdot h}$$

$$\delta 2 \leftarrow \frac{\delta 1 \cdot v1}{v2}$$

for $i \in 0 .. neq$

$$\delta_i \leftarrow \left[\frac{r \cdot v \cdot \left(3 \cdot k_f \cdot \Delta T\right)}{g \cdot \rho_f \cdot h_{fg}}\right]^{\frac{1}{4}}$$

$$U\omega_i \leftarrow \frac{g \cdot \rho_f \cdot (\delta_i)^2}{2 \cdot \mu} \cdot \sin\left(\frac{xloc}{r}\right)$$

$$xloc \leftarrow xloc + \Delta x$$

$$U\omega_0 \leftarrow v2$$

$$\Delta_0 \leftarrow \delta 2 \cdot axis2$$

$$\delta inc \leftarrow \frac{\delta_{18}}{1000}$$

$$Uinc \leftarrow \frac{U\omega_{18}}{1000}$$

$$h \leftarrow r\cdot\left(1-\cos\left(\frac{\Delta x}{r}\right)\right)$$

$$U\omega_0 \leftarrow \sqrt{(v2)^2+2\cdot g\cdot h}$$

$$\Delta_0 \leftarrow \frac{v2\cdot\Delta_0}{U\omega_0}$$

for iter $\in$ 1 .. 10

$$C_0 \leftarrow \frac{5}{4\cdot r}\cdot\cos\left(\frac{\Delta x}{r}\right)\cdot\delta_0\cdot U\omega_0+\frac{5}{4}\cdot\frac{\delta_0\cdot U\omega_0-0}{\Delta x}-\frac{k_f\cdot\Delta T}{\rho_f\cdot h_{fg}\cdot(\delta_0+\Delta_0)}\cdot\sin\left(\frac{\Delta x}{r}\right)+\frac{\Delta_0\cdot U\omega_0-\delta 2\cdot axis2\cdot v2}{\Delta x}$$

$$C_1 \leftarrow \frac{34}{35}\cdot\pi\cdot\rho_f\cdot\cos\left(\frac{\Delta x}{r}\right)\cdot\delta_0\cdot(U\omega_0)^2+\frac{34}{35}\cdot\pi\cdot r\cdot\rho_f\cdot\left[\frac{\delta_0\cdot(U\omega_0)^2-0}{\Delta x}\right]-2\cdot\pi\cdot r^2\cdot\delta_0\cdot\rho_f\cdot g\cdot\left(\sin\left(\frac{\Delta x}{r}\right)\right)^2+\left(\frac{3}{2}\cdot\mu\cdot\frac{U\omega_0}{\delta_0}\right)+\rho_f\cdot\left[\frac{\Delta_0\cdot(U\omega_0)^2-\delta 2\cdot axis2\cdot v2^2}{\Delta x}\right]$$

$$\psi(0,0) \leftarrow \frac{\left[\frac{5}{4\cdot r}\cdot\cos\left(\frac{\Delta x}{r}\right)\cdot(\delta_0+\delta inc)\cdot U\omega_0+\frac{5}{4}\cdot\frac{(\delta_0+\delta inc)\cdot U\omega_0-0}{\Delta x}-\frac{k_f\cdot\Delta T}{\rho_f\cdot h_{fg}\cdot(\delta_0+\delta inc+\Delta_0)}\cdot\sin\left(\frac{\Delta x}{r}\right)+\frac{\Delta_0\cdot U\omega_0-0}{\Delta x}\right]-\blacksquare\ldots+\left[\frac{5}{4\cdot r}\cdot\cos\left(\frac{\Delta x}{r}\right)\cdot\delta_0\cdot U\omega_0+\frac{5}{4}\cdot\frac{\delta_0\cdot U\omega_0-0}{\Delta x}-\frac{k_f\cdot\Delta T}{\rho_f\cdot h_{fg}\cdot(\delta_0+\Delta_0)}\cdot\sin\left(\frac{\Delta x}{r}\right)+\frac{\Delta_0\cdot U\omega_0-0}{\Delta x}\right]}{\delta inc}$$

$$\psi(0,1) \leftarrow \frac{\left[\frac{5}{4\,r}\cdot\cos\left(\frac{\Delta x}{r}\right)\cdot\delta_0\cdot(U\omega_0+Uinc)+\frac{5}{4}\cdot\frac{\delta_0\cdot(U\omega_0+Uinc)-0}{\Delta x}\right]-\left(\frac{5}{4\cdot r}\cdot\cos\left(\frac{\Delta x}{r}\right)\cdot\delta_0\cdot U\omega_0+\frac{5}{4}\cdot\frac{\delta_0\cdot U\omega_0-0}{\Delta x}\right)}{Uinc}$$

$$\psi(1,0) \leftarrow \frac{\left[\frac{34}{35}\cdot\pi\cdot\rho_f\cdot\cos\left(\frac{\Delta x}{r}\right)\cdot(\delta_0+\delta inc)\cdot(U\omega_0)^2+\frac{34}{35}\cdot\pi\cdot r\cdot\rho_f\cdot\left[\frac{(\delta_0+\delta inc)\cdot(U\omega_0)^2-0}{\Delta x}\right]-2\cdot\pi\cdot r^2\cdot(\delta_0+\delta inc)\cdot\rho_f\cdot g\cdot\left(\sin\left(\frac{\Delta x}{r}\right)\right)^2+\frac{3}{2}\cdot\mu\cdot\frac{U\omega_0}{(\delta_0+\delta inc)}\right]-\blacksquare\ldots+\left[\frac{34}{35}\cdot\pi\cdot\rho_f\cdot\cos\left(\frac{\Delta x}{r}\right)\cdot\delta_0\cdot(U\omega_0)^2+\frac{34}{35}\cdot\pi\cdot r\cdot\rho_f\cdot\left[\frac{\delta_0\cdot(U\omega_0)^2-0}{\Delta x}\right]-2\cdot\pi\cdot r^2\cdot\delta_0\cdot\rho_f\cdot g\cdot\left(\sin\left(\frac{\Delta x}{r}\right)\right)^2+\frac{3}{2}\cdot\mu\cdot\frac{U\omega_0}{\delta_0}\right]}{\delta inc}$$

$$\left[\frac{34}{35}\cdot\pi\cdot\rho_f\cdot\cos\left(\frac{\Delta x}{r}\right)\cdot\delta_0\cdot(U\omega_0+Uinc)^2+\frac{34}{35}\cdot\pi\cdot r\cdot\rho_f\cdot\left[\frac{\delta_0\cdot(U\omega_0+Uinc)^2-0}{\Delta x}\right]-2\cdot\pi\cdot r^2\cdot\delta_0\cdot\rho_f\cdot g\cdot\left(\sin\left(\frac{\Delta x}{r}\right)\right)^2+\frac{3}{2}\cdot\mu\cdot\frac{(U\omega_0+Uinc)}{\delta_0}\right]-\blacksquare\ldots$$

$$\psi(1,1)\leftarrow\frac{+\left[\frac{34}{35}\cdot\pi\cdot\rho_f\cdot\cos\left(\frac{\Delta x}{r}\right)\cdot\delta_0\cdot(U\omega_0)^2+\frac{34}{35}\cdot\pi\cdot r\cdot\rho_f\cdot\left[\frac{\delta_0\cdot(U\omega_0)^2-0}{\Delta x}\right]-2\cdot\pi\cdot r^2\cdot\delta_0\cdot\rho_f\cdot g\cdot\left(\sin\left(\frac{\Delta x}{r}\right)\right)^2+\frac{3}{2}\cdot\mu\cdot\frac{U\omega_0}{\delta_0}\right]}{Uinc}$$

$$del\leftarrow-\left(\psi^{-1}\cdot C\right)$$

$$\delta_0\leftarrow\delta_0+del_0$$

$$U\omega_0\leftarrow U\omega_0+del_1$$

for $ie\in 1\ldots neq$

$$\Delta_{ie}\leftarrow\frac{U\omega_{ie-1}\cdot\Delta_{ie-1}}{U\omega_{ie}}$$

$$h\leftarrow r\cdot\left(1-\cos\left(\frac{\Delta x}{r}\right)\right)$$

$$U\omega_{ie}\leftarrow\sqrt{(U\omega_{ie-1})^2+2\cdot g\cdot h}$$

for $iter\in 1\ldots 10$

$$C_0\leftarrow\frac{5}{4\cdot r}\cdot\cos\left(\frac{\Delta x}{r}\right)\cdot\delta_{ie}\cdot U\omega_{ie}+\frac{5}{4}\cdot\frac{\delta_{ie}\cdot U\omega_{ie}-\delta_{ie-1}\cdot U\omega_{ie-1}}{\Delta x}-\frac{k_f\cdot\Delta T}{\rho_f\cdot h_{fg}\cdot(\delta_{ie}+\Delta_{ie})}\cdot\sin\left(\frac{\Delta x}{r}\right)+\frac{\Delta_{ie}\cdot U\omega_{ie}-\Delta_{ie-1}\cdot U\omega_{ie-1}}{\Delta x}$$

$$C_1\leftarrow\frac{34}{35}\cdot\pi\cdot\rho_f\cdot\cos\left(\frac{\Delta x}{r}\right)\cdot\delta_{ie}\cdot(U\omega_{ie})^2+\frac{34}{35}\cdot\pi\cdot r\cdot\rho_f\cdot\frac{\left[(\delta_{ie})\cdot(U\omega_{ie})^2-\delta_{ie-1}\cdot(U\omega_{ie-1})^2\right]}{\Delta x}-\delta_{ie}\cdot 2\cdot\pi\cdot r^2\cdot\rho_f\cdot g\cdot\left(\sin\left(\frac{\Delta x}{r}\right)\right)^2+\left(\frac{3}{2}\cdot\mu\cdot\frac{U\omega_{ie}}{\delta_{ie}}\right)+\rho_f\cdot\left[\frac{\Delta_{ie}\cdot(U\omega_{ie})^2-\Delta_{ie-1}\cdot(U\omega_{ie-1})^2}{\Delta x}\right]$$

$$\psi(0,0)\leftarrow\frac{\left[\frac{5}{4\,r}\cdot\cos\left(\frac{\Delta x}{r}\right)\cdot(\delta_{ie}+\delta inc)\cdot U\omega_{ie}+\frac{5}{4}\cdot\frac{(\delta_{ie}+\delta inc)\cdot U\omega_{ie}-\delta_{ie-1}\cdot U\omega_{ie-1}}{\Delta x}-\frac{k_f\cdot\Delta T}{\rho_f\cdot h_{fg}\cdot(\delta_{ie}+\delta inc+\Delta_{ie})}\cdot\sin\left(\frac{\Delta x}{r}\right)\right]-\blacksquare\ldots}{+\left[\frac{5}{4\,r}\cdot\cos\left(\frac{\Delta x}{r}\right)\cdot\delta_{ie}\cdot U\omega_{ie}+\frac{5}{4}\cdot\frac{\delta_{ie}\cdot U\omega_{ie}-\delta_{ie-1}\cdot U\omega_{ie-1}}{\Delta x}-\frac{k_f\cdot\Delta T}{\rho_f\cdot h_{fg}\cdot(\delta_{ie}+\Delta_{ie})}\cdot\sin\left(\frac{\Delta x}{r}\right)\right]}{\delta inc}$$

$$\psi(0,1) \leftarrow \frac{\left[\frac{5}{4\cdot r}\cdot\cos\left(\frac{\Delta x}{r}\right)\cdot\delta_{ie}\cdot(U\omega_{ie}+Uinc)+\frac{5}{4}\cdot\frac{\delta_{ie}\cdot(U\omega_{ie}+Uinc)-\delta_{ie-1}\cdot U\omega_{ie-1}}{\Delta x}\right]-\left(\frac{5}{4\,r}\cdot\cos\left(\frac{\Delta x}{r}\right)\cdot\delta_{ie}\cdot U\omega_{ie}+\frac{5}{4}\cdot\frac{\delta_{ie}\cdot U\omega_{ie}-\delta_{ie-1}\cdot U\omega_{ie-1}}{\Delta x}\right)}{Uinc}$$

$$\psi(1,0) \leftarrow \frac{\left[\frac{34}{35}\cdot\pi\cdot\rho_f\cdot\cos\left(\frac{\Delta x}{r}\right)\cdot(\delta_{ie}+\delta inc)\cdot(U\omega_{ie})^2+\frac{34}{35}\cdot\pi\cdot r\cdot\rho_f\cdot\frac{\left[(\delta_{ie}+\delta inc)\cdot(U\omega_{ie})^2-\delta_{ie-1}\cdot(U\omega_{ie-1})^2\right]}{\Delta x}-2\cdot\pi\cdot r^2\cdot(\delta_{ie}+\delta inc)\cdot\rho_f\cdot g\cdot\left(\sin\left(\frac{\Delta x}{r}\right)\right)^2+\frac{3}{2}\cdot\mu\cdot\frac{U\omega_{ie}}{(\delta_{ie}+\delta inc)}\right]-\blacksquare\ldots}{\delta inc}$$

$$+\left[\frac{34}{35}\cdot\pi\cdot\rho_f\cdot\cos\left(\frac{\Delta x}{r}\right)\cdot\delta_{ie}\cdot(U\omega_{ie})^2+\frac{34}{35}\cdot\pi\cdot r\cdot\rho_f\cdot\frac{\left[\delta_{ie}\cdot(U\omega_{ie})^2-\delta_{ie-1}\cdot(U\omega_{ie-1})^2\right]}{\Delta x}-2\cdot\pi\cdot r^2\cdot\delta_{ie}\cdot\rho_f\cdot g\cdot\left(\sin\left(\frac{\Delta x}{r}\right)\right)^2+\frac{3}{2}\cdot\mu\cdot\frac{U\omega_{ie}}{\delta_{ie}}\right]$$

$$\psi(1,1) \leftarrow \frac{\left[\frac{34}{35}\cdot\pi\cdot\rho_f\cdot\cos\left(\frac{\Delta x}{r}\right)\cdot\delta_{ie}\cdot(U\omega_{ie}+Uinc)^2+\frac{34}{35}\cdot\pi\cdot r\cdot\rho_f\cdot\frac{\left[\delta_{ie}\cdot(U\omega_{ie}+Uinc)^2-\delta_{ie-1}\cdot(U\omega_{ie-1})^2\right]}{\Delta x}-2\cdot\pi\cdot r^2\cdot\delta_{ie}\cdot\rho_f\cdot g\cdot\left(\sin\left(\frac{\Delta x}{r}\right)\right)^2+\frac{3}{2}\cdot\mu\cdot\frac{(U\omega_{ie}+Uinc)}{\delta_{ie}}\right]-\blacksquare\ldots}{Uinc}$$

$$+\left[\frac{34}{35}\cdot\pi\cdot\rho_f\cdot\cos\left(\frac{\Delta x}{r}\right)\cdot\delta_{ie}\cdot(U\omega_{ie})^2+\frac{34}{35}\cdot\pi\cdot r\cdot\rho_f\cdot\frac{\left[\delta_{ie}\cdot(U\omega_{ie})^2-\delta_{ie-1}\cdot(U\omega_{ie-1})^2\right]}{\Delta x}-2\cdot\pi\cdot r^2\cdot\delta_{ie}\cdot\rho_f\cdot g\cdot\left(\sin\left(\frac{\Delta x}{r}\right)\right)^2+\frac{3}{2}\cdot\mu\cdot\frac{U\omega_{ie}}{\delta_{ie}}\right]$$

$$del \leftarrow -\left(\psi^{-1}\cdot C\right)$$

$$\delta_{ie} \leftarrow \delta_{ie} + del_0$$

$$U\omega_{ie} \leftarrow U\omega_{ie} + del_1$$

for $iter \in 1..10$

$$C_0 \leftarrow \frac{5}{4\,r}\cdot\cos\left(\frac{\Delta x}{r}\right)\cdot\delta_{ie}\cdot U\omega_{ie}+\frac{5}{4}\cdot\frac{\delta_{ie}\cdot U\omega_{ie}-\delta_{ie-1}\cdot U\omega_{ie-1}}{\Delta x}-\frac{k_f\cdot\Delta T}{\rho_f\cdot h_{fg}\cdot\delta_{ie}}\cdot\sin\left(\frac{\Delta x}{r}\right)$$

$$C_1 \leftarrow \frac{34}{35}\cdot\pi\cdot\rho_f\cdot\cos\left(\frac{\Delta x}{r}\right)\cdot\delta_{ie}\cdot(U\omega_{ie})^2+\frac{34}{35}\cdot\pi\cdot r\cdot\rho_f\cdot\frac{\left[(\delta_{ie})\cdot(U\omega_{ie})^2-\delta_{ie-1}\cdot(U\omega_{ie-1})^2\right]}{\Delta x}-\delta_{ie}\cdot 2\cdot\pi\cdot r^2\cdot\rho_f\cdot g\cdot\left(\sin\left(\frac{\Delta x}{r}\right)\right)^2+\left(\frac{3}{2}\cdot\mu\cdot\frac{U\omega_{ie}}{\delta_{ie}}\right)$$

$$\left[\frac{5}{4\cdot r}\cdot\cos\left(\frac{\Delta x}{r}\right)\cdot(\delta_{ie}+\delta inc)\cdot U\omega_{ie}+\frac{5}{4}\cdot\frac{(\delta_{ie}+\delta inc)\cdot U\omega_{ie}-\delta_{ie-1}\cdot U\omega_{ie-1}}{\Delta x}-\frac{k_f\cdot\Delta T}{\rho_f\cdot h_{fg}\cdot(\delta_{ie}+\delta inc)}\cdot\sin\left(\frac{\Delta x}{r}\right)\right]-\blacksquare\ldots$$

$$\psi(0,0) \leftarrow \frac{+\left(\frac{5}{4\,r}\cdot\cos\left(\frac{\Delta x}{r}\right)\cdot\delta_{ie}\cdot U\omega_{ie}+\frac{5}{4}\cdot\frac{\delta_{ie}\cdot U\omega_{ie}-\delta_{ie-1}\cdot U\omega_{ie-1}}{\Delta x}-\frac{k_f\cdot\Delta T}{\rho_f\cdot h_{fg}\cdot\delta_{ie}}\cdot\sin\left(\frac{\Delta x}{r}\right)\right)}{\delta inc}$$

$$\psi(0,1) \leftarrow \frac{\left[\frac{5}{4\,r}\cdot\cos\left(\frac{\Delta x}{r}\right)\cdot\delta_{ie}\cdot(U\omega_{ie}+Uinc)+\frac{5}{4}\cdot\frac{\delta_{ie}\cdot(U\omega_{ie}+Uinc)-\delta_{ie-1}\cdot U\omega_{ie-1}}{\Delta x}\right]-\left(\frac{5}{4\,r}\cdot\cos\left(\frac{\Delta x}{r}\right)\cdot\delta_{ie}\cdot U\omega_{ie}+\frac{5}{4}\cdot\frac{\delta_{ie}\cdot U\omega_{ie}-\delta_{ie-1}\cdot U\omega_{ie-1}}{\Delta x}\right)}{Uinc}$$

$$\psi(1,0) \leftarrow \frac{\left[\frac{34}{35}\cdot\pi\cdot\rho_f\cdot\cos\left(\frac{\Delta x}{r}\right)\cdot(\delta_{ie}+\delta inc)\cdot(U\omega_{ie})^2+\frac{34}{35}\cdot\pi\cdot r\cdot\rho_f\cdot\frac{\left[(\delta_{ie}+\delta inc)\cdot(U\omega_{ie})^2-\delta_{ie-1}\cdot(U\omega_{ie-1})^2\right]}{\Delta x}-2\cdot\pi\cdot r^2\cdot(\delta_{ie}+\delta inc)\cdot\rho_f\cdot g\cdot\left(\sin\left(\frac{\Delta x}{r}\right)\right)^2+\frac{3}{2}\cdot\mu\cdot\frac{U\omega_{ie}}{(\delta_{ie}+\delta inc)}\right]-\blacksquare\ldots}{+\left[\frac{34}{35}\cdot\pi\cdot\rho_f\cdot\cos\left(\frac{\Delta x}{r}\right)\cdot\delta_{ie}\cdot(U\omega_{ie})^2+\frac{34}{35}\cdot\pi\cdot r\cdot\rho_f\cdot\frac{\left[\delta_{ie}\cdot(U\omega_{ie})^2-\delta_{ie-1}\cdot(U\omega_{ie-1})^2\right]}{\Delta x}-2\cdot\pi\cdot r^2\cdot\delta_{ie}\cdot\rho_f\cdot g\cdot\left(\sin\left(\frac{\Delta x}{r}\right)\right)^2+\frac{3}{2}\cdot\mu\cdot\frac{U\omega_{ie}}{\delta_{ie}}\right]}{\delta inc}$$

$$\psi(1,1) \leftarrow \frac{\left[\frac{34}{35}\cdot\pi\cdot\rho_f\cdot\cos\left(\frac{\Delta x}{r}\right)\cdot\delta_{ie}\cdot(U\omega_{ie}+Uinc)^2+\frac{34}{35}\cdot\pi\cdot r\cdot\rho_f\cdot\frac{\left[\delta_{ie}\cdot(U\omega_{ie}+Uinc)^2-\delta_{ie-1}\cdot(U\omega_{ie-1})^2\right]}{\Delta x}-2\cdot\pi\cdot r^2\cdot\delta_{ie}\cdot\rho_f\cdot g\cdot\left(\sin\left(\frac{\Delta x}{r}\right)\right)^2+\frac{3}{2}\cdot\mu\cdot\frac{(U\omega_{ie}+Uinc)}{\delta_{ie}}\right]-\blacksquare\ldots}{+\left[\frac{34}{35}\cdot\pi\cdot\rho_f\cdot\cos\left(\frac{\Delta x}{r}\right)\cdot\delta_{ie}\cdot(U\omega_{ie})^2+\frac{34}{35}\cdot\pi\cdot r\cdot\rho_f\cdot\frac{\left[\delta_{ie}\cdot(U\omega_{ie})^2-\delta_{ie-1}\cdot(U\omega_{ie-1})^2\right]}{\Delta x}-2\cdot\pi\cdot r^2\cdot\delta_{ie}\cdot\rho_f\cdot g\cdot\left(\sin\left(\frac{\Delta x}{r}\right)\right)^2+\frac{3}{2}\cdot\mu\cdot\frac{U\omega_{ie}}{\delta_{ie}}\right]}{Uinc}$$

$$del \leftarrow -\left(\psi^{-1}\cdot C\right)$$

$$\delta_{ie} \leftarrow \delta_{ie} + del_0$$

$$U\omega_{ie} \leftarrow U\omega_{ie} + del_1$$

for $iter \in 1..10$

$$C_0 \leftarrow \frac{5}{4\,r}\cdot\cos\left(\frac{\Delta x}{r}\right)\cdot\delta_{ie}\cdot U\omega_{ie}+\frac{5}{4}\cdot\frac{\delta_{ie}\cdot U\omega_{ie}-\delta_{ie-1}\cdot U\omega_{ie-1}}{\Delta x}-\frac{k_f\cdot\Delta T}{\rho_f\cdot h_{fg}\cdot\delta_{ie}}\cdot\sin\left(\frac{\Delta x}{r}\right)$$

$$C_1 \leftarrow \frac{34}{35}\cdot\pi\cdot\rho_f\cdot\cos\left(\frac{\Delta x}{r}\right)\cdot\delta_{ie}\cdot(U\omega_{ie})^2+\frac{34}{35}\cdot\pi\cdot r\cdot\rho_f\cdot\frac{\left[(\delta_{ie})\cdot(U\omega_{ie})^2-\delta_{ie-1}\cdot(U\omega_{ie-1})^2\right]}{\Delta x}-\delta_{ie}\cdot 2\cdot\pi\cdot r^2\cdot\rho_f\cdot g\cdot\left(\sin\left(\frac{\Delta x}{r}\right)\right)^2+\left(\frac{3}{2}\cdot\mu\cdot\frac{U\omega_{ie}}{\delta_{ie}}\right)$$

$$\psi(0,0) \leftarrow \frac{\left[\frac{5}{4\,r}\cdot\cos\left(\frac{\Delta x}{r}\right)\cdot(\delta_{ie}+\delta inc)\cdot U\omega_{ie}+\frac{5}{4}\cdot\frac{(\delta_{ie}+\delta inc)\cdot U\omega_{ie}-\delta_{ie-1}\cdot U\omega_{ie-1}}{\Delta x}-\frac{k_f\cdot\Delta T}{\rho_f\cdot h_{fg}\cdot(\delta_{ie}+\delta inc)}\cdot\sin\left(\frac{\Delta x}{r}\right)\right]-\blacksquare\ldots}{+\left(\frac{5}{4\,r}\cdot\cos\left(\frac{\Delta x}{r}\right)\cdot\delta_{ie}\cdot U\omega_{ie}+\frac{5}{4}\cdot\frac{\delta_{ie}\cdot U\omega_{ie}-\delta_{ie-1}\cdot U\omega_{ie-1}}{\Delta x}-\frac{k_f\cdot\Delta T}{\rho_f\cdot h_{fg}\cdot\delta_{ie}}\cdot\sin\left(\frac{\Delta x}{r}\right)\right)}{\delta inc}$$

$$\psi(0,1) \leftarrow \frac{\left[\frac{5}{4\,r}\cdot\cos\left(\frac{\Delta x}{r}\right)\cdot\delta_{ie}\cdot(U\omega_{ie}+Uinc)+\frac{5}{4}\cdot\frac{\delta_{ie}\cdot(U\omega_{ie}+Uinc)-\delta_{ie-1}\cdot U\omega_{ie-1}}{\Delta x}\right]-\left(\frac{5}{4\cdot r}\cdot\cos\left(\frac{\Delta x}{r}\right)\cdot\delta_{ie}\cdot U\omega_{ie}+\frac{5}{4}\cdot\frac{\delta_{ie}\cdot U\omega_{ie}-\delta_{ie-1}\cdot U\omega_{ie-1}}{\Delta x}\right)}{Uinc}$$

$$\psi(1,0) \leftarrow \frac{\left[\frac{34}{35}\cdot\pi\cdot\rho_f\cdot\cos\left(\frac{\Delta x}{r}\right)\cdot(\delta_{ie}+\delta inc)\cdot(U\omega_{ie})^2+\frac{34}{35}\cdot\pi\cdot r\cdot\rho_f\cdot\frac{\left[(\delta_{ie}+\delta inc)\cdot(U\omega_{ie})^2-\delta_{ie-1}\cdot(U\omega_{ie-1})^2\right]}{\Delta x}-2\cdot\pi\cdot r^2\cdot(\delta_{ie}+\delta inc)\cdot\rho_f\cdot g\cdot\left(\sin\left(\frac{\Delta x}{r}\right)\right)^2+\frac{3}{2}\cdot\mu\cdot\frac{U\omega_{ie}}{(\delta_{ie}+\delta inc)}\right]-\blacksquare\ldots}{+\left[\frac{34}{35}\cdot\pi\cdot\rho_f\cdot\cos\left(\frac{\Delta x}{r}\right)\cdot\delta_{ie}\cdot(U\omega_{ie})^2+\frac{34}{35}\cdot\pi\cdot r\cdot\rho_f\cdot\frac{\left[\delta_{ie}\cdot(U\omega_{ie})^2-\delta_{ie-1}\cdot(U\omega_{ie-1})^2\right]}{\Delta x}-\pi\cdot r^2\cdot 2\cdot\delta_{ie}\cdot\rho_f\cdot g\cdot\left(\sin\left(\frac{\Delta x}{r}\right)\right)^2+\frac{3}{2}\cdot\mu\cdot\frac{U\omega_{ie}}{\delta_{ie}}\right]}{\delta inc}$$

$$\psi(1,1) \leftarrow \frac{\left[\frac{34}{35}\cdot\pi\cdot\rho_f\cdot\cos\left(\frac{\Delta x}{r}\right)\cdot\delta_{ie}\cdot(U\omega_{ie}+Uinc)^2+\frac{34}{35}\cdot\pi\cdot r\cdot\rho_f\cdot\frac{\left[\delta_{ie}\cdot(U\omega_{ie}+Uinc)^2-\delta_{ie-1}\cdot(U\omega_{ie-1})^2\right]}{\Delta x}-2\cdot\pi\cdot r^2\cdot\delta_{ie}\cdot\rho_f\cdot g\cdot\left(\sin\left(\frac{\Delta x}{r}\right)\right)^2+\frac{3}{2}\cdot\mu\cdot\frac{(U\omega_{ie}+Uinc)}{\delta_{ie}}\right]-\blacksquare\ldots}{+\left[\frac{34}{35}\cdot\pi\cdot\rho_f\cdot\cos\left(\frac{\Delta x}{r}\right)\cdot\delta_{ie}\cdot(U\omega_{ie})^2+\frac{34}{35}\cdot\pi\cdot r\cdot\rho_f\cdot\frac{\left[\delta_{ie}\cdot(U\omega_{ie})^2-\delta_{ie-1}\cdot(U\omega_{ie-1})^2\right]}{\Delta x}-\pi\cdot r^2\cdot 2\cdot\delta_{ie}\cdot\rho_f\cdot g\cdot\left(\sin\left(\frac{\Delta x}{r}\right)\right)^2+\frac{3}{2}\cdot\mu\cdot\frac{U\omega_{ie}}{\delta_{ie}}\right]}{Uinc}$$

$$del \leftarrow -\left(\psi^{-1}\cdot C\right)$$

$$\delta_{ie} \leftarrow \delta_{ie} + del_0$$

$$U\omega_{ie} \leftarrow U\omega_{ie} + del_1$$

$$\delta \leftarrow \delta + \Delta$$

$$result3 \leftarrow augment(\delta, U\omega)$$

$$result3 \leftarrow augment(result2, result3)$$